

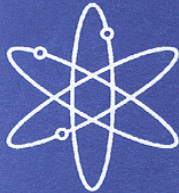
**NUREG/CR-6760
ORNL/TM-2000/321**



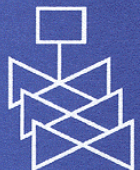
Study of the Effect of Integral Burnable Absorbers for PWR Burnup Credit



**Prepared by
C. E. Sanders and J. C. Wagner, ORNL**



Oak Ridge National Laboratory



**U.S. Nuclear Regulatory Commission
Office of Nuclear Regulatory Research
Washington, DC 20555-0001**



AVAILABILITY OF REFERENCE MATERIALS IN NRC PUBLICATIONS

NRC Reference Material

As of November 1999, you may electronically access NUREG-series publications and other NRC records at NRC's Public Electronic Reading Room at www.nrc.gov/NRC/ADAMS/index.html.

Publicly released records include, to name a few, NUREG-series publications; *Federal Register* notices; applicant, licensee, and vendor documents and correspondence; NRC correspondence and internal memoranda; bulletins and information notices; inspection and investigative reports; licensee event reports; and Commission papers and their attachments.

NRC publications in the NUREG series, NRC regulations, and *Title 10, Energy*, of the Code of *Federal Regulations*, may also be purchased from one of these two sources:

1. The Superintendent of Documents
U.S. Government Printing Office
P.O. Box 37082
Washington, DC 20402-9328
www.access.gpo.gov/su_docs
202-512-1800
2. The National Technical Information Service
Springfield, VA 22161-0002
www.ntis.gov
1-800-553-6847 or, locally, 703-605-6000

A single copy of each NRC draft report for comment is available free, to the extent of supply, upon written request as follows:

Address: Office of the Chief Information Officer,
Reproduction and Distribution
Services Section
U.S. Nuclear Regulatory Commission
Washington, DC 20555-0001

E-mail: DISTRIBUTION@nrc.gov

Facsimile: 301-415-2289

Some publications in the NUREG series that are posted at NRC's Web site address www.nrc.gov/NRC/NUREGS/indexnum.html are updated regularly and may differ from the last printed version.

Non-NRC Reference Material

Documents available from public and special technical libraries include all open literature items, such as books, journal articles, and transactions, *Federal Register* notices, Federal and State legislation, and congressional reports. Such documents as theses, dissertations, foreign reports and translations, and non-NRC conference proceedings may be purchased from their sponsoring organization.

Copies of industry codes and standards used in a substantive manner in the NRC regulatory process are maintained at—

The NRC Technical Library
Two White Flint North
11545 Rockville Pike
Rockville, MD 20852-2738

These standards are available in the library for reference use by the public. Codes and standards are usually copyrighted and may be purchased from the originating organization or, if they are American National Standards, from—

American National Standards Institute
11 West 42nd Street
New York, NY 10036-8002
www.ansi.org
212-642-4900

The NUREG series comprises (1) technical and administrative reports and books prepared by the staff (NUREG/XXXX) or agency contractors (NUREG/CR-XXXX), (2) proceedings of conferences (NUREG/CP-XXXX), (3) reports resulting from international agreements (NUREG/IA-XXXX), (4) brochures (NUREG/BR-XXXX), and (5) compilations of legal decisions and orders of the Commission and Atomic and Safety Licensing Boards and of Directors' decisions under Section 2.206 of NRC's regulations (NUREG-0750).

DISCLAIMER: This report was prepared as an account of work sponsored by an agency of the U.S. Government. Neither the U.S. Government nor any agency thereof, nor any employee, makes any warranty, expressed or implied, or assumes any legal liability or responsibility for any third party's use, or the results of such use, of any information, apparatus, product, or process disclosed in this publication, or represents that its use by such third party would not infringe privately owned rights.

Study of the Effect of Integral Burnable Absorbers for PWR Burnup Credit

Manuscript Completed: August 2001
Date Published: March 2002

Prepared by
C. E. Sanders and J. C. Wagner, ORNL

Oak Ridge National Laboratory
Managed by UT-Battelle, LLC
Oak Ridge, TN 37831-6370

R. Y. Lee, NRC Project Manager

Prepared for
Division of Systems Analysis and Regulatory Effectiveness
Office of Nuclear Regulatory Research
U.S. Nuclear Regulatory Commission
Washington, DC 20555-0001
NRC Job Code W6479



ABSTRACT

The Interim Staff Guidance on burnup credit issued by the U.S. Nuclear Regulatory Commission's Spent Fuel Project Office recommends restricting the use of burnup credit to assemblies that have not used burnable absorbers. This restriction eliminates a large portion of the currently discharged spent fuel assemblies from cask loading, and thus severely limits the practical usefulness of burnup credit. This report examines the effect of integral burnable absorbers (IBAs) on reactivity to provide technical justification for relaxing the current restriction for dry storage and transportation, and subsequently, for developing the necessary guidelines for relaxing the current restriction. The effect of IBAs on reactivity for various IBA designs is shown and discussed. Further, the reactivity effect of IBAs for typical initial fuel enrichment and absorber loadings is quantified as a function of burnup. The report concludes with a discussion of the issues for consideration and preliminary recommendations to expand the use of burnup credit to include spent fuel assemblies with IBAs.

CONTENTS

	<u>Page</u>
ABSTRACT	iii
LIST OF FIGURES	vii
LIST OF TABLES	xi
FOREWORD	xiii
ACKNOWLEDGEMENTS	xv
1 INTRODUCTION	1
2 INTEGRAL BURNABLE ABSORBER DESIGNS CONSIDERED	3
2.1 INTEGRAL FUEL BURNABLE ABSORBER RODS.....	3
2.2 UO ₂ -Gd ₂ O ₃ INTEGRAL BURNABLE ABSORBER RODS.....	3
2.3 UO ₂ -Er ₂ O ₃ INTEGRAL BURNABLE ABSORBER RODS.....	4
2.4 Al ₂ O ₃ -B ₄ C INTEGRAL BURNABLE ABSORBER RODS.....	4
3 REACTIVITY EFFECT OF INTEGRAL BURNABLE ABSORBER RODS.....	5
3.1 INTRODUCTION	5
3.2 CODE DESCRIPTION	6
3.3 CALCULATIONS.....	7
3.3.1 Integral Fuel Burnable Absorber Rods	7
3.3.1.1 Integral Fuel Burnable Absorber Analyses for 1.57 mg ¹⁰ B/inch.....	8
3.3.1.2 Integral Fuel Burnable Absorber Analyses for 2.355 mg ¹⁰ B/inch.....	17
3.3.2 UO ₂ -Gd ₂ O ₃ Integral Burnable Absorber Rods.....	17
3.3.2.1 Combustion Engineering Designs	20
3.3.2.2 Siemens Designs	27
3.3.3 UO ₂ -Er ₂ O ₃ Integral Burnable Absorber Rods	36
3.3.4 Al ₂ O ₃ -B ₄ C Integral Burnable Absorber Rods.....	42
3.3.5 Additional Studies	49
3.3.5.1 Parametric Assembly Design Studies.....	49
3.3.5.1.1 Variations of gadolinia loading and initial fuel enrichment	49
3.3.5.1.2 Variations of integral fuel burnable absorber loading and initial fuel enrichment.....	52
3.3.5.2 Residual Reactivity Effect of Integral Burnable Absorbers.....	55
3.3.5.3 Cooling Time.....	58
3.3.5.4 Reactivity Behavior in a Poisoned Storage Cell.....	59
3.3.5.5 Axial Burnup.....	62
4 SUMMARY AND IMPLICATIONS	67
5 RECOMMENDATIONS	69
6 REFERENCES	71

LIST OF FIGURES

<u>Figures</u>	<u>Page</u>
1 Typical reactivity behavior of PWR fuel with and without IBAs (neutron poisons).....	6
2 HELIOS calculational model of an IFBA case containing 156 IFBA rods	9
3 Fuel rod array (17 × 17) representing the loading pattern for 80 IFBA rods.....	10
4 Comparison of k_{inf} values with IFBA rods (80 IFBA rods, 3.4 wt % ^{235}U enriched fuel) and without IFBA rods (3.4 wt % ^{235}U enriched fuel)	11
5 Comparison of Δk values as a function of burnup between assemblies with and without IFBA rods (80 IFBA rods) for initial enrichments of 3.4 and 4.4 wt % ^{235}U . The results are also plotted on the enlarged scale on the right-hand-side y-axis for clarity.....	12
6 Fuel rod array (17 × 17) representing the loading pattern for 104 IFBA rods.....	13
7 Comparison of Δk values as a function of burnup between assemblies with and without IFBA rods (104 IFBA rods) for initial enrichments of 3.4 and 4.0 wt % ^{235}U . The results are also plotted according to the enlarged scale on the right-hand-side y-axis for clarity.....	14
8 Fuel rod array (17 × 17) representing the loading pattern for 156 IFBA rods.....	15
9 Comparison of Δk values as a function of burnup between assemblies with and without IFBA rods (156 IFBA rods) for initial enrichments of 4.0 and 4.4 wt % ^{235}U . The results are also plotted on the enlarged scale on the right-hand-side y-axis for clarity.....	16
10 Comparison of Δk values as a function of burnup between assemblies with and without IFBA rods, with varied number of IFBA rods and an enrichment of 4.617 wt % ^{235}U . The results are also plotted on the enlarged scale on the right-hand-side y-axis for clarity.....	18
11 Comparison of Δk values as a function of burnup between assemblies with and without IFBA rods (104 IFBA rods) for initial enrichments of 4.25 and 4.617 wt % ^{235}U . The results are also plotted on the enlarged scale on the right-hand-side y-axis for clarity.....	19
12 Fuel rod array (16 × 16) representing the loading pattern of the D and E fuel assemblies	21
13 Fuel rod array (16 × 16) representing the loading pattern of the D1 and E1 fuel assemblies	22
14 Fuel rod array (16 × 16) representing the loading pattern of the D2 and E2 fuel assemblies	23
15 HELIOS calculational model of the D1 fuel assembly containing eight $\text{UO}_2\text{-Gd}_2\text{O}_3$ rods	24

LIST OF FIGURES (continued)

<u>Figure</u>	<u>Page</u>
16	Comparison of Δk values as a function of burnup between the D assembly designs with gadolinia-bearing rods and the D assembly design (Figure 12) without gadolinia-bearing rods. The results are also plotted according to the enlarged scale on the right-hand-side y-axis for clarity..... 25
17	Comparison of Δk values as a function of burnup between the E assembly designs with gadolinia-bearing rods and the E assembly design (Figure 12) without gadolinia-bearing rods. The results are also plotted on the enlarged scale on the right-hand-side y-axis for clarity..... 26
18	Fuel rod array (17×17) representing the M1 loading pattern..... 28
19	Fuel rod array (17×17) representing the M2 loading pattern..... 29
20	Fuel rod array (17×17) representing the M3 loading pattern..... 30
21	Fuel rod array (17×17) representing the M4 loading pattern..... 31
22	HELIOS calculational model of M1 fuel assembly 32
23	Comparison of k_{inf} values with and without gadolinia-bearing rods (M1 assembly)..... 33
24	Comparison of Δk values as a function of burnup between assemblies with and without gadolinia-bearing rods (M1 and M2 assemblies). The results are also plotted on the enlarged scale on the right-hand-side y-axis for clarity..... 34
25	Comparison of Δk values as a function of burnup between assemblies with (M3 and M4) and without gadolinia-bearing rods. The results are also plotted on the enlarged scale on the right-hand-side y-axis for clarity. 35
26	HELIOS calculational model of a fuel assembly containing 60 erbia-bearing fuel rods 37
27	Fuel rod array (14×14) representing the loading pattern for 20 $UO_2-Er_2O_3$ rods..... 38
28	Fuel rod array (14×14) representing the loading pattern for 60 $UO_2-Er_2O_3$ rods..... 39
29	Comparison of k_{inf} values with erbia-bearing rods (60) present..... 40
30	Comparison of Δk values as a function of burnup between assemblies with and without $UO_2-Er_2O_3$ fuel rods. The fuel rods have a ^{235}U enrichment of 4.3 wt %, and the $UO_2-Er_2O_3$ rods contain 2.0 wt % erbia..... 41
31	HELIOS calculational model of a fuel assembly containing 12 $Al_2O_3-B_4C$ rods..... 43

LIST OF FIGURES (continued)

<u>Figure</u>	<u>Page</u>
32 Fuel rod array (14 × 14) representing the loading pattern for four Al ₂ O ₃ -B ₄ C rods.....	44
33 Fuel rod array (14 × 14) representing the loading pattern for eight Al ₂ O ₃ -B ₄ C rods.....	45
34 Fuel rod array (14 × 14) representing the loading pattern for 12 Al ₂ O ₃ -B ₄ C rods	46
35 Comparison of k_{inf} values with and without Al ₂ O ₃ -B ₄ C rods (12 Al ₂ O ₃ -B ₄ C rods).....	47
36 Comparison of Δk values as a function of burnup between assemblies with and without Al ₂ O ₃ -B ₄ C rods. The fuel rods have a ²³⁵ U enrichment of 4 wt %, and the Al ₂ O ₃ -B ₄ C rods have 4 wt % B ₄ C.	48
37 Comparison of Δk values versus burnup with varying gadolinia weight percentage. The fuel enrichments are 3.78/3.28 wt % ²³⁵ U.....	50
38 Comparison of Δk values versus burnup with various ²³⁵ U enrichments. The eight IBA rods have 6 wt % Gd ₂ O ₃	51
39 Comparison of Δk values versus burnup with varying IFBA loadings. The ²³⁵ U enrichment is 4 wt % for all cases.	52
40 Comparison of Δk values versus burnup with the 32 IFBA loading pattern showing varying ²³⁵ U enrichments. The results are also plotted on the enlarged scale on the right-hand-side y-axis for clarity.	53
41 Comparison of Δk values versus burnup with the 156 IFBA loading pattern showing varying ²³⁵ U enrichments. The results are also plotted on the enlarged scale on the right-hand-side y-axis for clarity.	54
42 Reactivity worth of gadolinium isotopes versus burnup for M1 assembly.....	56
43 Reactivity worth of boron versus burnup for a Westinghouse 17 × 17 fuel assembly containing 64 IFBA rods	57
44 Comparison of Δk values as a function of burnup and cooling time between assemblies with and without IFBA rods (104 IFBA rods) for and initial enrichment of 4.0 wt % ²³⁵ U	58
45 Comparison of Δk values as a function of burnup for IFBA assemblies in differing geometric configurations.....	60

LIST OF FIGURES (continued)

<u>Figure</u>		<u>Page</u>
46	Comparison of Δk values as a function of burnup for assemblies with $\text{UO}_2\text{-Gd}_2\text{O}_3$ rods in differing geometric configurations.....	61

LIST OF TABLES

<u>Table</u>	<u>Page</u>
1 Summary of parameters used for the depletion calculations	7
2 Westinghouse 17 × 17 fuel assembly specifications	8
3 CE 16 × 16 fuel assembly specifications.....	20
4 Fuel assembly data for the D and E sets of assembly designs	20
5 Siemens 17 × 17 fuel assembly specifications	27
6 Fuel assembly data for the M1–M4 assembly designs.....	27
7 CE 14 × 14 fuel assembly specifications.....	36
8 Summary of maximum positive Δk values observed for IFBA cases.....	55
9 Summary of maximum positive Δk values observed for IFBA cases in a cask environment.....	61
10 Comparison of k_{eff} results in the GBC-32 cask for fuel with full-length (144 inch) IFBA rods when the axial burnup distribution is included.....	64
11 Comparison of k_{eff} results in the GBC-32 cask for fuel with IFBA rods when the axial burnup distribution is included and the IFBA coating corresponds to the central 120 inches of the axial fuel length	64
12 Comparison of k_{eff} results in the GBC-32 cask for fuel with IFBA rods when the axial burnup distribution is included and the IFBA coating corresponds to the central 108 inches of the axial fuel length	65

FOREWORD

In 1999 the United States Nuclear Regulatory Commission (U.S. NRC) issued initial recommended guidance for using reactivity credit due to fuel irradiation (i.e., burnup credit) in the criticality safety analysis of spent pressurized-water-reactor (PWR) fuel in storage and transportation packages. This guidance was issued by the NRC Spent Fuel Project Office (SFPO) as Revision 1 to Interim Staff Guidance 8 (ISG8R1) and published in the *Standard Review Plan for Transportation Packages for Spent Nuclear Fuel*, NUREG-1617 (March 2000). With this initial guidance as a basis, the NRC Office of Nuclear Regulatory Research initiated a program to provide the SFPO with technical information that would:

- enable realistic estimates of the subcritical margin for systems with spent nuclear fuel (SNF) and an increased understanding of the phenomena and parameters that impact the margin, and
- support the development of technical bases and recommendations for effective implementation of burnup credit and provide realistic SNF acceptance criteria while maintaining an adequate margin of safety.

One restriction recommended by the ISG8R1 is to preclude assemblies irradiated with burnable absorbers from being used in a cask that implements burnup credit. Since a large portion (perhaps 50% or more) of the discharged SNF inventory has been exposed to burnable absorbers, this restriction was identified as a potentially unnecessary and costly restriction that could be removed with improved understanding of the impact of burnable absorbers on SNF reactivity in transportation and storage environments. Burnable absorbers used in PWR fuel designs can be classed into two categories: burnable poison rods that can be separated from an assembly and integral burnable absorbers (IBAs) that are a fixed part of the assembly. This report presents a parametric study that quantifies the changes in the SNF neutron multiplication factor due to the presence of IBAs during fuel irradiation and discusses the behavior that causes the changes. Based on this study and discussion, the report proposes recommendations for modifying ISG8R1 to allow loading of burnup credit casks with assemblies exposed to IBAs.



Farouk Eltawila, Director
Division of Systems Analysis and Regulatory Effectiveness

ACKNOWLEDGEMENTS

This work was supported by the Office of Nuclear Regulatory Research, U.S. Nuclear Regulatory Commission (NRC), under Project JCN W6479, Development and Applicability of Criticality Safety Software for Licensing Review. The authors acknowledge review and useful comments by Carl J. Withee of the Spent Fuel Project Office and Richard Y. Lee of the Office of Nuclear Regulatory Research.

The authors gratefully acknowledge Richard J. Cacciapouti (Duke Engineering and Services), Hae-Ryong Hwang (Korea Power Engineering Company, Inc.), and John R. Massari (Constellation Nuclear Services) for their invaluable contributions to this report by supplying fuel data and related information. The authors acknowledge Patrick O'Leary and Michelle Pitts (Framatome ANP) for their initial review and constructive comments on this report. The thorough review of the manuscript by our colleagues M. D. DeHart, I. C. Gauld, C. V. Parks, and R. M. Westfall is very much appreciated. Finally, the authors are thankful to Carolyn Moser for her editorial comments and to Willena C. Carter for her careful preparation of this report.

1 INTRODUCTION

The concept of taking credit for the reduction in reactivity due to fuel burnup is commonly referred to as *burnup credit*. The reduction in reactivity that occurs with fuel burnup is due to the change in concentration (net reduction) of fissile nuclides and the production of actinide and fission-product neutron absorbers. The change in the concentration of these nuclides with fuel burnup, and consequently the reduction in reactivity, is dependent upon the depletion environment (e.g., the neutron spectrum). As a result, the utilization of credit for fuel burnup necessitates consideration of variations in fuel designs and operating conditions.

Continuing advancements in fuel assembly design have enabled enhanced fuel utilization, thereby increasing the performance of reactor cores (i.e., extending core lifetimes). One characteristic of these advanced fuel assembly designs is the expanded use of burnable absorber (neutron poison) materials, either as an integral part of the fuel assembly or as a separate assembly used in conjunction with the fuel assembly. Burnable absorbers may be classified into two distinct categories: (1) burnable poison rods (BPRs) and (2) integral burnable absorbers (IBAs). BPRs are rods containing neutron-absorbing material that are inserted into the guide tubes of a pressurized water reactor (PWR) assembly during normal operation and are commonly used for reactivity control and enhanced fuel utilization. In contrast, IBAs are burnable poisons that are a nonremovable, or integral, part of the fuel assembly once it is manufactured. An example of an IBA is the Westinghouse Integral Fuel Burnable Absorber (IFBA) rod, which has a coating of zirconium diboride (ZrB_2) on the fuel pellets. Integral burnable absorbers are used extensively in many current PWR fuel assembly designs. Although BPRs have also been commonly used in PWRs, this report focuses on the effect of IBAs only. The effect of BPRs is addressed in Ref. 1.

The Interim Staff Guidance on burnup credit² issued by the Nuclear Regulatory Commission's Spent Fuel Project Office recommends that licensees restrict the use of burnup credit to assemblies that have not used burnable absorbers. This restriction eliminates a large portion of the currently discharged spent fuel assemblies from cask loading and thus severely limits the practical usefulness of burnup credit. Therefore, this report examines the effect of IBAs on reactivity for various designs and enrichment/poison loading combinations as a function of burnup. All IBA types that have been widely used in United States (U.S.) commercial PWRs are included in this evaluation, and to the extent possible, analyses are presented for a realistic range of initial fuel enrichment and poison loading combinations that are representative of actual assemblies. The effects are quantified, and trends with initial fuel enrichment and poison loading are noted. The report concludes with a discussion of the issues for consideration and preliminary recommendations for expanding the use of burnup credit to include spent fuel assemblies with IBAs.

2 INTEGRAL BURNABLE ABSORBER DESIGNS CONSIDERED

Several different types of IBAs have been used in commercial nuclear fuel assembly designs. However, all of the various designs are similar in that they contain thermal neutron absorbing material as an integral, nonremovable part of the fuel assembly. Variations in the IBA material, composition, placement within rods, and rod configurations exist among current PWR fuel assembly designs. These IBA characteristics may also be varied in combination with the initial fuel assembly enrichment and core location to achieve core operating and fuel management goals. For completeness, this report presents analyses for all IBA types that have been widely used in U.S. commercial PWRs. These include Westinghouse assembly designs with IFBAs, Combustion Engineering (CE) and Siemens assembly designs with $\text{UO}_2\text{-Gd}_2\text{O}_3$ rods, CE assembly designs with $\text{UO}_2\text{-Er}_2\text{O}_3$ rods, and CE assembly designs with $\text{Al}_2\text{O}_3\text{-B}_4\text{C}$ rods. To the extent possible, analyses were performed for a representative, realistic range of fuel initial enrichment and poison loading combinations. We cannot, however, confirm that all types that have ever been used in U.S. PWRs are included in this evaluation. For clarity, each of the unique IBA types considered in this report is described below.

The fuel assembly design data used for this analysis were collected from a variety of nonproprietary sources. For many of the IBA types, complete detailed specifications were not openly available in any single document. Therefore, the complete fuel design specifications required for this analysis were assembled from multiple sources and are documented in this report for reference.

2.1 INTEGRAL FUEL BURNABLE ABSORBER RODS

Some Westinghouse fuel assembly designs include IFBA rods, which contain enriched uranium dioxide (UO_2) fuel pellets with a thin coating of ZrB_2 on the outer surface. To our knowledge, IFBA rods are exclusive to Westinghouse and have been used in Westinghouse reactor cores since about 1987. Specifications of the assembly designs that utilize IFBA rods include boron loading in the ZrB_2 coating, the number of IFBA rods, and the placement or loading pattern of the IFBA rods within the fuel assembly. The number of IFBA rods within a fuel assembly may vary from zero to ~60% of the total number of fuel rods. For a Westinghouse 17×17 assembly, which contains 264 fuel rods, loading patterns with 0, 8, 16, 32, 48, 64, 80, 104, 128, and 156 IFBA rods are known to exist. In addition, the boron loading in the ZrB_2 coating and the initial ^{235}U enrichment are varied to meet core management goals.

2.2 $\text{UO}_2\text{-Gd}_2\text{O}_3$ INTEGRAL BURNABLE ABSORBER RODS

A number of nuclear fuel vendors — including CE, Framatome ANP (formerly Babcock & Wilcox [B&W]), and Siemens — have manufactured gadolinia-uranium ($\text{UO}_2\text{-Gd}_2\text{O}_3$) IBA rods. These $\text{UO}_2\text{-Gd}_2\text{O}_3$ rods, or gadolinia rods, are fuel rods with gadolinia (Gd_2O_3) as an integral part of the fuel matrix and are also used extensively in boiling water reactors (BWRs). The weight percent or loading of Gd_2O_3 in each gadolinia-bearing rod and the number of gadolinia rods within an assembly are both variable. Further, the ^{235}U enrichment among the gadolinia-bearing and nongadolinia-bearing fuel rods is varied to a small extent in some designs.

2.3 UO₂-Er₂O₃ INTEGRAL BURNABLE ABSORBER RODS

In addition to UO₂-Gd₂O₃ rods, CE has manufactured an IBA containing erbia (Er₂O₃). Similar to the UO₂-Gd₂O₃ rods, the erbia rods include the burnable absorber Er₂O₃ as an integral part of the fuel matrix. The weight percent or loading of the erbia and the number of erbia rods within an assembly are both variable, as is the ²³⁵U enrichment.

2.4 Al₂O₃-B₄C INTEGRAL BURNABLE ABSORBER RODS

Another IBA manufactured by CE consists of solid rods containing alumina pellets with uniformly dispersed boron carbide particles (Al₂O₃-B₄C) clad in zircaloy. Unlike the IFBA, UO₂-Gd₂O₃, and UO₂-Er₂O₃ rods, these rods do not contain fuel. The weight percent of B₄C and the number of rods per assembly are variable. These rods are similar to BPRs but are classified herein as IBAs because they are an integral, nonremoval part of the fuel assembly.

3 REACTIVITY EFFECT OF INTEGRAL BURNABLE ABSORBER RODS

3.1 INTRODUCTION

For PWR fuels without IBAs, reactivity decreases with burnup in a nearly linear fashion. In contrast, for PWR fuel assembly designs that make significant use of IBAs, reactivity actually increases as fuel burnup proceeds, reaching a maximum at a burnup where the IBA is nearly depleted, and then decreasing with burnup in an almost linear fashion. For fuel assembly designs that make modest use of IBAs, reactivity decreases with burnup slowly, up to the point at which the IBA is nearly depleted, and then decreases with burnup in a nearly linear manner. The assemblies are typically designed such that the burnable absorber is effectively depleted in the first third of the assembly life, and as a result, the assembly reactivity typically peaks within this period of burnup. The reactivity behavior of a PWR fuel assembly with and without IBAs (neutron poisons) present as a function of burnup is illustrated in Figure 1.

The presence of IBAs during depletion hardens the neutron spectrum, resulting in lower ^{235}U depletion and higher production of fissile plutonium isotopes. Enhanced plutonium production and the concurrent diminished fission of ^{235}U due to increased plutonium fission can increase the reactivity of the fuel at discharge and beyond, depending on the IBA assembly design characteristics. However, as mentioned, the assemblies are typically designed such that the burnable absorber is effectively depleted in the first third of the assembly life, and thus is exposed to a hardened spectrum during the first third of its exposure only. Unlike BPRs, which are inserted into assembly guide tubes, IBAs do not displace the moderator in the assembly lattice, and thus generally have a less significant impact on the neutron spectrum.

Although a great deal of work has been performed on IBA design and development for greater fuel utilization and core performance, few studies have been undertaken to assess the significance of IBAs on the reactivity of discharged fuel. Recent work has provided examples of the typical magnitudes of the reactivity effects of IBAs, including IFBA, $\text{UO}_2\text{-Gd}_2\text{O}_3$, and $\text{UO}_2\text{-Er}_2\text{O}_3$ rods.³ Although the analyses were limited to a single case for each type of IBA, indications from this study are that the neutron-multiplication factor for an assembly without IBAs is always greater (as a function of burnup) than the neutron-multiplication factor for an assembly that use $\text{UO}_2\text{-Gd}_2\text{O}_3$ or $\text{UO}_2\text{-Er}_2\text{O}_3$ rods. Conversely, the neutron-multiplication factor for an assembly without IFBA rods was found to be slightly less ($\sim 0.2\% \Delta k$ at target discharge burnup) than the neutron-multiplication factor for an assembly with IFBA rods. The study concludes that neglecting the IBAs yields conservative results for gadolinia- and erbia-bearing fuel and nonconservative results for IFBA fuel, and that the reactivity effect from IBAs is generally small and well behaved.

The following sections describe the calculational methods used for this evaluation and present detailed analyses to demonstrate the reactivity effect of IBAs as a function of burnup. The analyses include variations in the IBA type, concentration, and initial fuel enrichment.

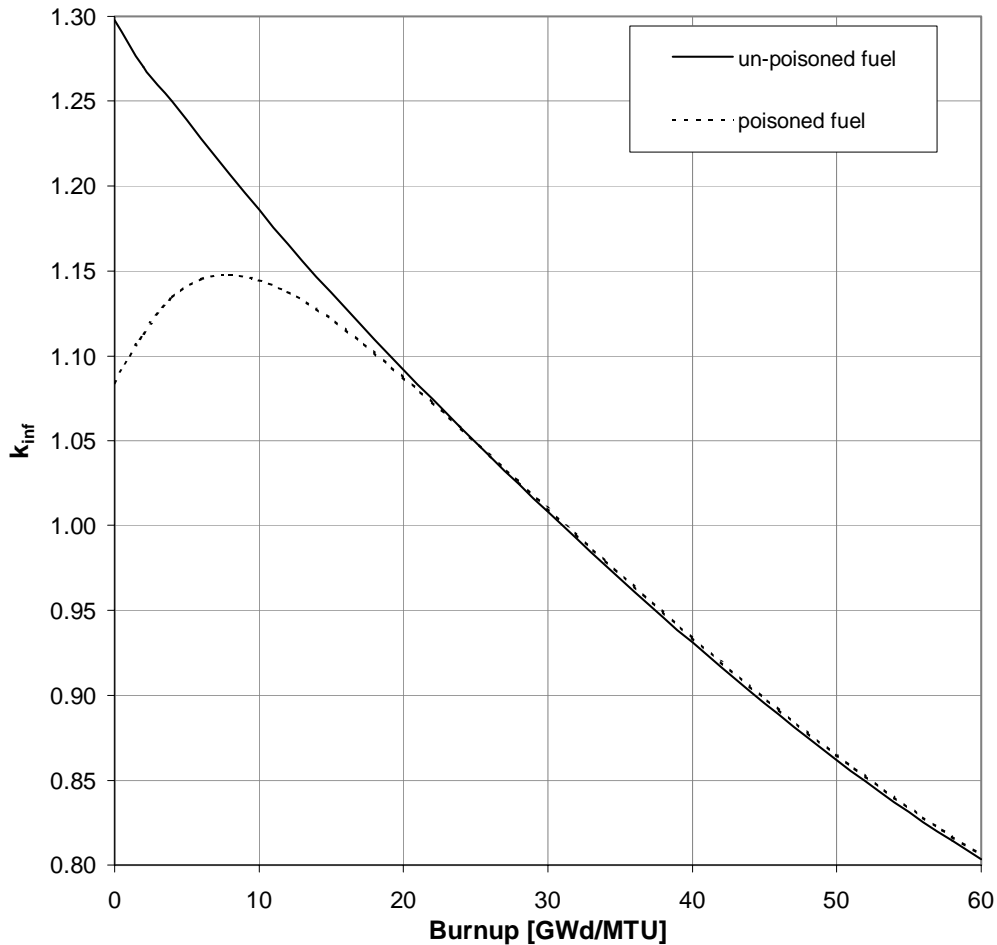


Figure 1 Typical reactivity behavior of PWR fuel with and without IBAs (neutron poisons)

3.2 CODE DESCRIPTION

The calculations presented in the following sections were performed using the HELIOS-1.6 code package,⁴ which primarily consists of three programs: AURORA, HELIOS, and ZENITH. HELIOS is a two-dimensional (2-D), generalized-geometry transport theory code based on the method of collision probabilities with current coupling. AURORA, the input processor, is used to define the geometry, materials, and calculational parameters. ZENITH, the output processor, reads the results saved by HELIOS (in a binary database) and outputs the results in text format. The HELIOS code system also contains the ORION program for viewing and checking model geometries and materials.

HELIOS was employed for this analysis because of its capability to explicitly model the relatively complicated, heterogeneous assembly lattices associated with IBAs. The various structures within each of the assembly models were coupled using angular current discretization (interface currents). Unless stated otherwise, all calculations are for an infinite radial array of fuel assemblies and utilize the 45-group neutron cross-section library (based on ENDF/B-VI data) that is distributed with the HELIOS-1.6 code package.

3.3 CALCULATIONS

All depletion calculations were performed with HELIOS using the properties and parameters given in Table 1. Using the isotopic compositions from the depletion calculations, branch or restart calculations were performed with HELIOS to determine the neutron-multiplication factor as a function of burnup for out-of-reactor conditions (i.e., 20°C with no soluble boron present), zero cooling time, and a full nuclide set. All nuclides that are included in the HELIOS 45-group cross-section library were included in the calculations. For each unique IBA assembly design considered, a calculation was performed for (1) the actual assembly specification (including the presence of the IBA) and (2) the condition in which the IBA is not included (in the calculation, IBA rods are replaced by “normal” fuel rods with the same enrichment). Throughout the following sections, the Δk values between these two conditions are reported to assess the effect of IBAs on the reactivity of spent nuclear fuel (SNF).

Table 1 Summary of parameters used for the depletion calculations

Parameter	Value used in analyses
Moderator temperature (K)	600
Fuel temperature (K)	1000
Fuel density (g/cm ³)	10.44 (UO ₂)
Clad temperature (K)	600
Clad density (g/cm ³)	5.78 (Zr)
Power density (MW/MTU)	60*
Moderator boron concentration (ppm)	650

* Various cases were also calculated using a power density of 30 MW/MTU (which is a more realistic value). The results showed that the Δk values presented in the following sections are not sensitive to variations in the power density.

The majority of the calculations were done with an infinite radial array of assemblies to gain an understanding of behaviors and trends and so that the results would be general (i.e., not dependent on storage cell specifications, such as poison loading). A number of the criticality calculations were repeated in Section 3.3.5 to assess the effect for poisoned storage cells, variations in cooling time, and inclusion of an axial burnup distribution. The results of these studies indicate that the calculated effects are not sensitive to cooling time and confirm the trends demonstrated with infinite assembly arrays.

3.3.1 Integral Fuel Burnable Absorber Rods

The IFBA, developed by Westinghouse, consists of a thin coating of ZrB₂ on the outer surface of the fuel pellets. Various IFBA loading combinations (¹⁰B concentration and number of IFBA rods) and enrichment combinations were studied in order to establish the reactivity effect as a function of burnup. The absorber loading and enrichment combinations considered are based on actual fuel assemblies and were selected to encompass the range of known variations including the number of IFBA rods, ¹⁰B concentration, and initial fuel enrichment. All of the IFBA rod analyses were performed with a Westinghouse 17 × 17 assembly. Dimensional specifications for the fuel assembly are given in Table 2.

Table 2 Westinghouse 17 × 17 fuel assembly specifications

Parameter	Dimension (cm)
Rod pitch	1.260
Assembly pitch	21.5
Cladding outside diameter	0.8898
Cladding inside diameter	0.8001
Pellet outside diameter	0.7840
Guide/instrument tube outside diameter	1.204
Guide/instrument tube inside diameter	1.124
Array size	17 × 17
Number of fuel rods	264
Number of guide/instrument tubes	25

Analyses are presented in this section for IFBA assembly designs with 80, 104, and 156 IFBA rods; two different boron loadings (1.57 and 2.355 mg ¹⁰B/in.); and corresponding variations in initial fuel enrichment. With the exception of the loading patterns, the specifications for the actual IFBA assembly characteristics (i.e., number of IFBA rods, ¹⁰B loading, and initial enrichment) were obtained from Ref. 5. The IFBA loading patterns used in these analyses are from Ref. 6. Figure 2 displays the geometry of one of the IFBA assemblies (containing 156 IFBA rods) as modeled in HELIOS.

The presentation of the IFBA analyses is divided into two subsections, based on the boron loading. The two subsections compare results for linear poison material (boron) loadings of 1.57 and 2.355 mg ¹⁰B/in. of pellet, respectively.

3.3.1.1 Integral Fuel Burnable Absorber Analyses for 1.57 mg ¹⁰B/inch

The first IFBA assembly design considered is a 17 × 17 assembly with 80 IFBA rods, as shown in Figure 3. Calculations were performed for (1) the actual assembly specification (as shown in Figure 3) and (2) the condition in which the IFBA rods were replaced by non-IFBA fuel rods with the same enrichment as the other fuel rods. The k_{inf} values as a function of burnup from the two calculations are compared in Figure 4. The Δk values between these two conditions are determined to assess the effect of the IFBAs on reactivity.

Separate calculations were performed with enrichments of 3.4 and 4.4 wt % ²³⁵U to cover the range of initial enrichments for this particular IFBA loading found in the available fuel data,⁵ which consisted of actual fuel assembly data from the Seabrook plant. The results (Δk as a function of burnup) are shown in Figure 5, where it can be seen that both cases achieve a positive Δk (i.e., the k_{inf} value with IFBA rods present becomes greater than the k_{inf} value without IFBA rods present). The Δk for the case with 3.4 wt % ²³⁵U enrichment becomes positive at a burnup of around 20 GWd/MTU, reaching a maximum of approximately 0.18% Δk at around 34 GWd/MTU. The Δk for the case with 4.4 wt % ²³⁵U enrichment becomes positive at a burnup of around 25 GWd/MTU, with a maximum of 0.15% Δk near 50 GWd/MTU. Consistent with previously published work,³ these results indicate that the IFBA-bearing fuel k_{inf} is not always less than the non-IFBA fuel k_{inf} .

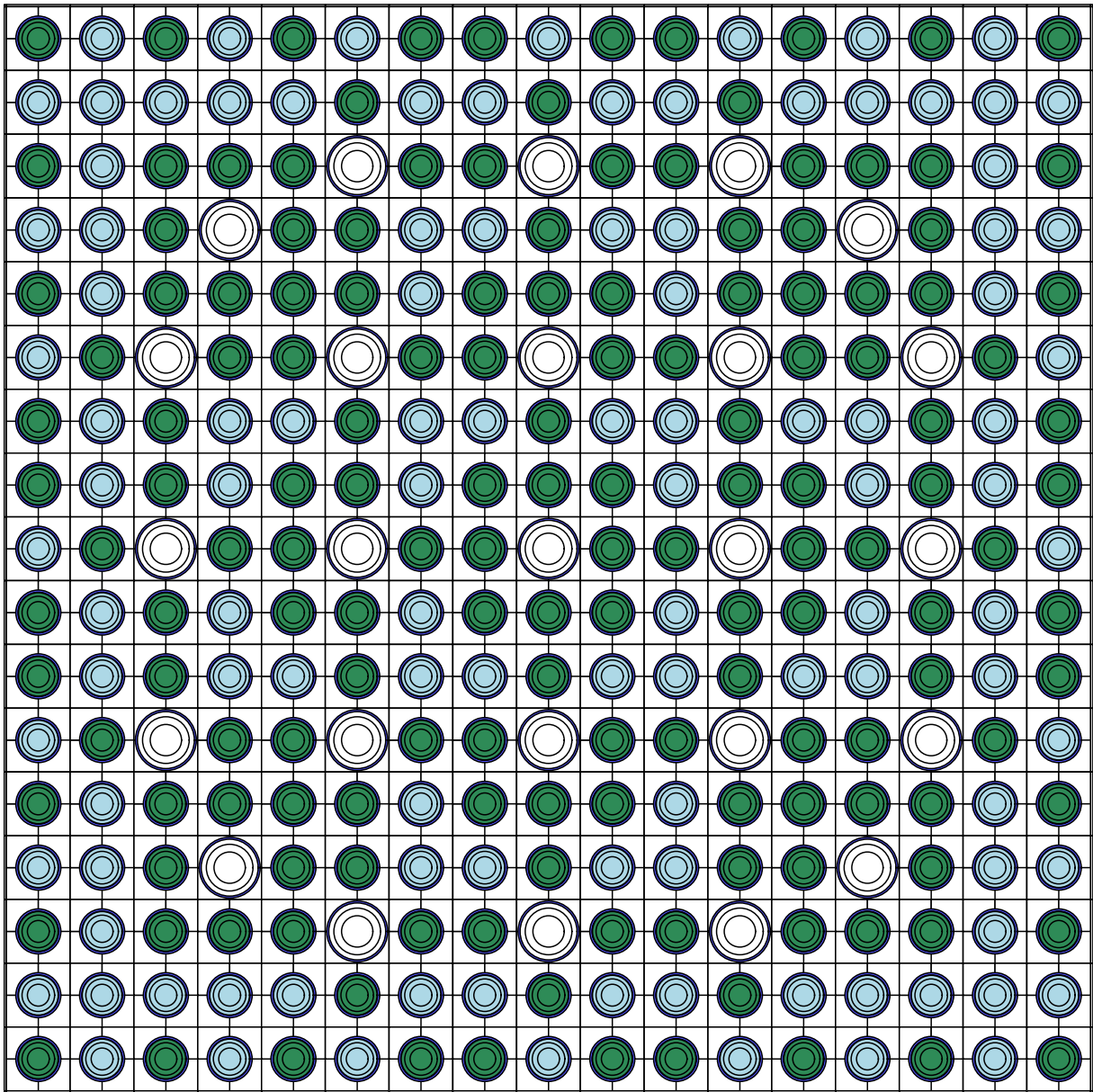


Figure 2 HELIOS computational model of an IFBA case containing 156 IFBA rods

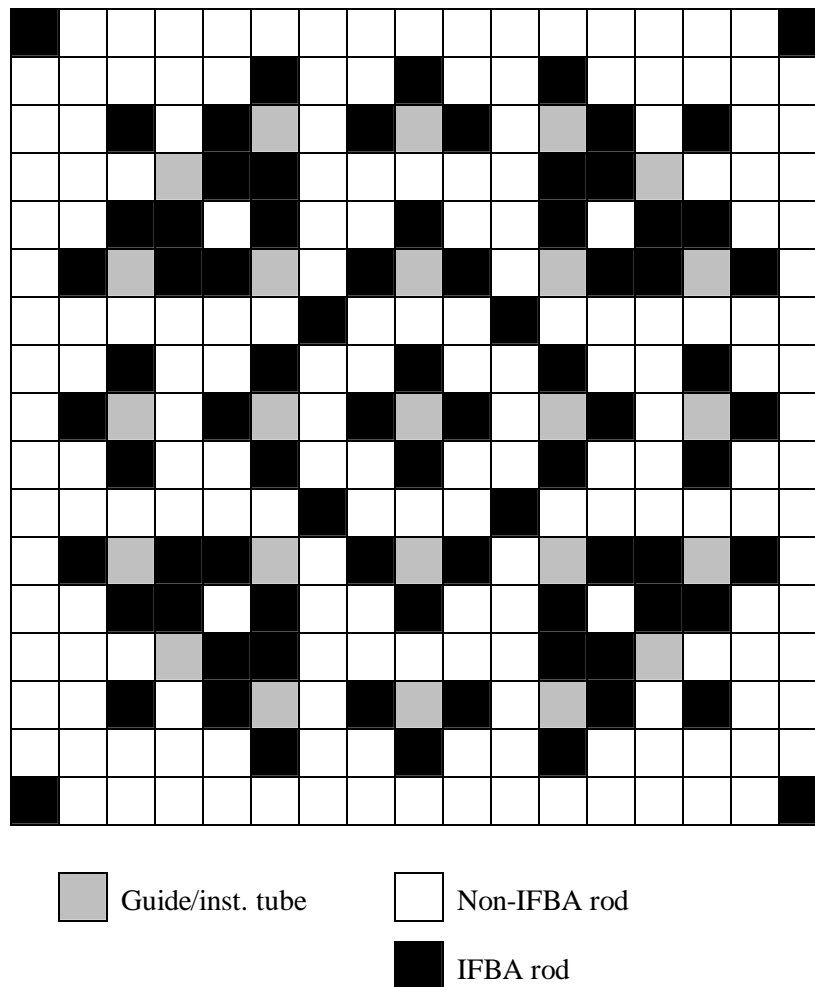


Figure 3 Fuel rod array (17 × 17) representing the loading pattern for 80 IFBA rods

The second IFBA design considered contains 104 IFBA rods, as shown in Figure 6. As with all designs considered in this subsection, the poison loading is 1.57 mg ¹⁰B/in. of pellet. Once again, the initial enrichment was varied to span the range within the actual fuel data. The results (Δk as a function of burnup) are shown in Figure 7, where it can be seen that both cases achieve positive Δk values. The Δk values for the case with 3.4 wt % ²³⁵U enrichment become positive at a burnup of about 21 GWd/MTU, reach a maximum of 0.24% Δk at around 35 GWd/MTU, and then decrease. The Δk values for the case with 4.0 wt % ²³⁵U enrichment become positive at a burnup of about 24 GWd/MTU, with a maximum of 0.23% Δk at 44 GWd/MTU. Note that the Δk values reach a maximum and are decreasing with increased burnup beyond that point. These results are consistent with the results shown for 80 IFBA rods, further confirming that the reactivity of an IFBA-bearing fuel assembly is not always less than that of a non-IFBA fuel assembly.

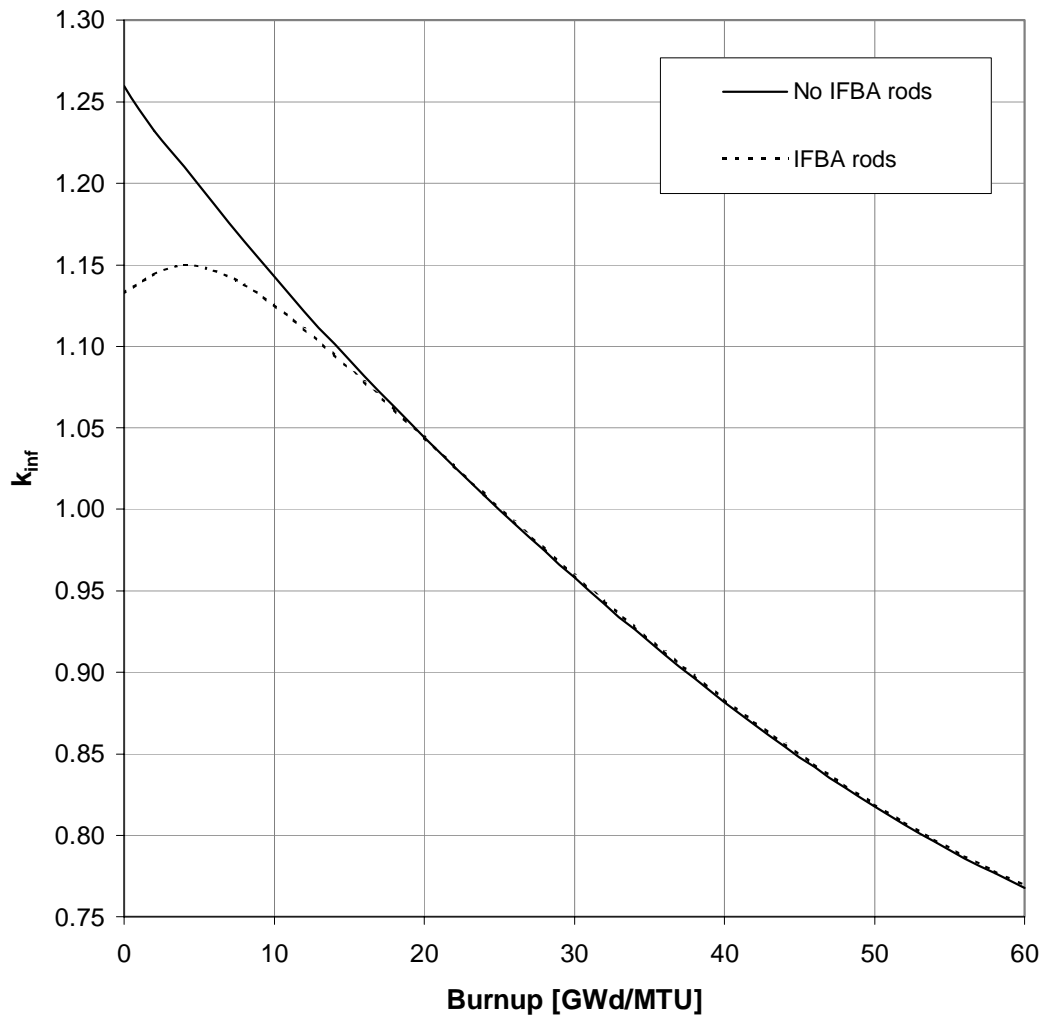


Figure 4 Comparison of k_{inf} values with IFBA rods (80 IFBA rods, 3.4 wt % ^{235}U enriched fuel) and without IFBA rods (3.4 wt % ^{235}U enriched fuel)

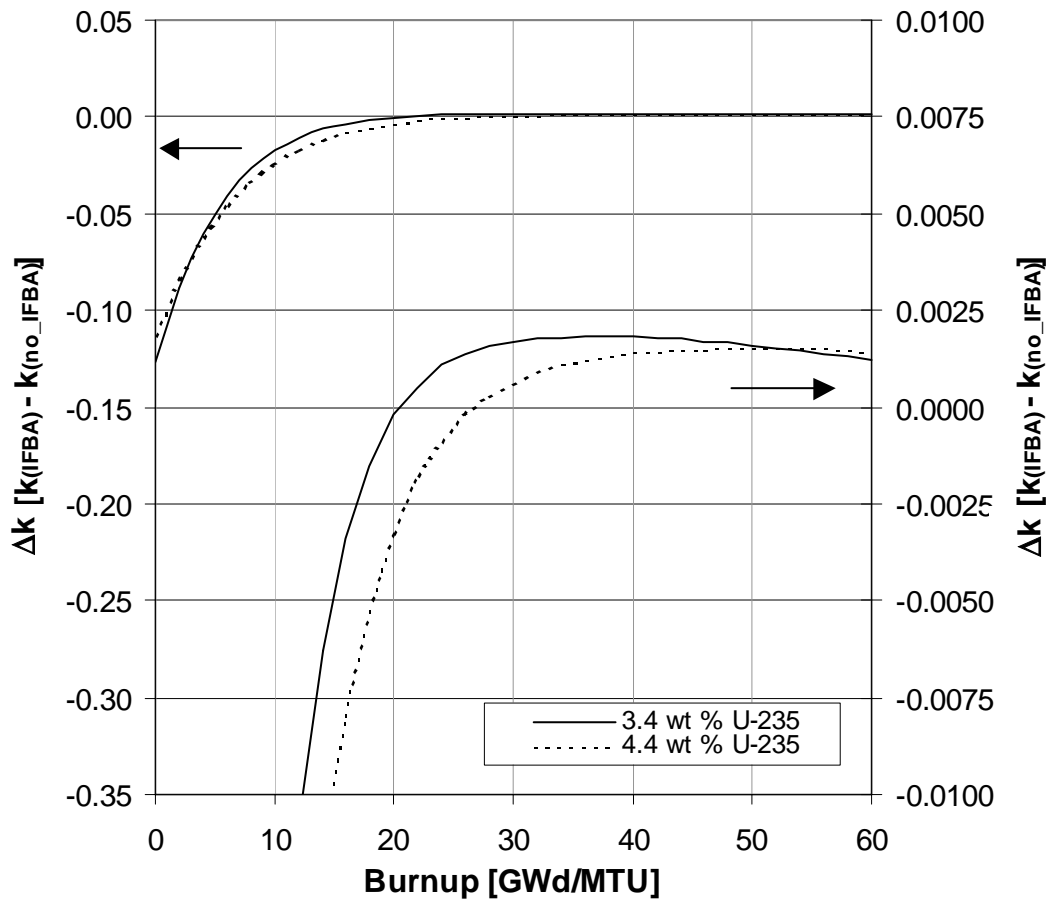


Figure 5 Comparison of Δk values as a function of burnup between assemblies with and without IFBA rods (80 IFBA rods) for initial enrichments of 3.4 and 4.4 wt % ^{235}U . The results are also plotted on the enlarged scale on the right-hand-side y-axis for clarity.

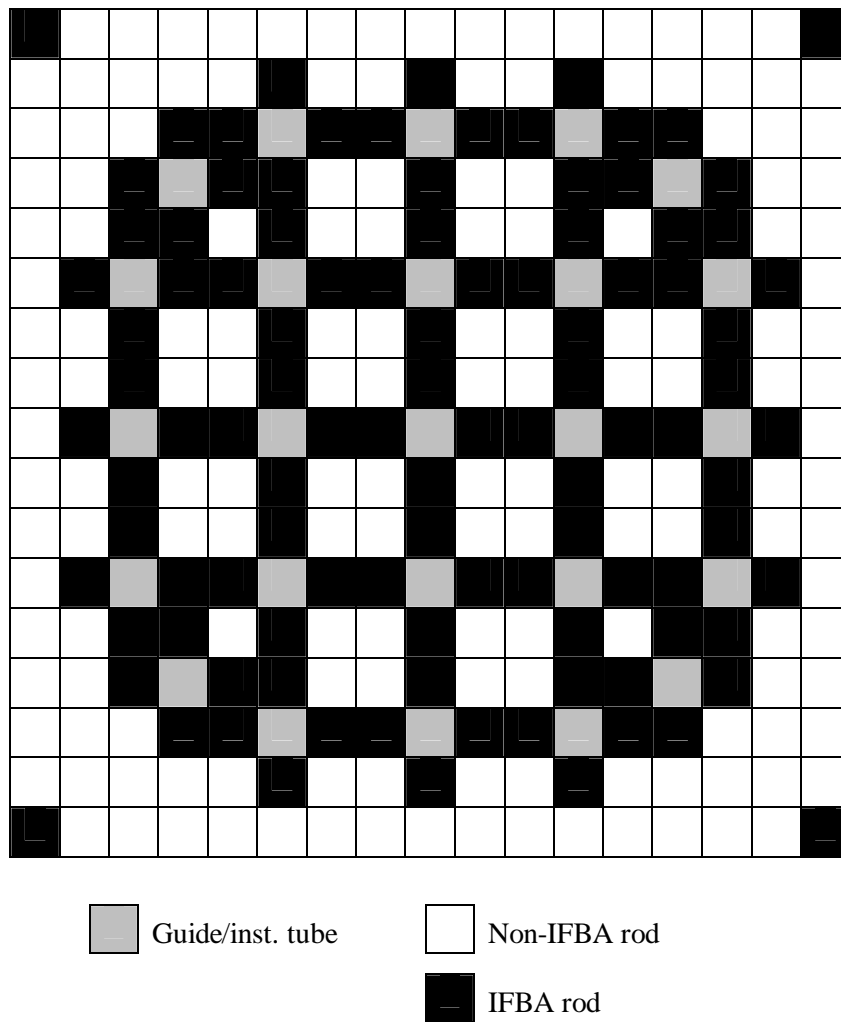


Figure 6 Fuel rod array (17 × 17) representing the loading pattern for 104 IFBA rods

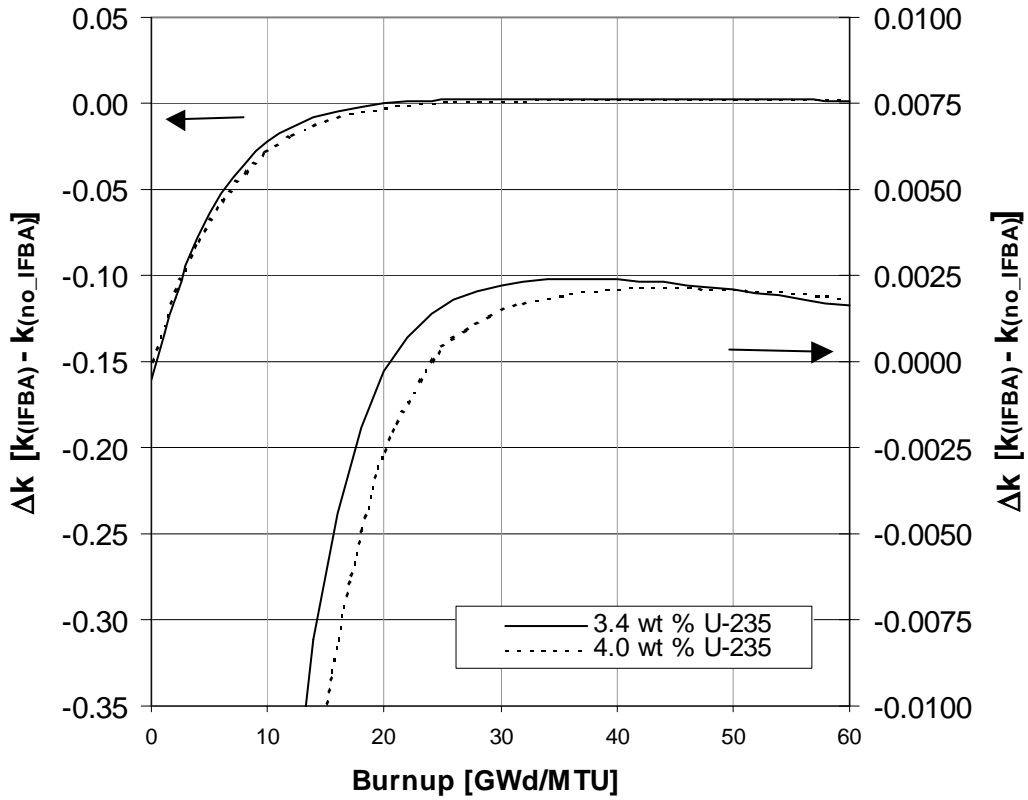


Figure 7 Comparison of Δk values as a function of burnup between assemblies with and without IFBA rods (104 IFBA rods) for initial enrichments of 3.4 and 4.0 wt % ^{235}U . The results are also plotted according to the enlarged scale on the right-hand-side y-axis for clarity.

The third and final IFBA design considered for this particular ^{10}B loading contains 156 IFBA rods, as shown in Figure 8. Based on actual fuel data, the ^{235}U enrichment was varied between 4.0 and 4.4 wt %. The results (Δk as a function of burnup) are shown in Figure 9. The Δk for the case with 4.0 wt % ^{235}U enrichment becomes positive at a burnup of around 25 GWd/MTU, reaching a maximum of 0.31% Δk at around 40 GWd/MTU. The Δk for the case with 4.4 wt % ^{235}U enrichment becomes positive at a burnup of around 27 GWd/MTU, with a maximum of 0.29 % Δk near 50 GWd/MTU. Comparison of Figures 7 and 9 indicates that the maximum positive Δk value increases with the number of IFBA rods.

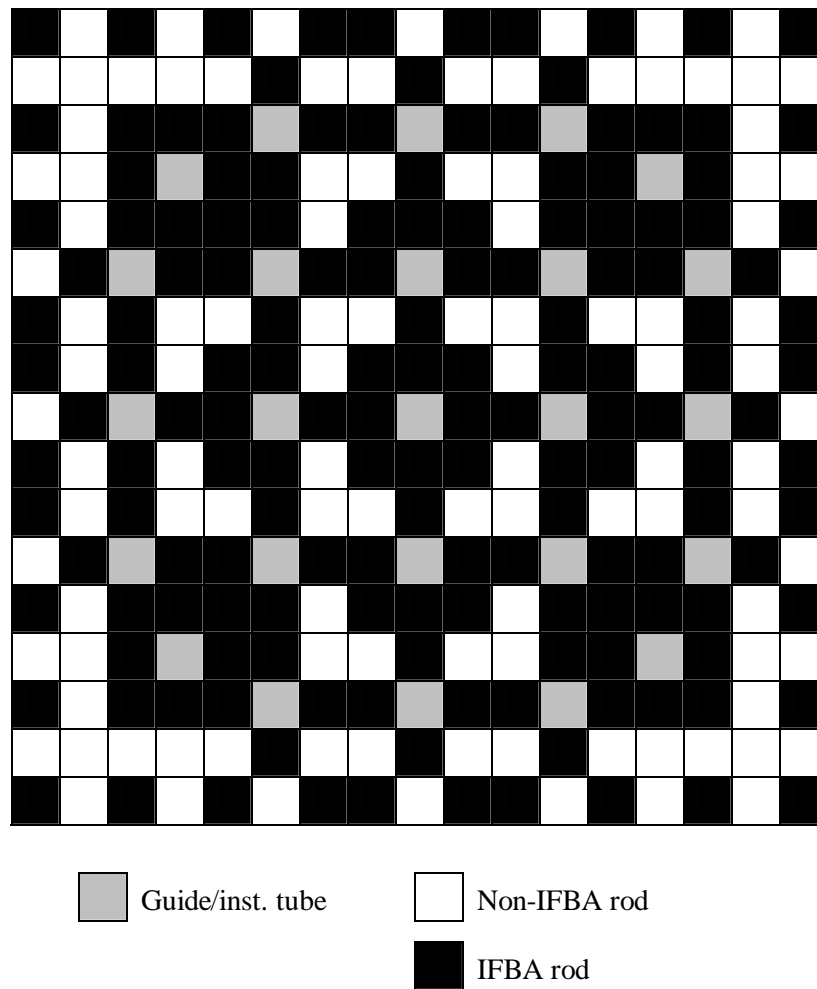


Figure 8 Fuel rod array (17×17) representing the loading pattern for 156 IFBA rods

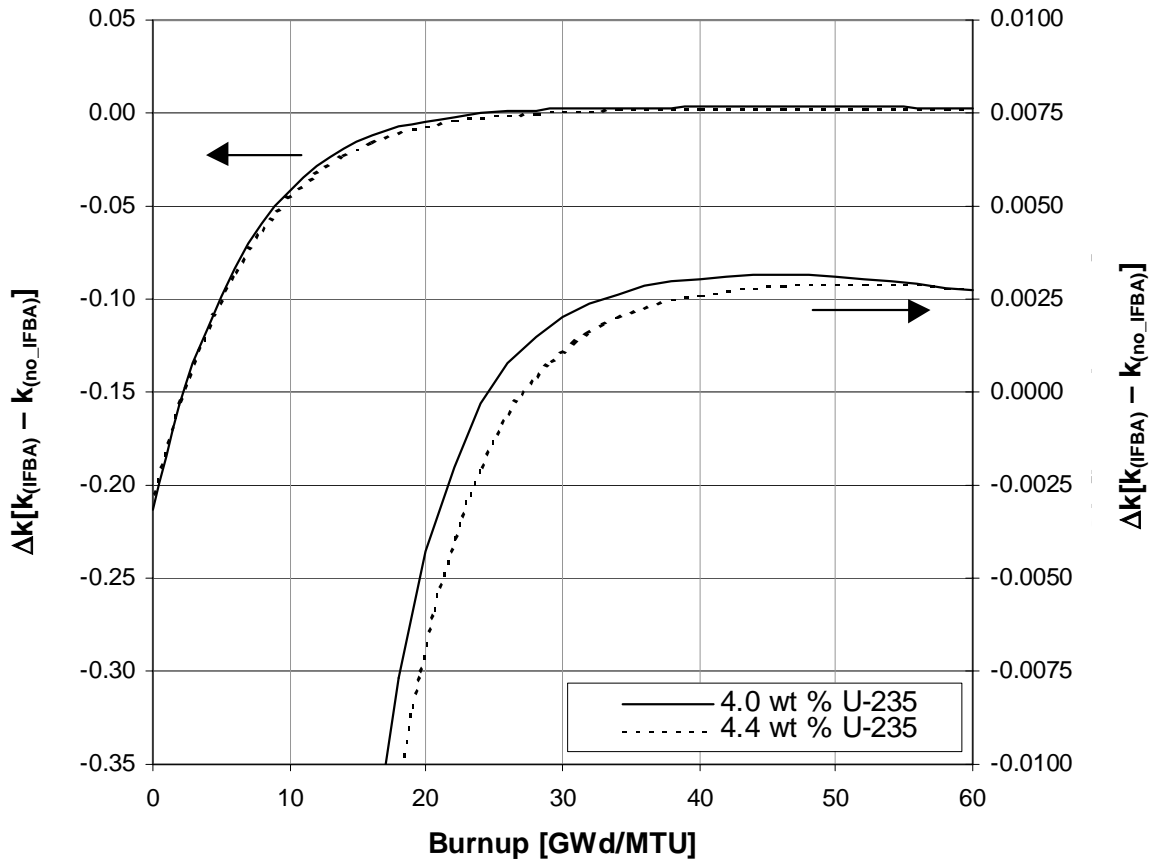


Figure 9 Comparison of Δk values as a function of burnup between assemblies with and without IFBA rods (156 IFBA rods) for initial enrichments of 4.0 and 4.4 wt % ^{235}U . The results are also plotted on the enlarged scale on the right-hand-side y-axis for clarity.

3.3.1.2 Integral Fuel Burnable Absorber Analyses for 2.355 mg ¹⁰B/inch

The three IFBA loading patterns considered in the previous subsection (80, 104 and 156 IFBA rods) were also studied with a poison loading of 2.355 mg ¹⁰B/in., for corresponding enrichments based on actual fuel data. The Δk values for the three IFBA rod configurations are shown in Figure 10. These results confirm that for a given fuel enrichment, the positive reactivity effect increases with poison loading (i.e., number of IFBA rods).

An assembly design containing 104 IFBA rods was also evaluated with an enrichment of 4.25 wt % ²³⁵U. The Δk values are shown in Figure 11, along with the reactivity differences from the previous calculation with 104 IFBA rods and 4.617 wt % ²³⁵U enrichment. The results indicate that the maximum positive Δk value increases slightly with decreasing initial fuel enrichment.

These results are consistent with the results shown in the previous subsection, demonstrating that the k_{inf} values for fuel containing IFBA rods are not always less than the k_{inf} values for fuel without IFBA rods. For burnups greater than ~20 GWd/MTU, the IFBA rods are shown to have a small positive reactivity effect as compared to assemblies without IFBA rods. This transition point moves up with increasing fuel enrichment and increasing number of IFBA rods. For all of the IFBA cases considered, the maximum positive reactivity effect was determined to be 0.41%. However, it should be pointed out that this maximum value corresponds to the most heavily poisoned assembly design (156 IFBA rods with 2.355 mg ¹⁰B/in.) and, judging from the available data, is not representative of typical IFBA assemblies.

For fixed initial fuel enrichment, the positive reactivity effect has been shown to increase with increasing poison loading (i.e., both increasing ¹⁰B loading and increasing number of IFBA rods). Finally, the results in this and the previous subsection make clear that for a fixed poison loading the positive reactivity effect increases slightly with decreasing fuel enrichment.

3.3.2 UO₂-Gd₂O₃ Integral Burnable Absorber Rods

A number of nuclear fuel vendors — including CE, Framatome ANP (formerly B&W), and Siemens — have manufactured gadolinia-uranium (UO₂-Gd₂O₃) IBA rods. These UO₂-Gd₂O₃ rods, or gadolinia rods, are fuel rods with Gd₂O₃ as an integral part of the fuel matrix. The weight percent or loading of Gd₂O₃ in each gadolinia-bearing rod and the number of gadolinia rods within an assembly are both variable. Further, the ²³⁵U enrichment among the gadolinia-bearing and nongadolinia-bearing fuel rods is varied to a small extent in some designs, with the gadolinia-bearing fuel rods typically having lower ²³⁵U enrichment than the nongadolinia-bearing fuel rods. (Because of the lower heat conductivity of the UO₂-Gd₂O₃ fuel as compared to UO₂ fuel the ²³⁵U enrichment in the UO₂-Gd₂O₃ fuel rod is often reduced to meet the design criterion for maximum fuel temperature.⁷) A known inherent penalty associated with gadolinia rods is that gadolinia displaces uranium in the fuel matrix, resulting in a reduced heavy-metal mass.

Various gadolinia loadings (wt % Gd₂O₃ and number of gadolinia-bearing rods) and enrichment combinations were studied in order to establish the reactivity effect as a function of burnup. The absorber loading and enrichment combinations considered are based on actual fuel assemblies and were selected to encompass the range of known variations.

Analyses are presented in the following subsections for two distinct fuel assembly designs that employ gadolinia-bearing rods: the CE 16 × 16 assembly design (which includes large water holes) and the Siemens 17 × 17 design. The Siemens assembly design does not include oversized water holes, and thus is expected

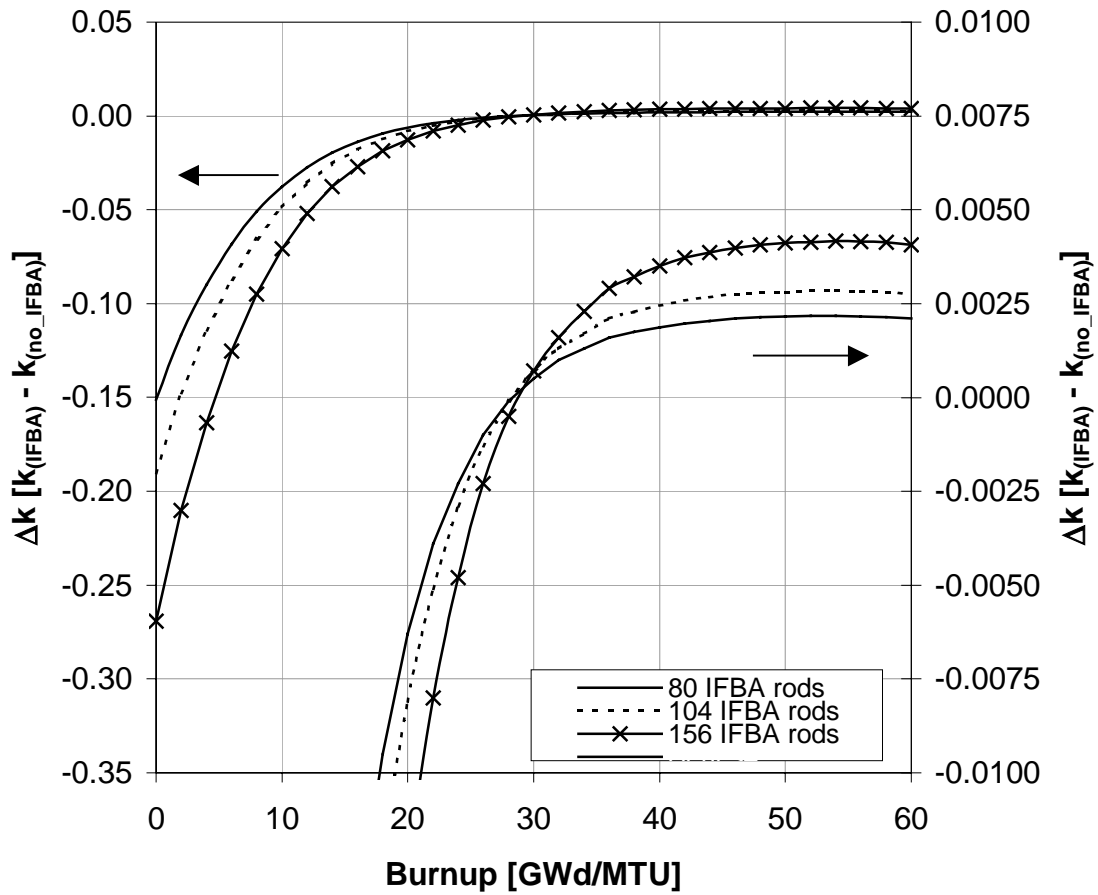


Figure 10 Comparison of Δk values as a function of burnup between assemblies with and without IFBA rods, with varied number of IFBA rods and an enrichment of 4.617 wt % ^{235}U . The results are also plotted on the enlarged scale on the right-hand-side y-axis for clarity.

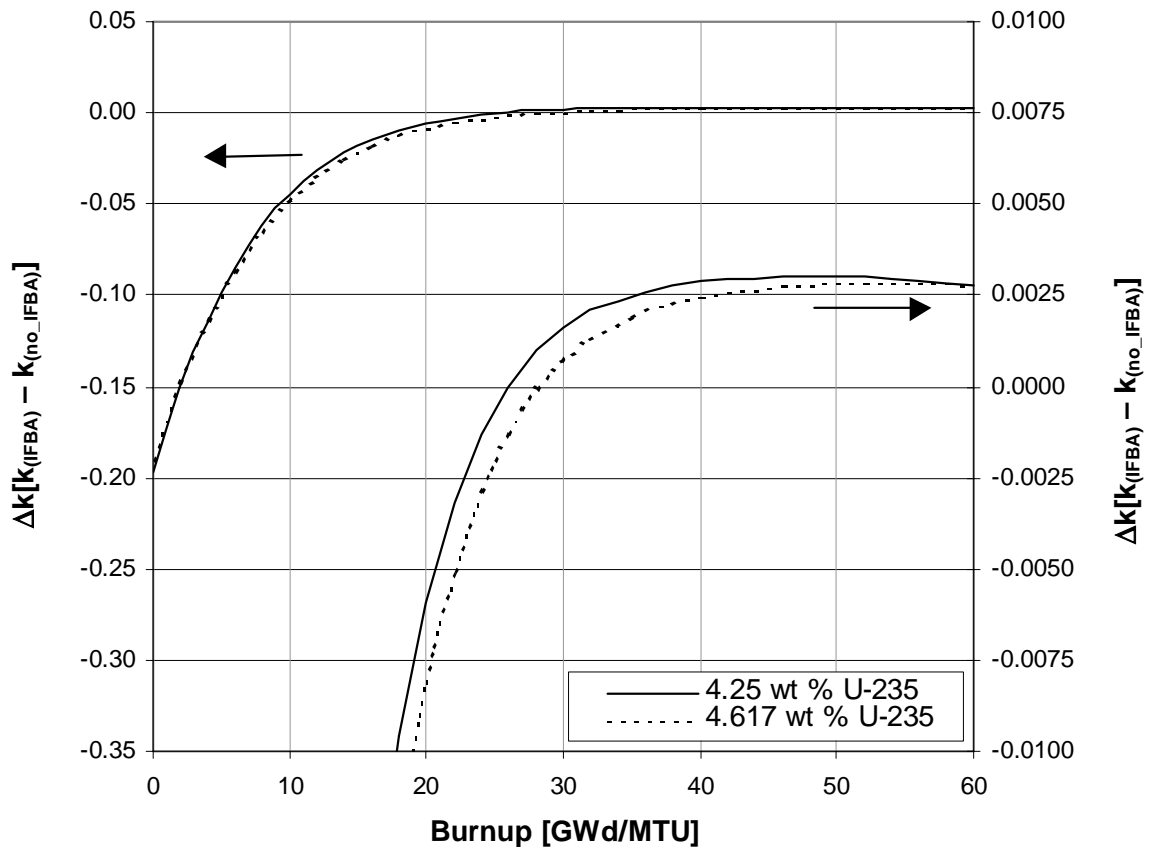


Figure 11 Comparison of Δk values as a function of burnup between assemblies with and without IFBA rods (104 IFBA rods) for initial enrichments of 4.25 and 4.617 wt % ^{235}U . The results are also plotted on the enlarged scale on the right-hand-side y-axis for clarity.

to be representative of other similar fuel assembly designs (e.g., Framatome ANP and Westinghouse designs that employ gadolinia-bearing rods).

3.3.2.1 Combustion Engineering Designs

The specifications for the CE gadolinia-bearing fuel assembly designs were obtained from Ref. 8. The fuel dimension specifications for these CE 16×16 assemblies are listed in Table 3. To facilitate the discussion, the assembly designs are classified into two sets, based on their initial pin enrichments. The assembly designs within the two designated sets, the D sets (D, D1 and D2) and the E sets (E, E1 and E2), have variable numbers of gadolinia-bearing rods, as defined in Table 4. The corresponding fuel loading diagrams are illustrated in Figures 12 through 14. Figure 15 displays the D1 geometry as modeled in HELIOS.

Table 3 CE 16×16 fuel assembly specifications

Parameter	Dimension (cm)
Rod pitch	1.285
Assembly pitch	20.78
Cladding outside diameter	0.97028
Cladding inside diameter	0.84328
Pellet outside diameter	0.82550
Water hole outside diameter	2.4892
Water hole inside diameter	2.286
Array size	16×16
Number of fuel rods	236
Number of water holes	5

Table 4 Fuel assembly data for the D and E sets of assembly designs

Fuel assembly	UO ₂ fuel rod enrichment	No. of UO ₂ fuel rods/assembly	No. of UO ₂ -Gd ₂ O ₃ rods/assembly	Gd ₂ O ₃ / ²³⁵ U wt % for UO ₂ -Gd ₂ O ₃ rods
D	4.42/3.92	184/52	0	N/A
D1	4.42/3.92	176/52	8	6.0/4.42*
D2	4.42/3.92	172/52	12	6.0/4.42
E	4.60/4.10	184/52	0	N/A
E1	4.60/4.10	176/52	8	8.0/4.60
E2	4.60/4.10	172/52	12	8.0/4.60

*Read as 6.0 wt % Gd₂O₃ and 4.42 wt % ²³⁵U enrichment in UO₂-Gd₂O₃ rods.

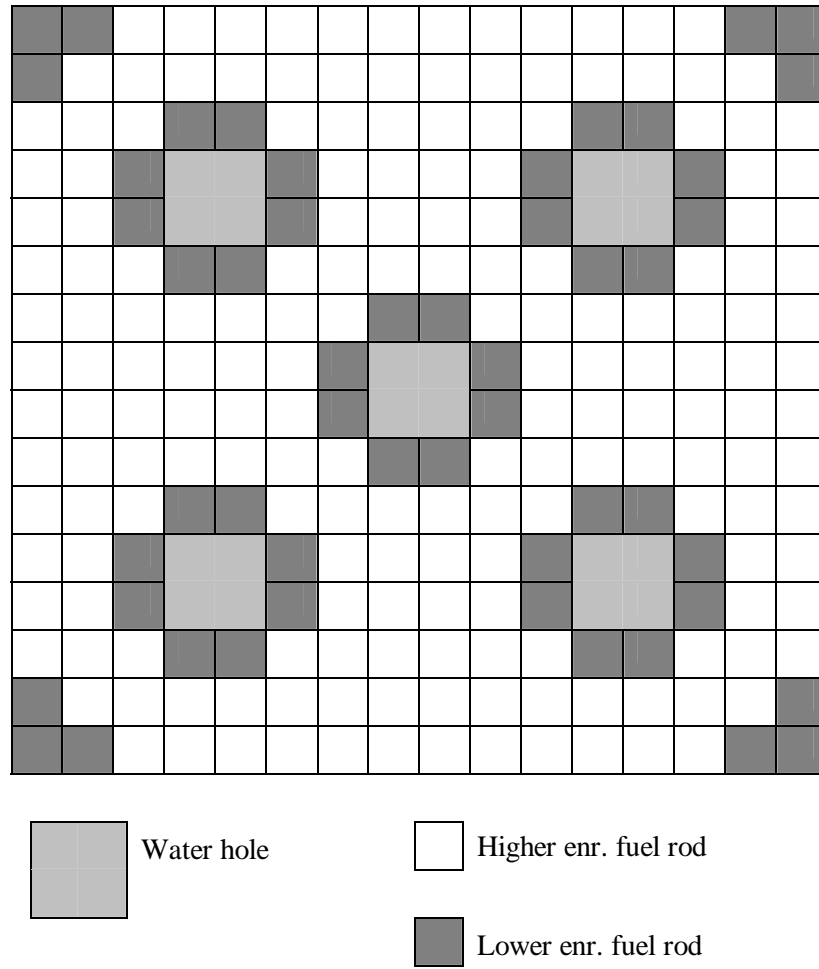


Figure 12 Fuel rod array (16 × 16) representing the loading pattern of the D and E fuel assemblies

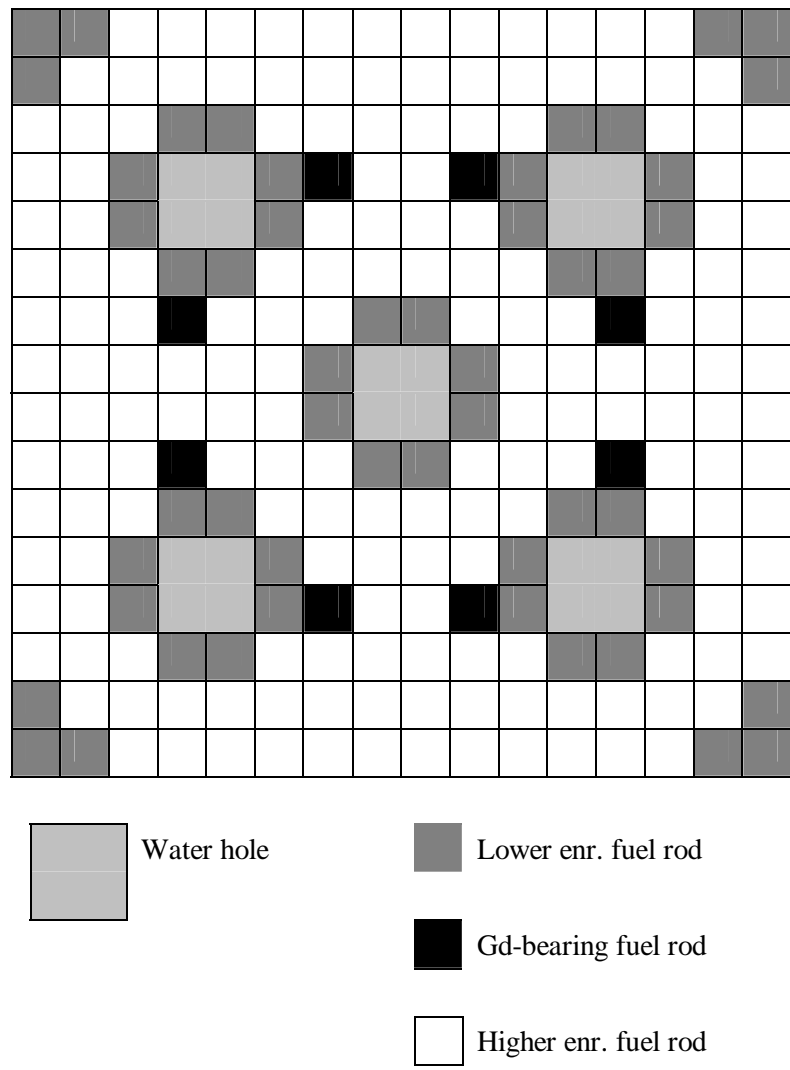


Figure 13 Fuel rod array (16 × 16) representing the loading pattern of the D1 and E1 fuel assemblies

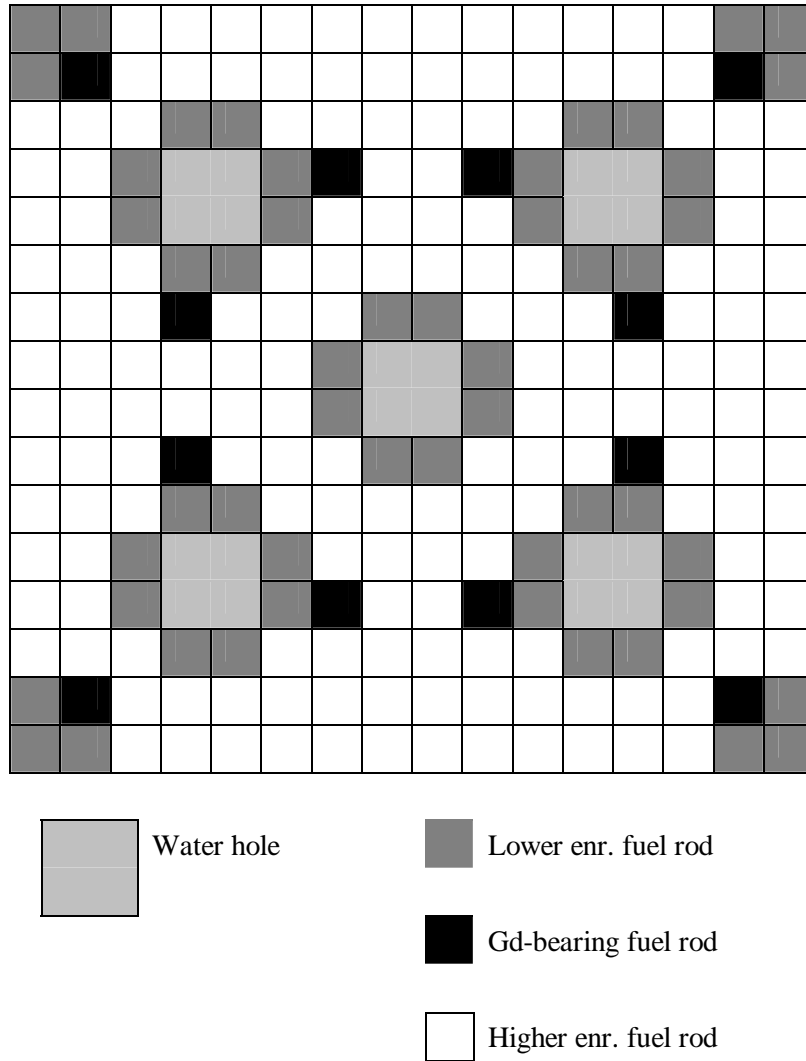


Figure 14 Fuel rod array (16 × 16) representing the loading pattern of the D2 and E2 fuel assemblies

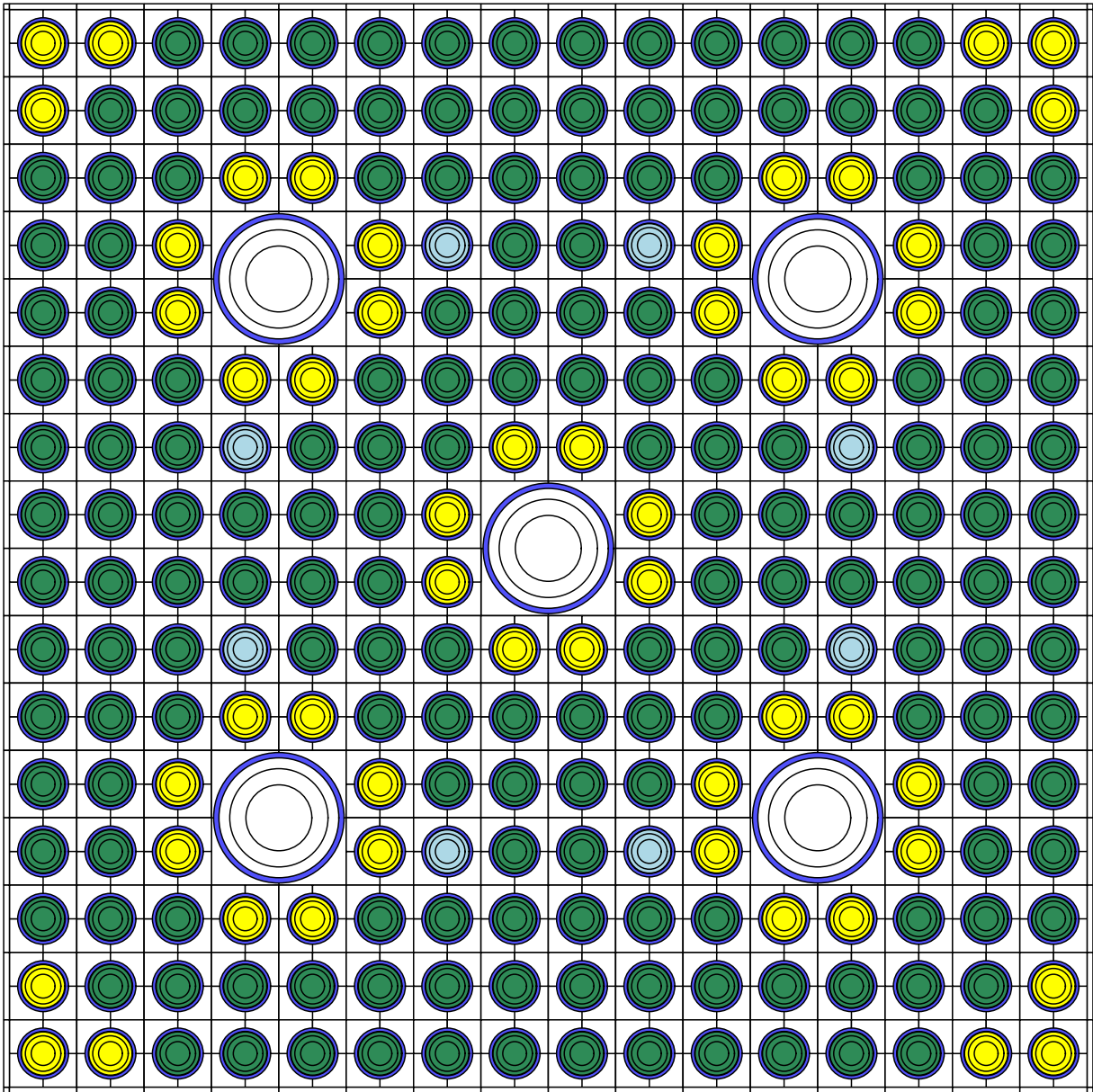


Figure 15 HELIOS calculational model of the D1 fuel assembly containing eight $\text{UO}_2\text{-Gd}_2\text{O}_3$ rods

The D and E fuel designs were used to study the effect of various numbers of gadolinia-bearing rods. The D, D1, and D2 fuel assemblies were modeled according to Tables 3 and 4. The resulting Δk values between the gadolinia-bearing (D1 and D2) and nongadolinia-bearing fuel (D) as a function of burnup are shown in Figure 16. The Δk values do not become positive for either of the gadolinia-bearing fuel assembly designs. In other words, the k_{inf} values for the gadolinia-bearing fuel remain less than the k_{inf} values for the nongadolinia fuel. Also note that the D2 fuel assembly, with 12 gadolinia-bearing rods, has slightly more negative Δk values than the D1 fuel assembly, which has only 8 gadolinia-bearing rods.

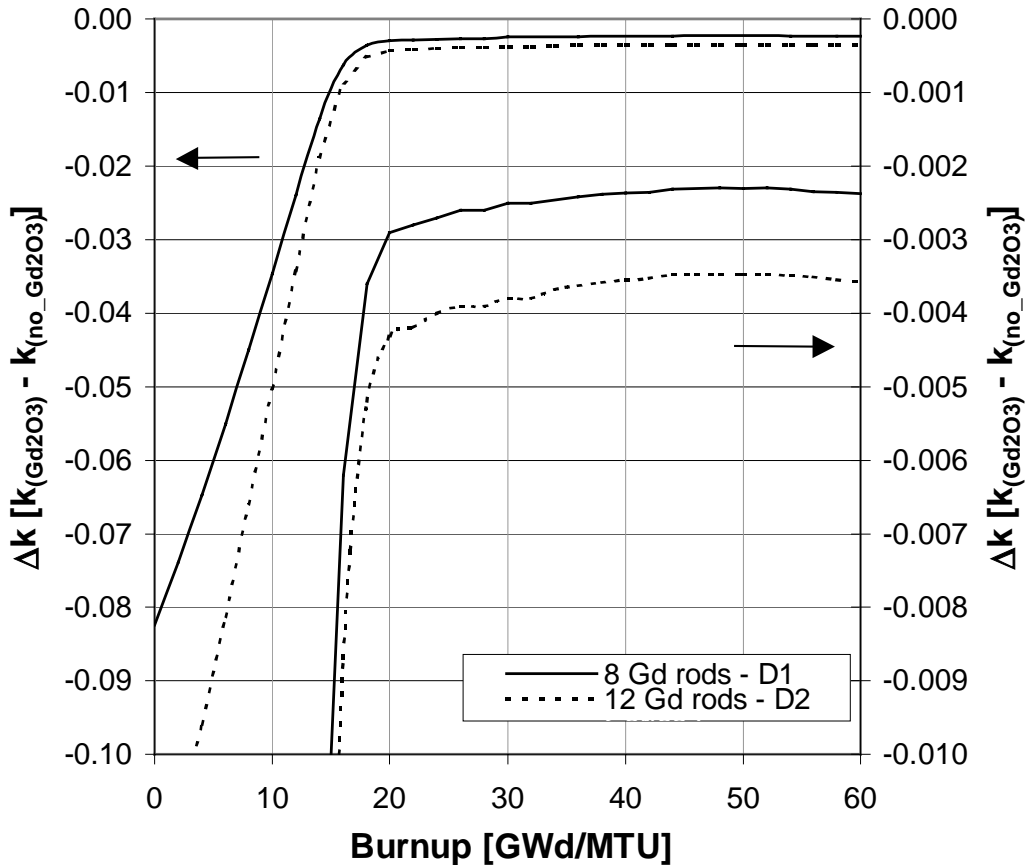


Figure 16 Comparison of Δk values as a function of burnup between the D assembly designs with gadolinia-bearing rods and the D assembly design (Figure 12) without gadolinia-bearing rods. The results are also plotted according to the enlarged scale on the right-hand-side y-axis for clarity.

The effect of the gadolinia-bearing rods was also studied for the E fuel assembly designs, modeled according to Tables 3 and 4. The resulting Δk values as a function of burnup are shown in Figure 17. Again, the Δk values for both of the gadolinia-bearing fuel assemblies (E1 and E2) remain negative throughout the entire burnup period. Also note that Δk values are slightly more negative for the higher ^{235}U enriched/higher gadolinia-loading E fuel assembly designs than for the lower ^{235}U enriched/lower gadolinia-loading D fuel assembly designs.

The results from both the D and E fuel assembly designs indicate that the gadolinia-bearing fuel k_{inf} values are less than the non-gadolinia-bearing fuel k_{inf} values throughout burnup. The extent by which the reactivity of the gadolinia-bearing fuel assembly is reduced increases with increasing gadolinia loading (wt % Gd_2O_3 and the number of gadolinia-bearing rods).

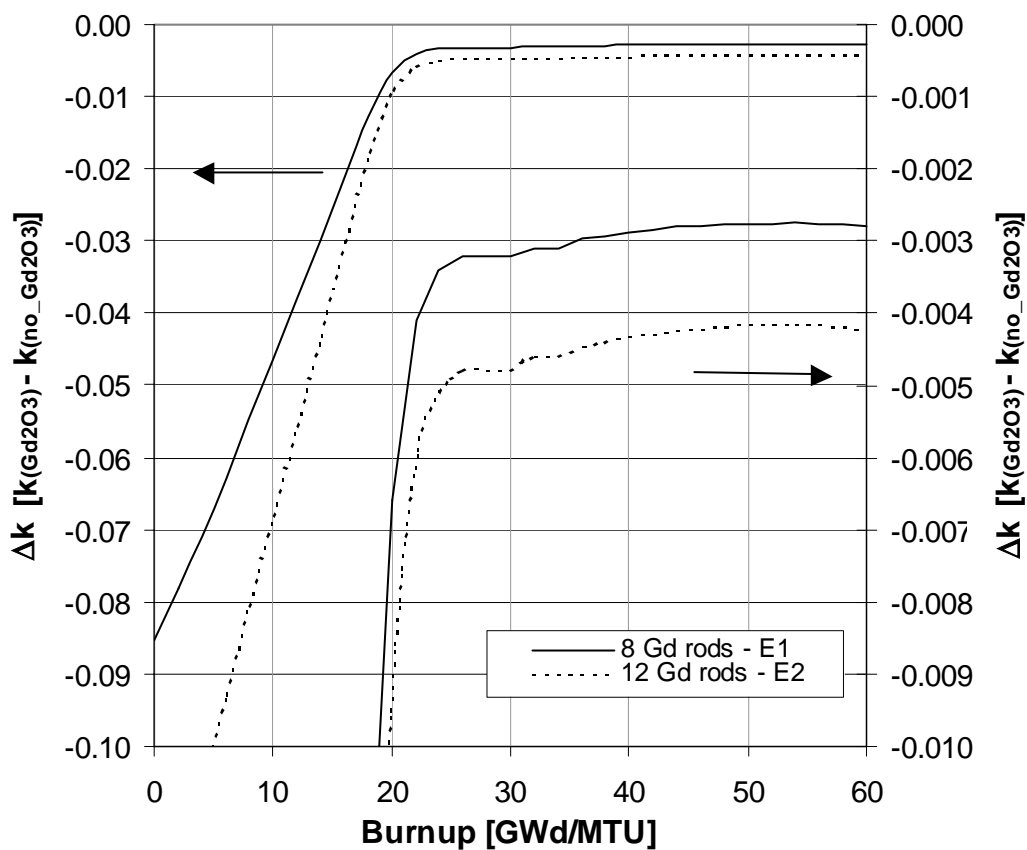


Figure 17 Comparison of Δk values as a function of burnup between the E assembly designs with gadolinia-bearing rods and the E assembly design (Figure 12) without gadolinia-bearing rods. The results are also plotted on the enlarged scale on the right-hand-side y-axis for clarity.

3.3.2.2 Siemens Designs

In addition to the CE assembly designs analyzed in the previous subsection, Siemens assembly designs with gadolinia-bearing rods were analyzed. Four different 17×17 fuel assembly designs with various gadolinia loadings were considered. The common assembly specifications are listed in Table 5.

Table 5 Siemens 17×17 fuel assembly specifications

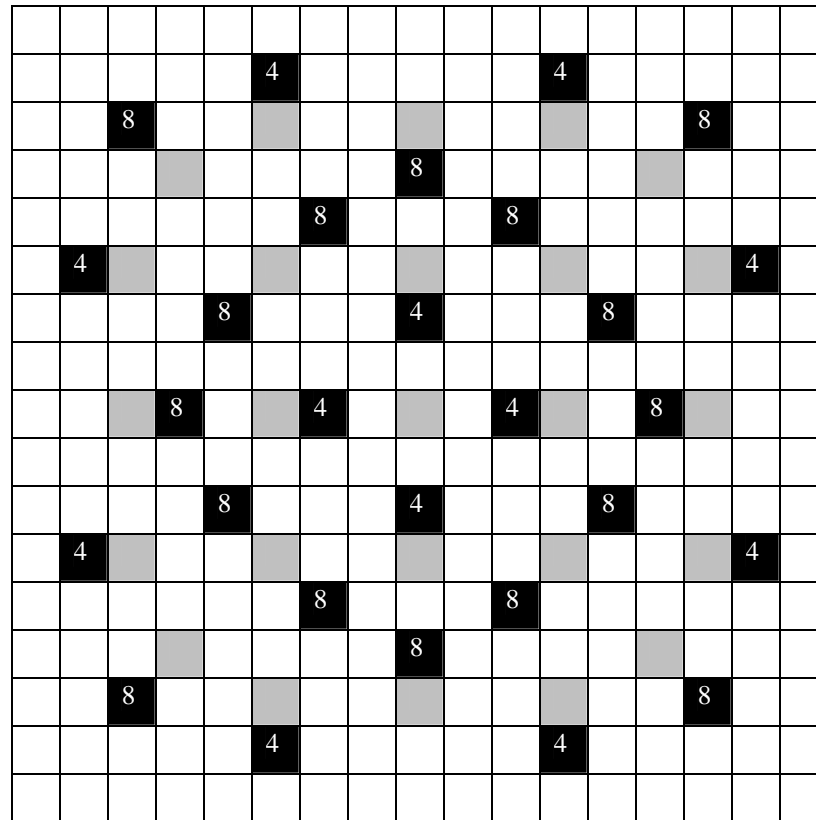
Parameter	Dimension (cm)
Rod pitch	1.260
Assembly pitch	21.5
Cladding outside diameter	0.95504
Cladding inside diameter	0.83312
Pellet outside diameter	0.81661
Guide/instrument tube outside diameter	1.2192
Guide/instrument tube inside diameter	1.1379
Array size	17×17
Number of fuel rods	264
Number of guide/instrument tubes	25

The assembly designs considered (designated M1–M4) are summarized in Table 6 and illustrated in Figures 18–21. Unpoisoned, equivalent enrichment reference cases (corresponding to M1–M4, respectively) were also analyzed and used for comparison. These unpoisoned cases were exactly the same as the actual cases, with the exception that the $\text{UO}_2\text{-Gd}_2\text{O}_3$ rods were replaced with equivalent enrichment UO_2 rods. The HELIOS calculational model for the M1 assembly design is shown in Figure 22.

Table 6 Fuel assembly data for the M1–M4 assembly designs

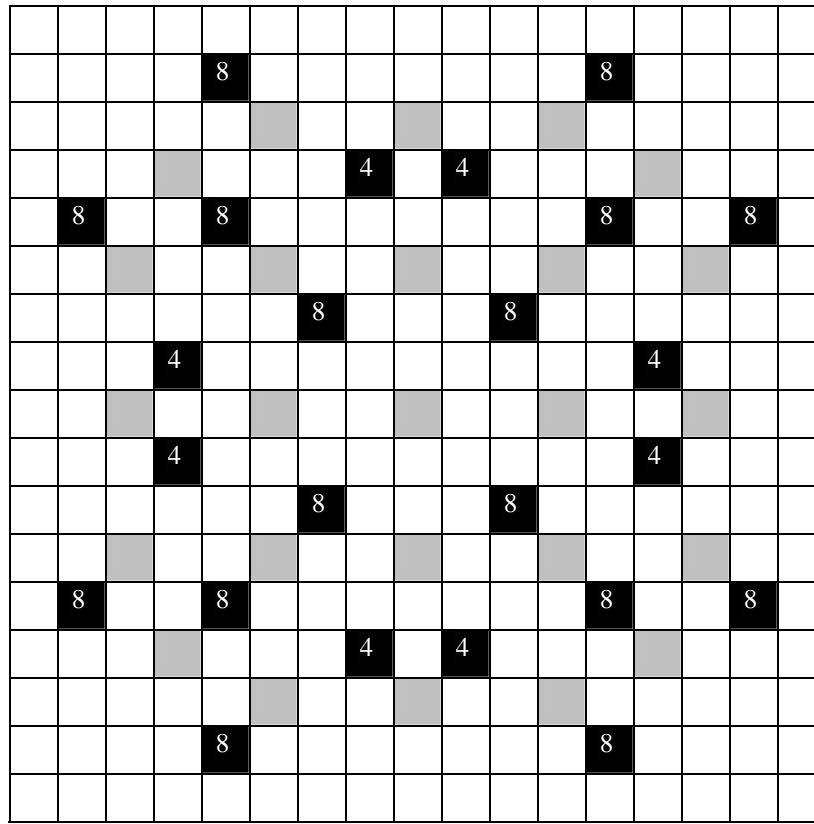
Fuel assembly	UO_2 fuel rod enrichment	No. of UO_2 fuel rods/assembly	No. of $\text{UO}_2\text{-Gd}_2\text{O}_3$ rods/assembly	$\text{Gd}_2\text{O}_3/^{235}\text{U}$ wt % for $\text{UO}_2\text{-Gd}_2\text{O}_3$ rods
M1	4.25	236	16	8.0/3.91*
			12	4.0/4.08
M2	4.25	240	16	8.0/3.91
			8	4.0/4.08
M3	4.25	244	16	6.0/3.99
			4	2.0/4.16
M4	4.25	260	4	2.0/4.16

*Read as 8.0 wt % Gd_2O_3 and 3.91 wt % ^{235}U enrichment in $\text{UO}_2\text{-Gd}_2\text{O}_3$ rods.



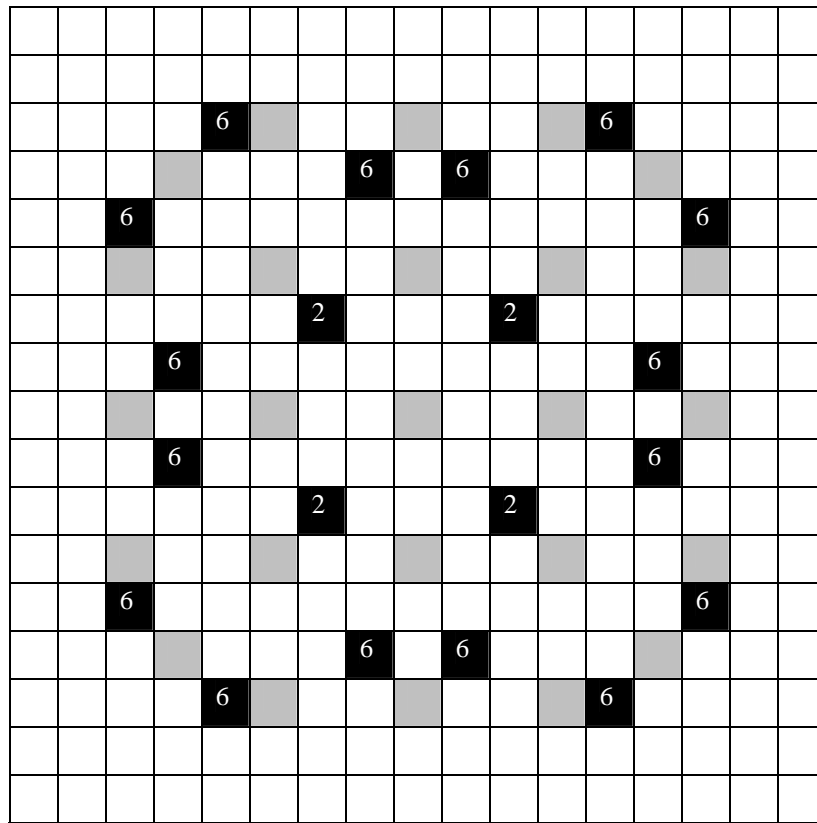
- Guide/inst. tube
- Fuel rod
- 4 Gd-bearing fuel rod with 4 wt % Gd_2O_3
- 8 Gd-bearing fuel rod with 8 wt % Gd_2O_3

Figure 18 Fuel rod array (17 × 17) representing the M1 loading pattern



- Guide/inst. tube
- Fuel rod
- 4 Gd-bearing fuel rod with 4 wt % Gd_2O_3
- 8 Gd-bearing fuel rod with 8 wt % Gd_2O_3

Figure 19 Fuel rod array (17 × 17) representing the M2 loading pattern



- Guide/inst. tube
- Fuel rod
- 2 Gd-bearing fuel rod with 2 wt % Gd_2O_3
- 6 Gd-bearing fuel rod with 6 wt % Gd_2O_3

Figure 20 Fuel rod array (17 × 17) representing the M3 loading pattern

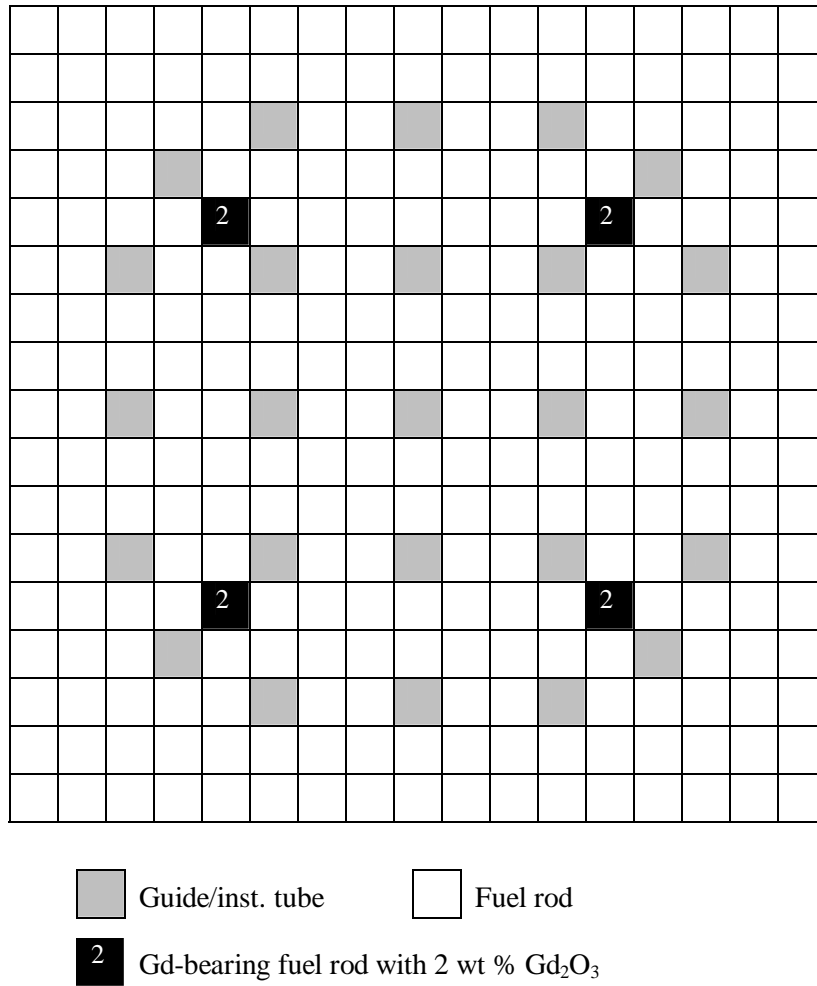


Figure 21 Fuel rod array (17 × 17) representing the M4 loading pattern

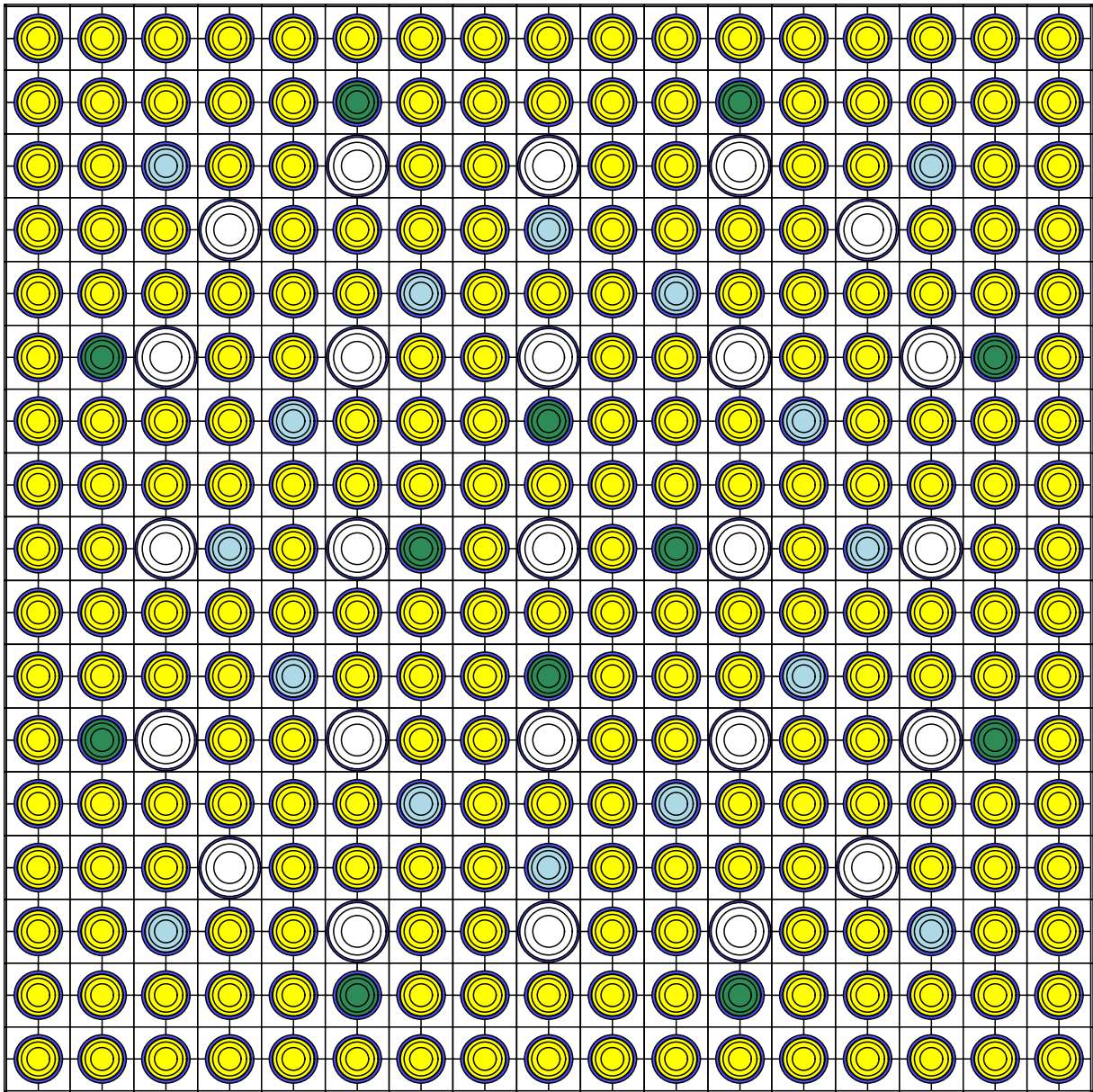


Figure 22 HELIOS calculational model of M1 fuel assembly

The k_{inf} values as a function of burnup for the unpoisoned reference case (corresponding to M1) and the poisoned M1 case are compared in Figure 23. The Δk values as a function of burnup for the M1–M4 assemblies are shown in Figures 24 and 25, where it can be seen that all of the gadolinia-bearing fuel assembly designs yield negative Δk values. As mentioned earlier, each of the four cases has a separate reference case that does not contain any gadolinia.

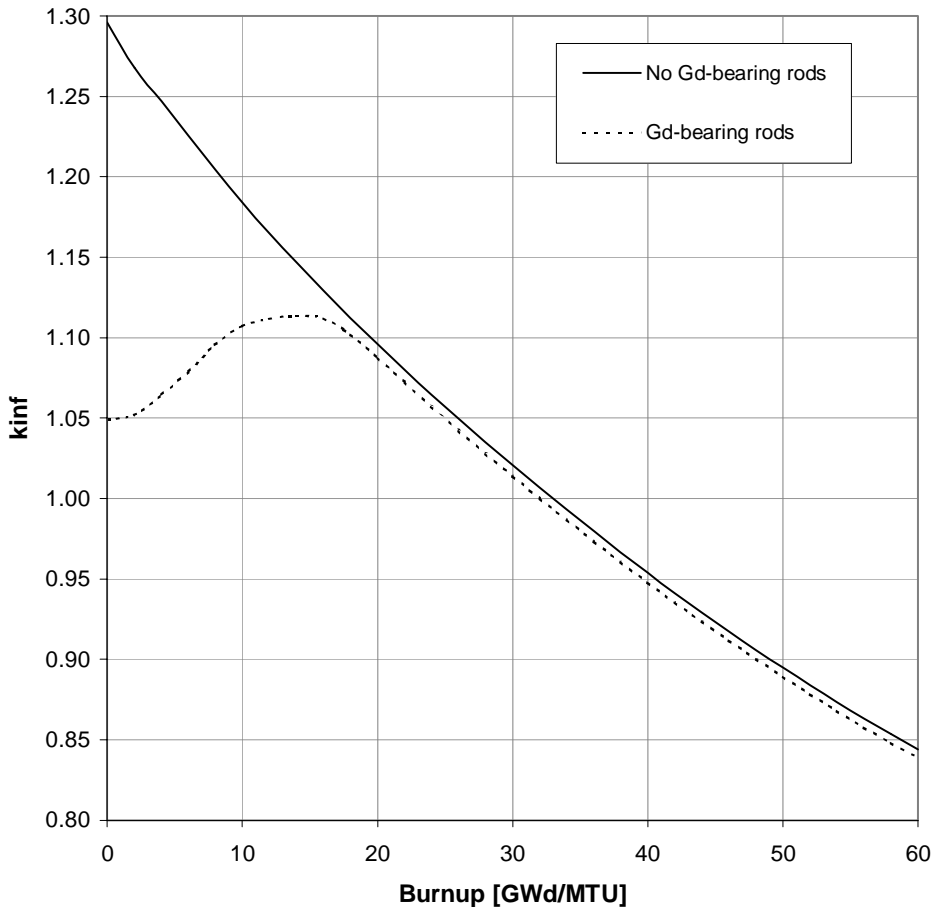


Figure 23 Comparison of k_{inf} values with and without gadolinia-bearing rods (M1 assembly)

These results are consistent with the results shown in the previous subsection, confirming that the k_{inf} values for fuel assemblies with gadolinia-bearing rods are always less than the k_{inf} values for fuel assemblies without gadolinia-bearing rods. Further, the amount by which the k_{inf} values are lower increases with increasing gadolinia loading. The reason for this negative reactivity with gadolinia-bearing rods is discussed in Section 3.3.5 (Subsection 3.3.5.2).

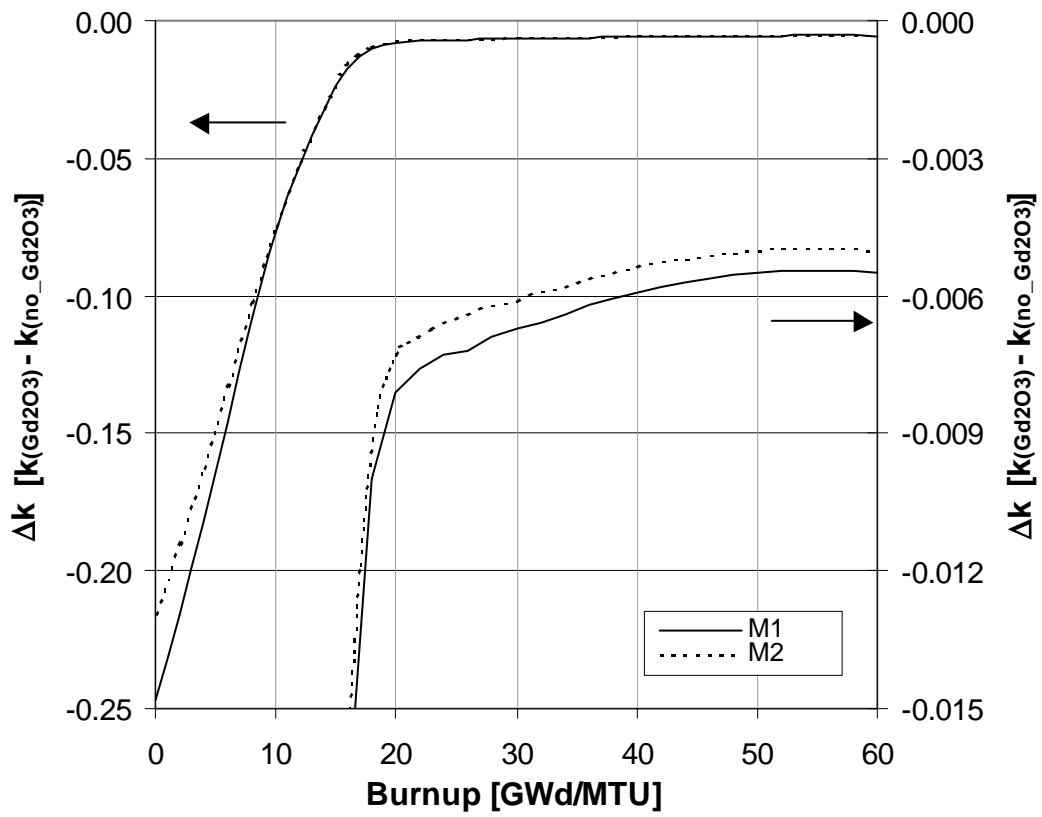


Figure 24 Comparison of Δk values as a function of burnup between assemblies with and without gadolinia-bearing rods (M1 and M2 assemblies). The results are also plotted on the enlarged scale on the right-hand-side y-axis for clarity.

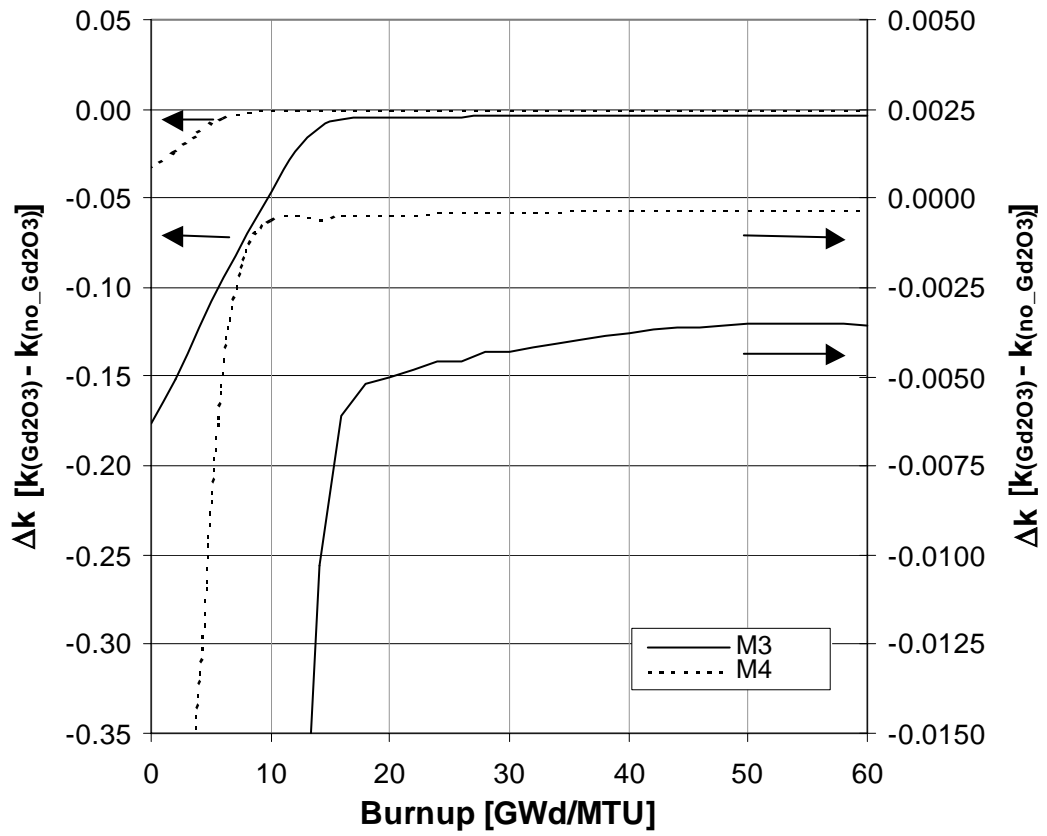


Figure 25 Comparison of Δk values as a function of burnup between assemblies with (M3 and M4) and without gadolinia-bearing rods. The results are also plotted on the enlarged scale on the right-hand-side y-axis for clarity.

3.3.3 UO₂-Er₂O₃ Integral Burnable Absorber Rods

In addition to UO₂-Gd₂O₃ rods, CE has manufactured an IBA containing erbia (Er₂O₃). Assemblies with erbia-bearing rods are far less prevalent than assemblies with gadolinia-bearing rods. Similar to the UO₂-Gd₂O₃ rods, the erbia-bearing rods include the burnable absorber (Er₂O₃) as an integral part of the fuel matrix. The weight percent of the erbia and the number of erbia-bearing rods within an assembly are both variable, as well as the ²³⁵U enrichment.

Common specifications for the CE 14 × 14 erbia-bearing fuel assembly design⁹ are listed in Table 7. Figure 26 shows the geometry of one of the fuel assemblies considered (containing 60 erbia rods). The two unique erbia-bearing fuel assembly lattices considered in this analysis are shown in Figures 27 and 28. The enrichment of all rods is 4.3 wt % ²³⁵U, and the weight percent of Er₂O₃ in the erbia-bearing rods is 2.0.

Calculations were performed for (1) the actual assembly specifications (as shown in Figures 27 and 28) and (2) a case in which the UO₂-Er₂O₃ rods were replaced with equivalent enrichment (4.3 wt % ²³⁵U) UO₂ rods. The k_{inf} values as a function of burnup for the two conditions are compared in Figure 29. The results (Δk values) from the calculations are shown in Figure 30. It can be seen that the k_{inf} values for the non-erbia-bearing fuel assembly remain higher than the k_{inf} values corresponding to the erbia-bearing fuel assemblies (i.e., the Δk values are always negative). Further, the Δk values become more negative with increasing erbia loading.

Table 7 CE 14 × 14 fuel assembly specifications

Parameter	Dimension (cm)
Rod pitch	1.47
Assembly pitch	20.8
Cladding outside diameter	1.1176
Cladding inside diameter	0.97536
Pellet outside diameter	0.95631
Water hole outside diameter	2.4079
Water hole inside diameter	2.3063
Array size	14 × 14
Number of fuel rods	176
Number of water holes	5

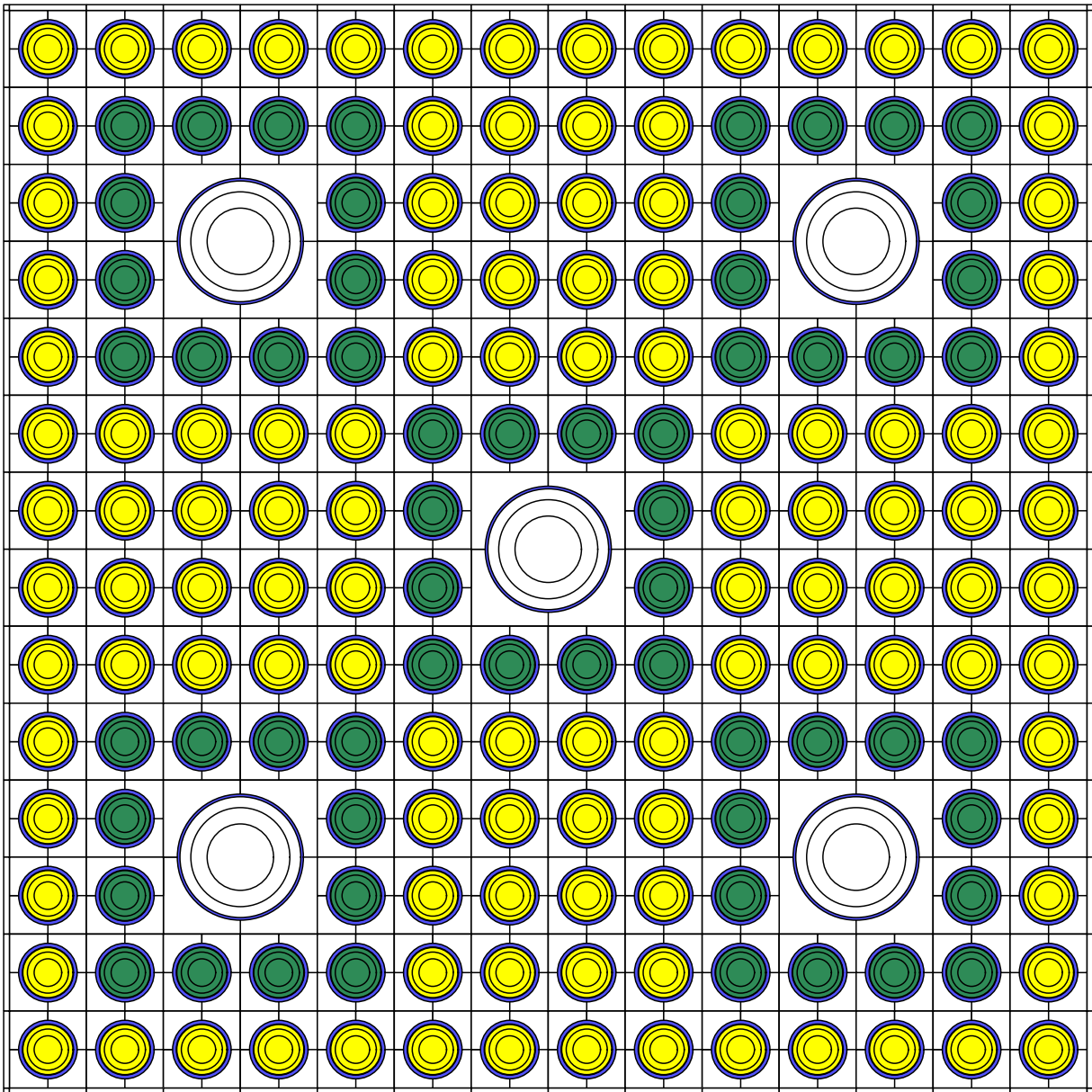


Figure 26 HELIOS calculational model of a fuel assembly containing 60 erbia-bearing fuel rods

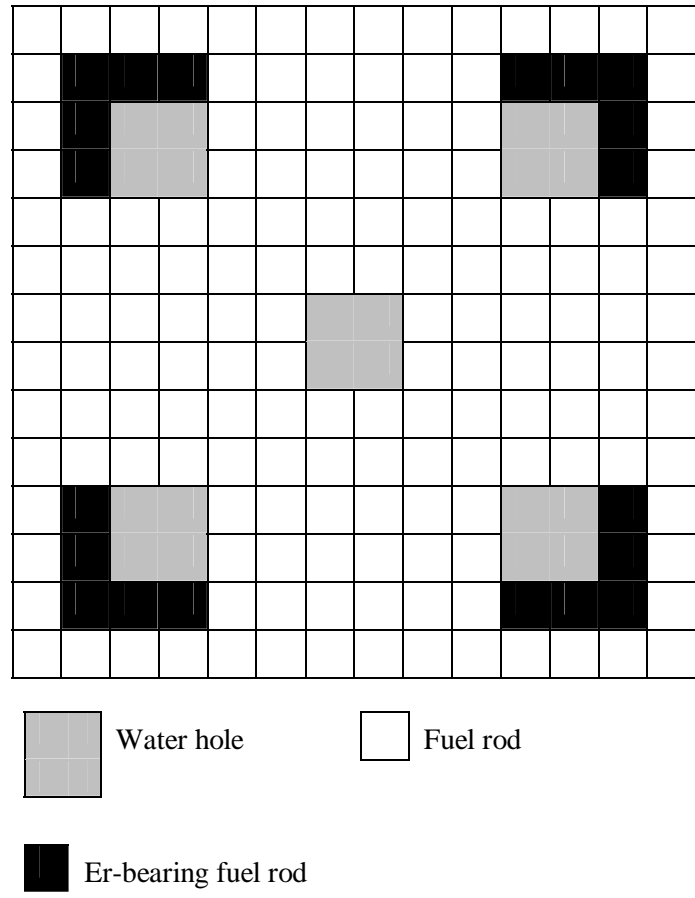


Figure 27 Fuel rod array (14 × 14) representing the loading pattern for 20 UO₂-Er₂O₃ rods

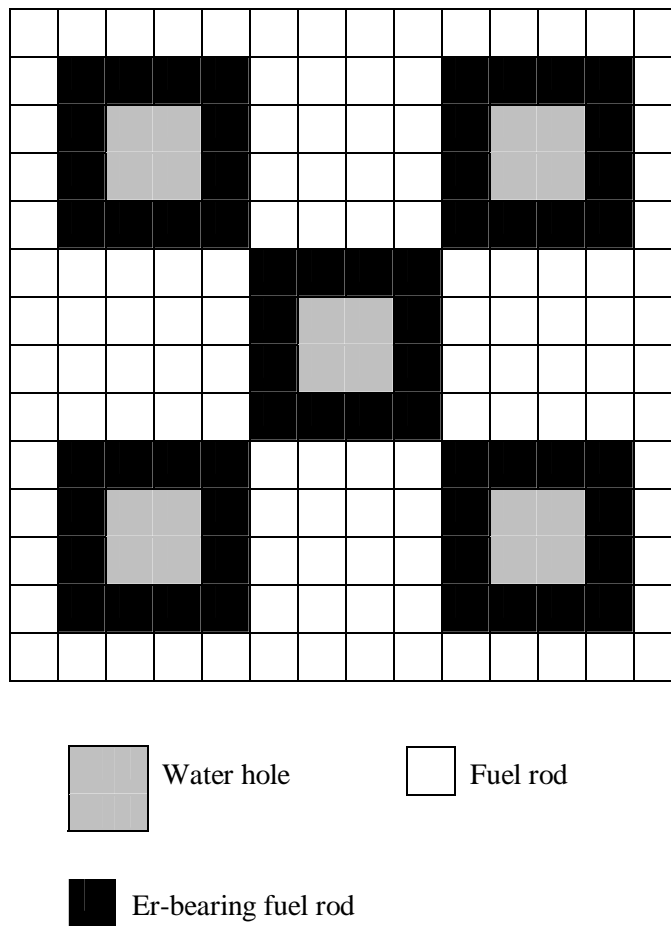


Figure 28 Fuel rod array (14 × 14) representing the loading pattern for 60 $\text{UO}_2\text{-Er}_2\text{O}_3$ rods

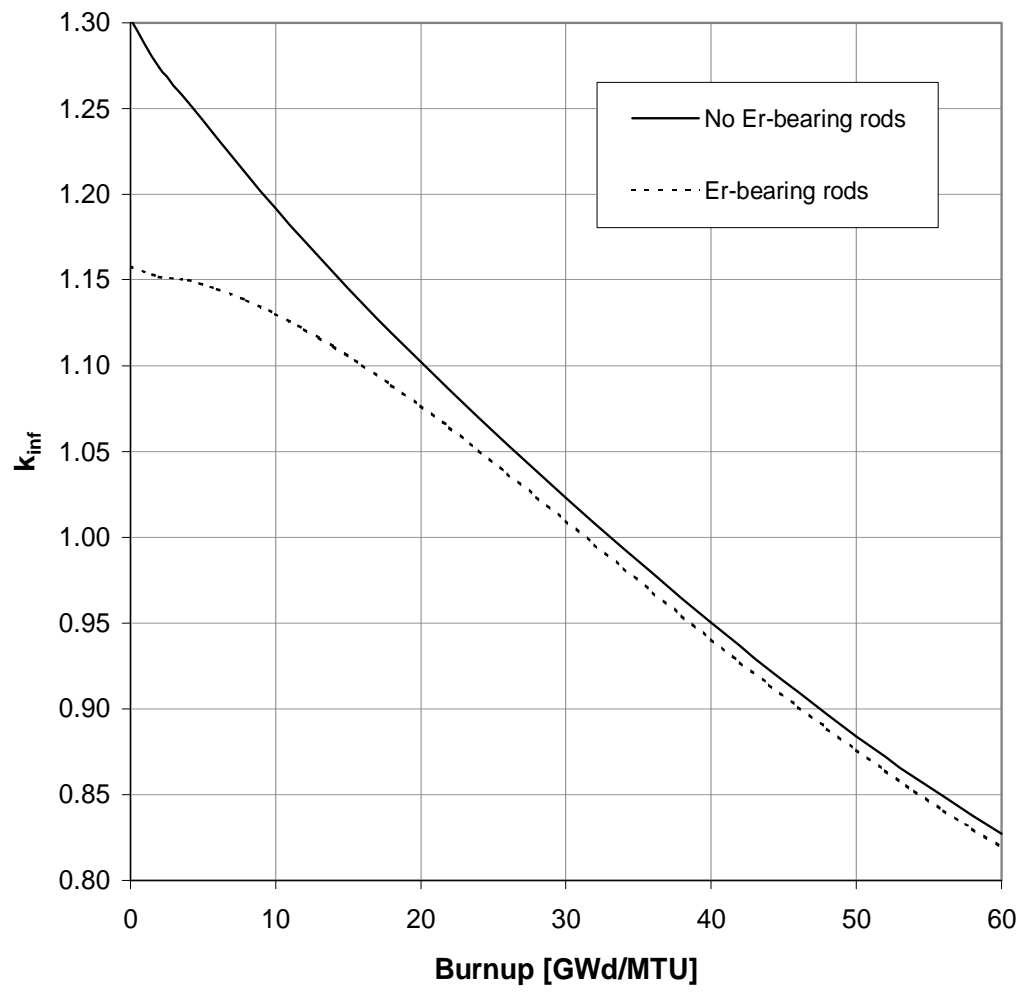


Figure 29 Comparison of k_{inf} values with erbia-bearing rods (60) present

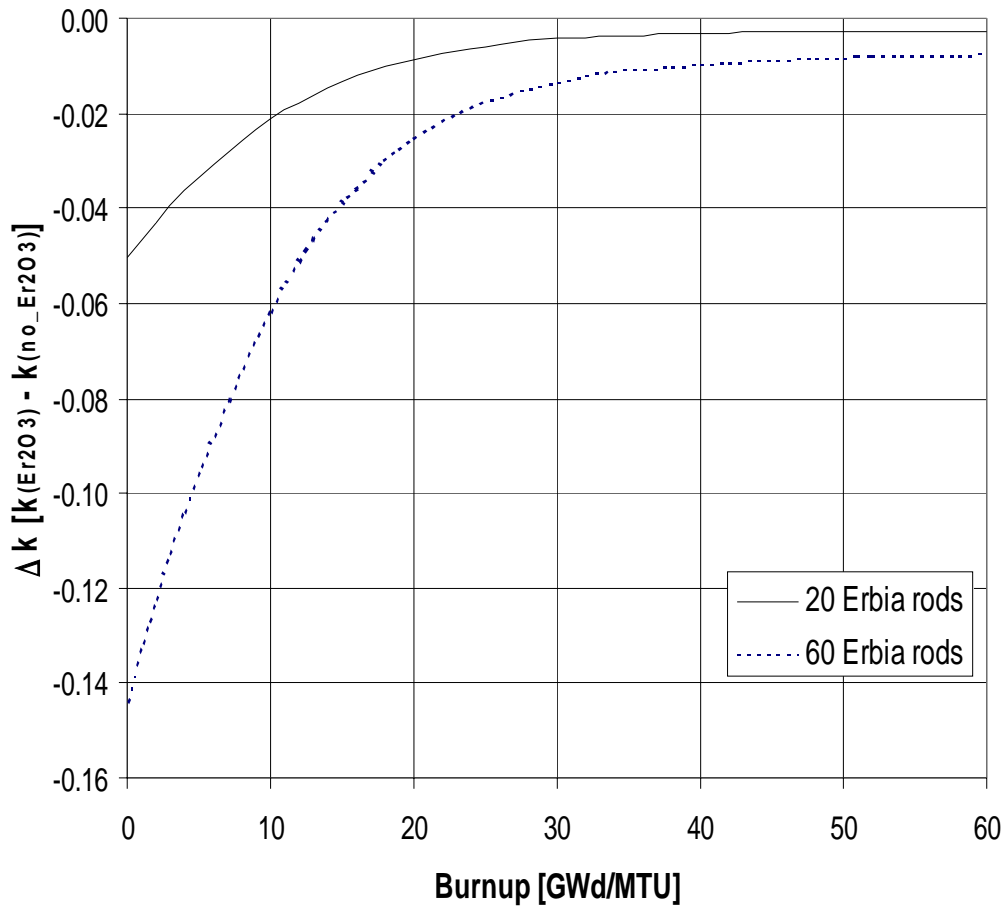


Figure 30 Comparison of Δk values as a function of burnup between assemblies with and without $\text{UO}_2\text{-Er}_2\text{O}_3$ fuel rods. The fuel rods have a ^{235}U enrichment of 4.3 wt %, and the $\text{UO}_2\text{-Er}_2\text{O}_3$ rods contain 2.0 wt % erbia.

3.3.4 Al₂O₃-B₄C Integral Burnable Absorber Rods

Another IBA manufactured by CE consists of solid rods containing aluminum pellets with uniformly dispersed boron carbide particles (Al₂O₃-B₄C), clad in zircaloy. Unlike the IFBA, UO₂-Gd₂O₃, and UO₂-Er₂O₃ rods, these rods do not contain fuel and hence are often referred to as burnable poison rods. However, because the B₄C rods are an *integral*, nonremovable part of the fuel assembly, they are included in this study. The weight percent of B₄C and the number of Al₂O₃-B₄C rods per assembly are variable.

The limited specifications for actual CE fuel assembly designs with Al₂O₃-B₄C rods were obtained from Ref. 9. Figure 31 displays the geometry of one of the CE fuel assembly designs considered, containing 12 Al₂O₃-B₄C rods. The fuel dimension specifications for these CE 14 × 14 assemblies are listed in Table 7, and the assembly lattices are shown in Figures 32–34. The Al₂O₃-B₄C rods contain 4.0 wt % B₄C and the UO₂ rods have an initial enrichment of 4.0 wt % ²³⁵U.

For the unpoisoned reference cases, the Al₂O₃-B₄C rods were replaced with equivalent enrichment (4.0 wt % ²³⁵U) fuel rods. The k_{inf} values as a function of burnup with and without Al₂O₃-B₄C rods present are compared in Figure 35. The Δk values as a function of burnup are shown in Figure 36, where it can be seen that the cases with Al₂O₃-B₄C rods maintain negative Δk values throughout the entire burnup period.

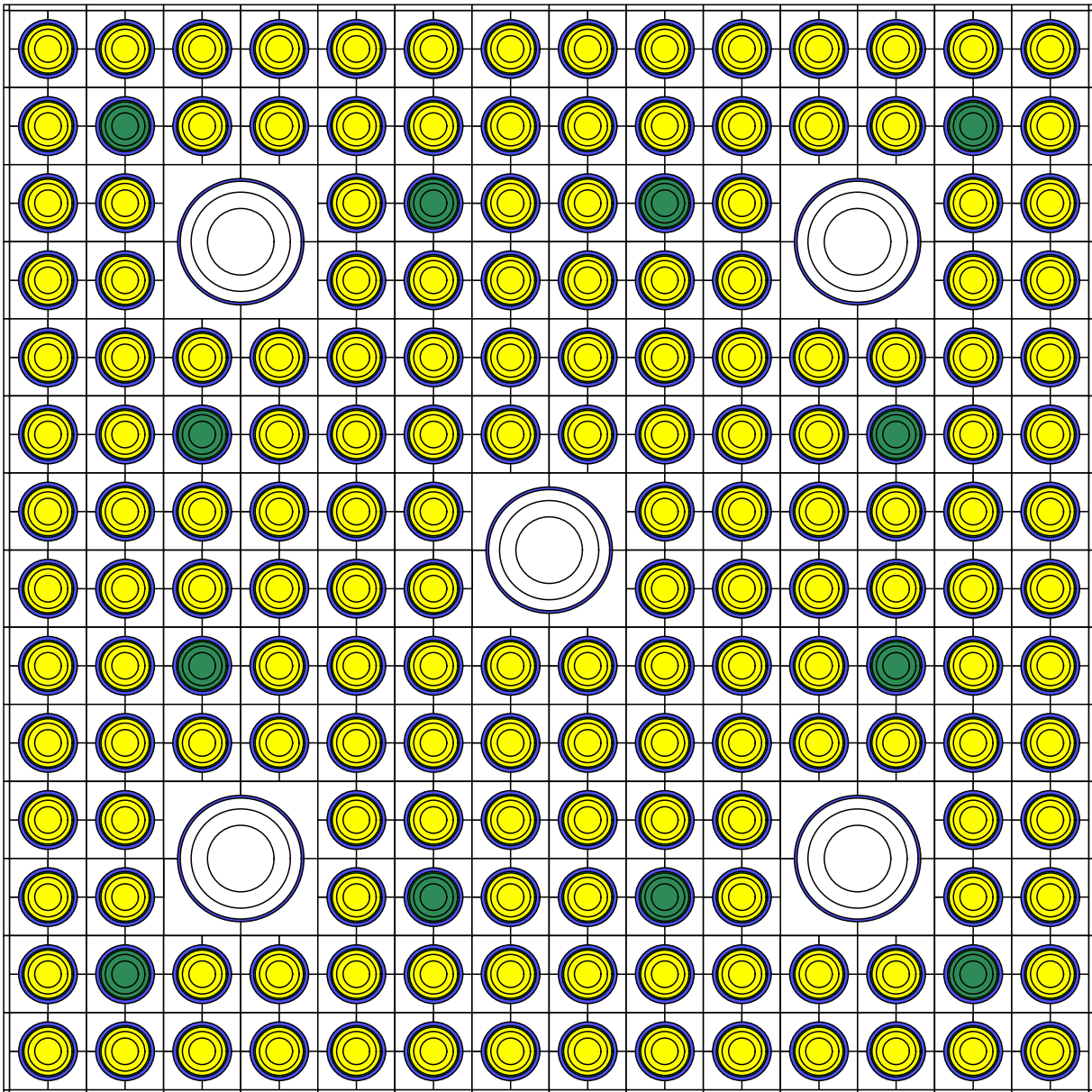


Figure 31 HELIOS calculational model of a fuel assembly containing 12 $\text{Al}_2\text{O}_3\text{-B}_4\text{C}$ rods

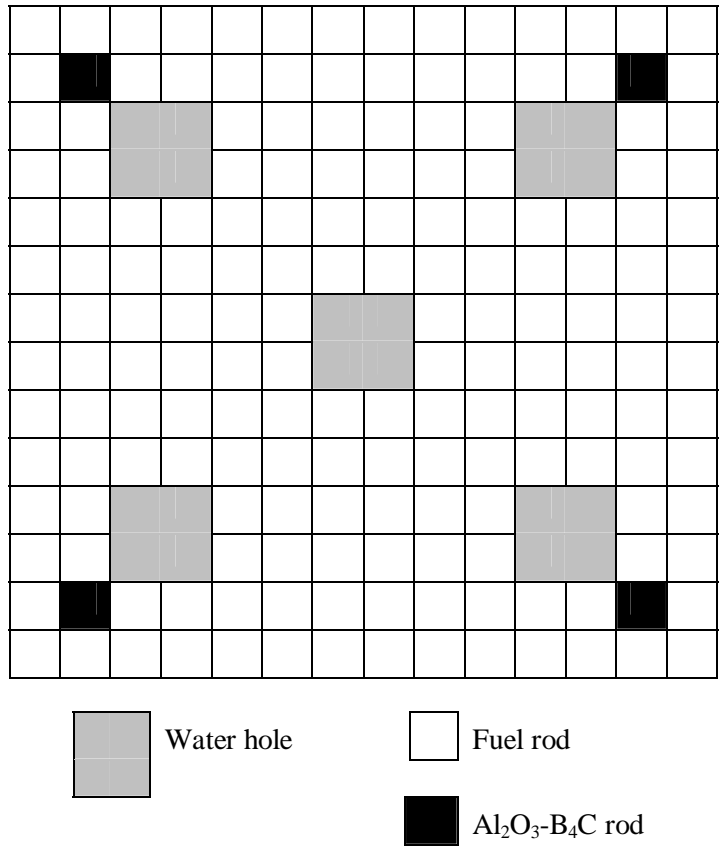


Figure 32 Fuel rod array (14 × 14) representing the loading pattern for four $\text{Al}_2\text{O}_3\text{-B}_4\text{C}$ rods

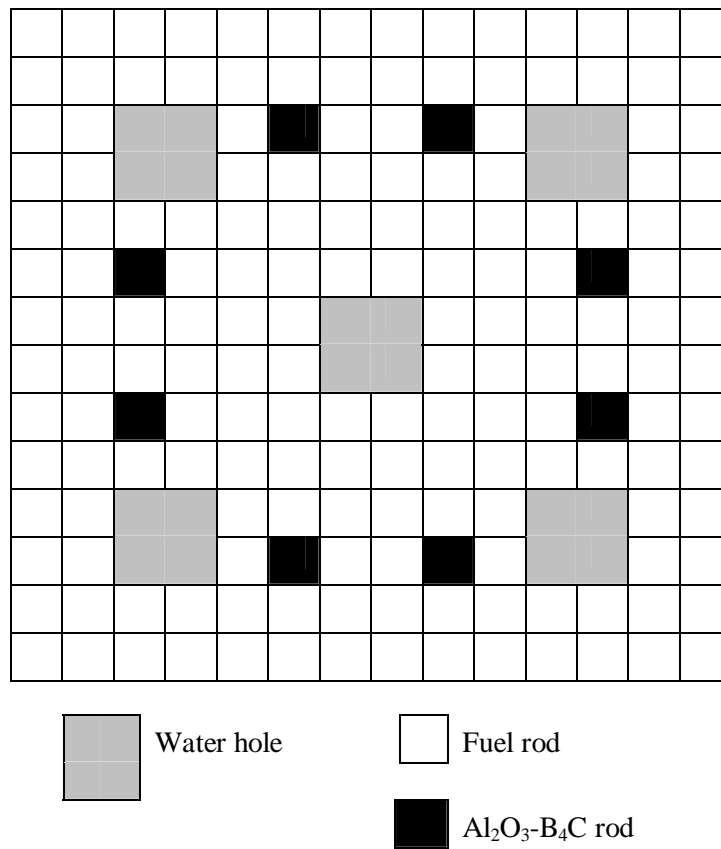


Figure 33 Fuel rod array (14×14) representing the loading pattern for eight $\text{Al}_2\text{O}_3\text{-B}_4\text{C}$ rods

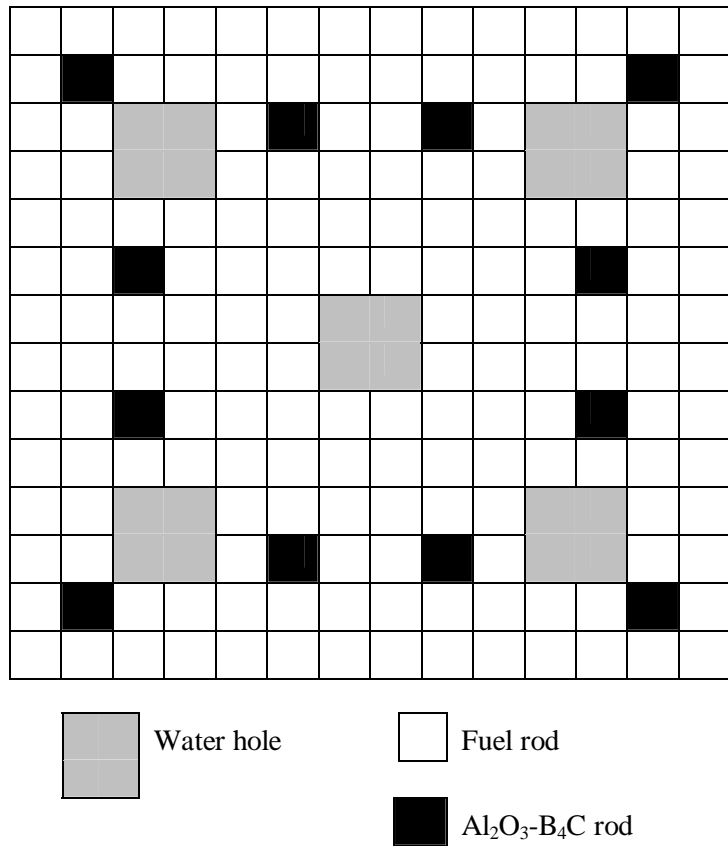


Figure 34 Fuel rod array (14 × 14) representing the loading pattern for 12 $\text{Al}_2\text{O}_3\text{-B}_4\text{C}$ rods

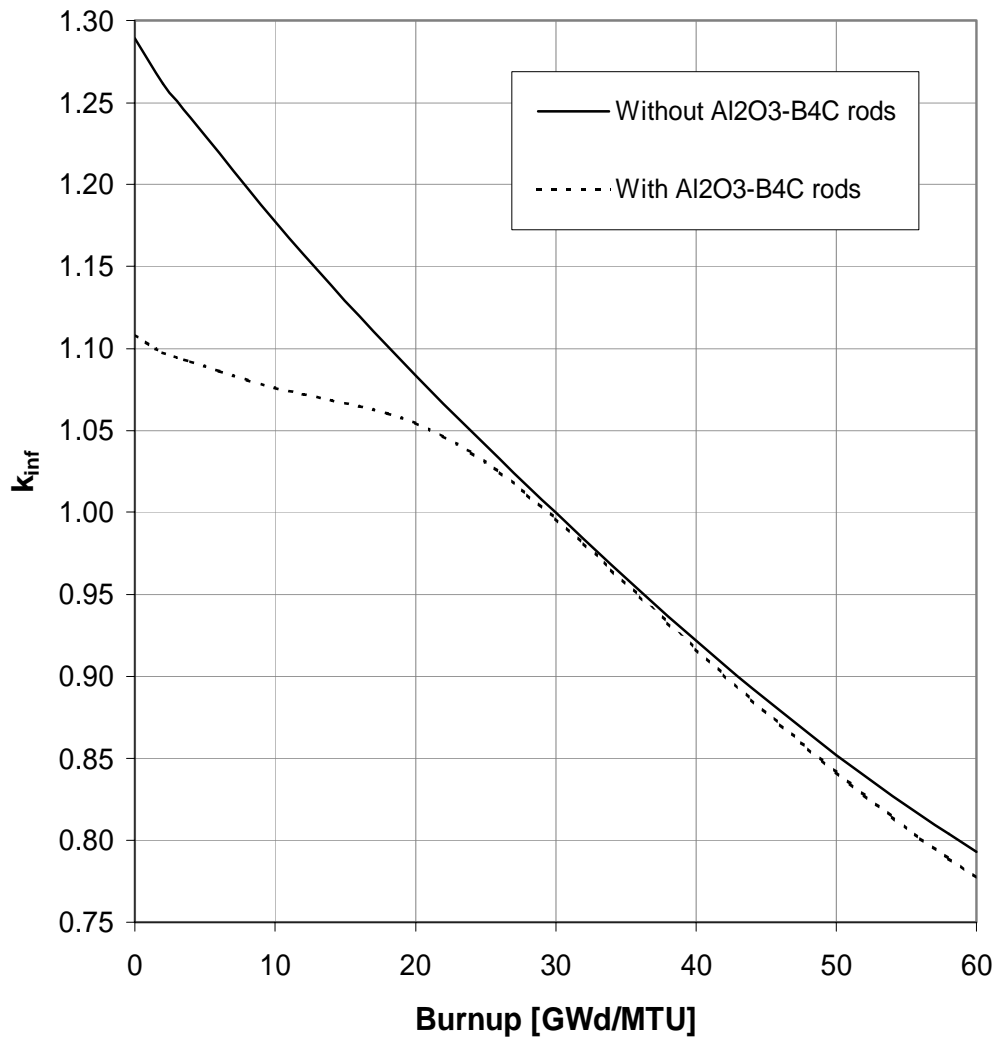


Figure 35 Comparison of k_{inf} values with and without Al₂O₃-B₄C rods (12 Al₂O₃-B₄C rods)

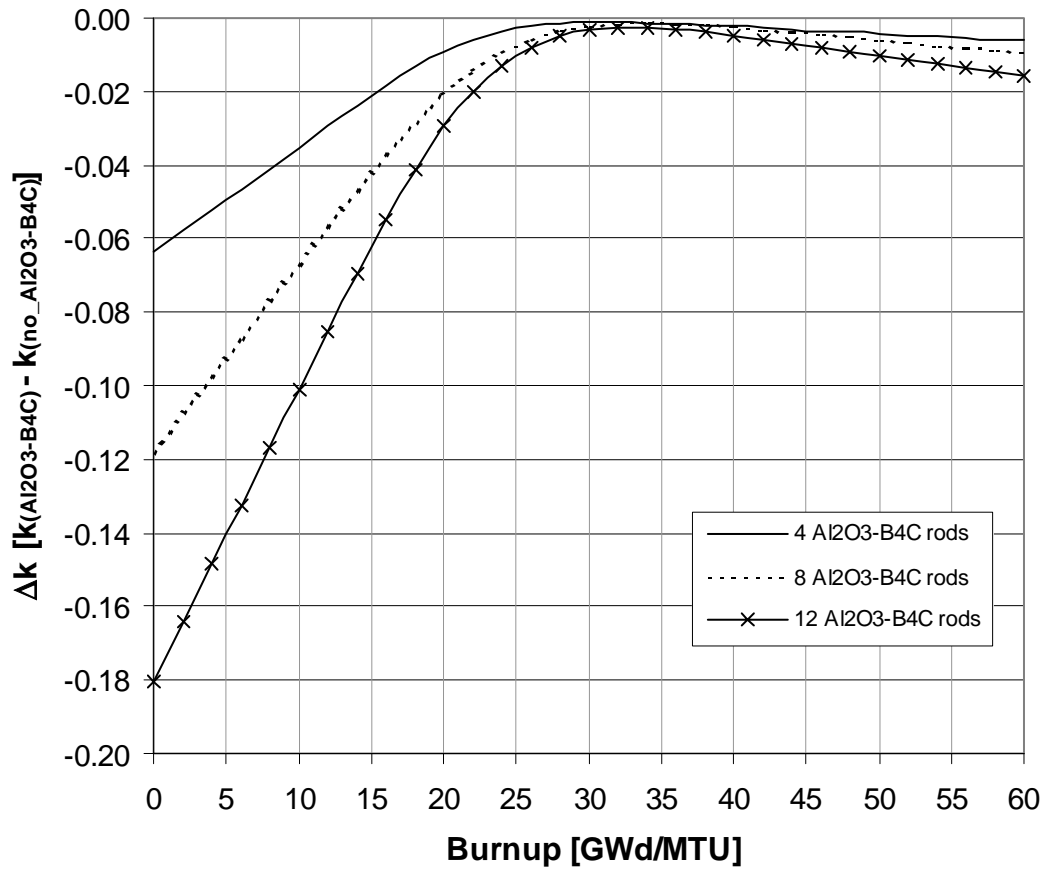


Figure 36 Comparison of Δk values as a function of burnup between assemblies with and without Al₂O₃-B₄C rods. The fuel rods have a ²³⁵U enrichment of 4 wt %, and the Al₂O₃-B₄C rods have 4 wt % B₄C.

3.3.5 Additional Studies

Because this study was performed in support of burnup credit, several of the calculations presented in the previous sections were repeated with modeling assumptions and conditions common to burnup credit analyses to assess their impact on the results. This section presents infinite assembly array calculations to study the effect of variations in assembly designs (i.e., poison loading and initial fuel enrichment) and variations in cooling time, and to investigate the reactivity worth of residual IBA materials. The section also presents studies of reactivity behavior in a poisoned storage cell and the effect of including an axial burnup distribution in a cask model.

3.3.5.1 Parametric Assembly Design Studies

All of the analyses presented in the previous sections are based on actual fuel assembly designs obtained from plant data. The additional studies presented in this section are an attempt to better understand the impact of IBA rods for variations outside those shown in the previous sections. These studies are intended to clarify trends and/or relationships between the variable characteristics (e.g., poison loading and initial fuel enrichment). Note that although these studies are based on actual fuel assembly designs, the parameters are varied outside of the known range. Consequently, the results in this section should be used to enhance understanding, and not for quantifying reactivity effects.

3.3.5.1.1 Variations of gadolinia loading and initial fuel enrichment

The first additional study involves variations in poison loading and fuel enrichment in a CE fuel assembly design with $\text{UO}_2\text{-Gd}_2\text{O}_3$ rods. The reference case consists of the 16×16 fuel assembly with no burnable absorber rods, as shown in Figure 12. The dimensions and specification of the fuel assembly are provided in Tables 3 and 4. For the cases with IBA rods present, the assembly layout is as shown in Figure 13.

Calculations were performed using varying weight percentages of gadolinia in the $\text{UO}_2\text{-Gd}_2\text{O}_3$ rods to investigate the sensitivity to gadolinia loading. Gadolinia enrichments of 4, 6, and 8 wt % were considered, while the ^{235}U enrichment was fixed at 3.78/3.28. The Δk values for the various gadolinia enrichment cases as function of burnup are shown in Figure 37. These results are consistent with earlier results for actual fuel assembly designs, showing that the Δk values become more negative with increasing gadolinia loading.

The calculational model with 6 wt % gadolinia in the $\text{UO}_2\text{-Gd}_2\text{O}_3$ rods was further investigated by considering cases with uniform fuel rod enrichments of 3, 4, and 5 wt % ^{235}U . The Δk values for the various enrichments are shown in Figure 38. All of the cases maintain negative Δk values, and the initial ^{235}U enrichment is shown to have a relatively small effect.

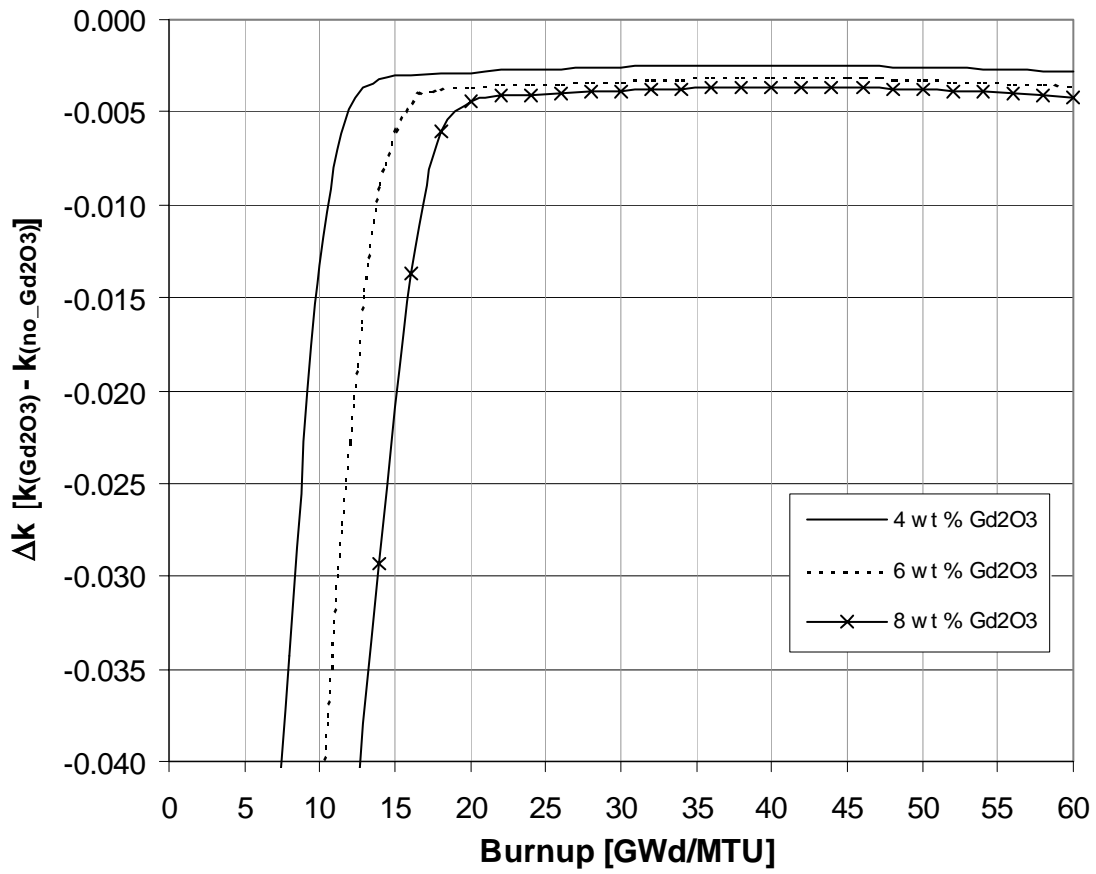


Figure 37 Comparison of Δk values versus burnup with varying gadolinia weight percentage. The fuel enrichments are 3.78/3.28 wt % ^{235}U .

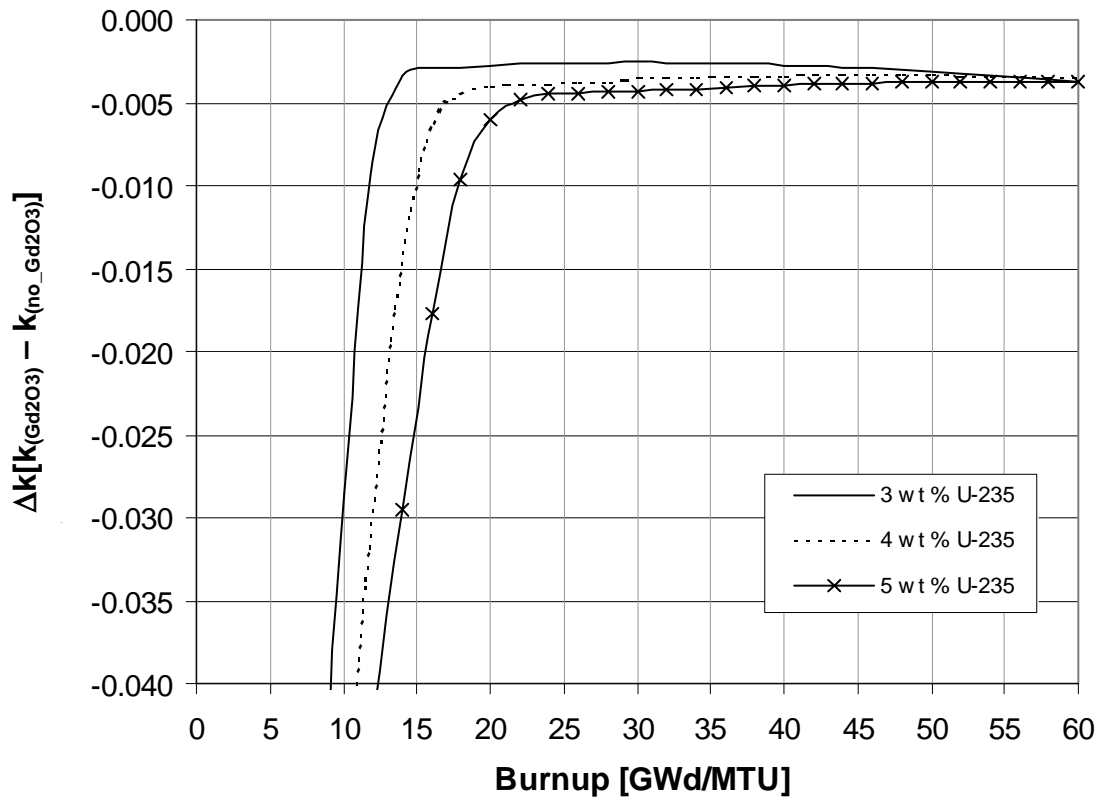


Figure 38 Comparison of Δk values versus burnup with various ^{235}U enrichments. The eight IBA rods have 6 wt % Gd_2O_3 .

3.3.5.1.2 Variations of integral fuel burnable absorber loading and initial fuel enrichment

The second additional study involves variations in IFBA loading and fuel enrichment in a 17×17 assembly. The dimensions and fuel assembly specifications can be found in Table 2. Analyses were performed for IFBA assembly designs¹⁰ with 32, 64, 80, 104, 128, and 156 IFBA rods and ²³⁵U enrichments of 3.0, 4.0, and 5.0 wt % with a boron loading of 1.57 mg ¹⁰B/in. The Δk values for the various IFBA loading patterns as a function of burnup for initial ²³⁵U enrichment of 4.0 wt % are shown in Figure 39. These results are consistent with those shown in Section 3.3.1 because the maximum positive Δk values increase as the number of IFBA rods increase.

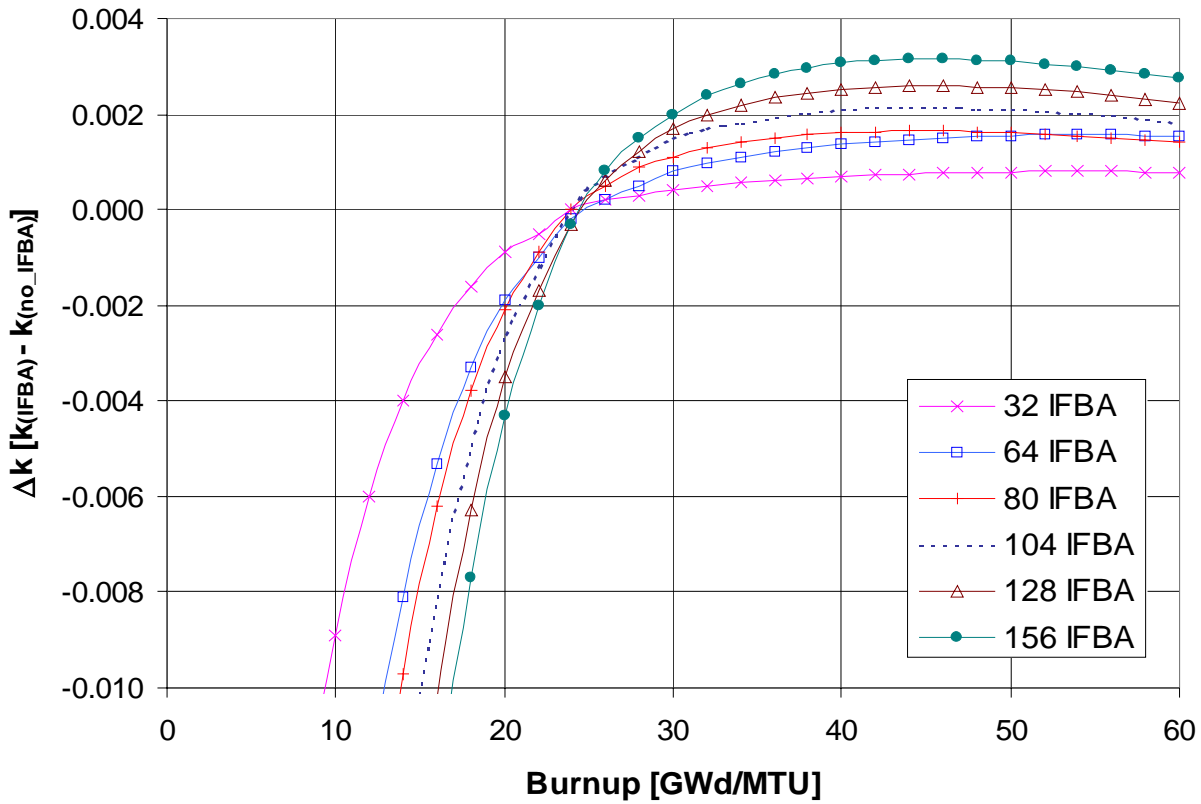


Figure 39 Comparison of Δk values versus burnup with varying IFBA loadings. The ²³⁵U enrichment is 4 wt % for all cases.

To illustrate the effect of initial fuel enrichment, Δk values for 3.0, 4.0, and 5.0 wt % ²³⁵U are shown in Figures 40 and 41 for IFBA loading patterns of 32 and 156, respectively. As is consistent with the results shown in Section 3.3.1, the positive Δk values increase with decreasing enrichment. Note that the 3.0 and 4.0 wt % ²³⁵U cases reach a maximum Δk and then begin to decrease. The maximum positive Δk values for the various IFBA cases are summarized in Table 8.

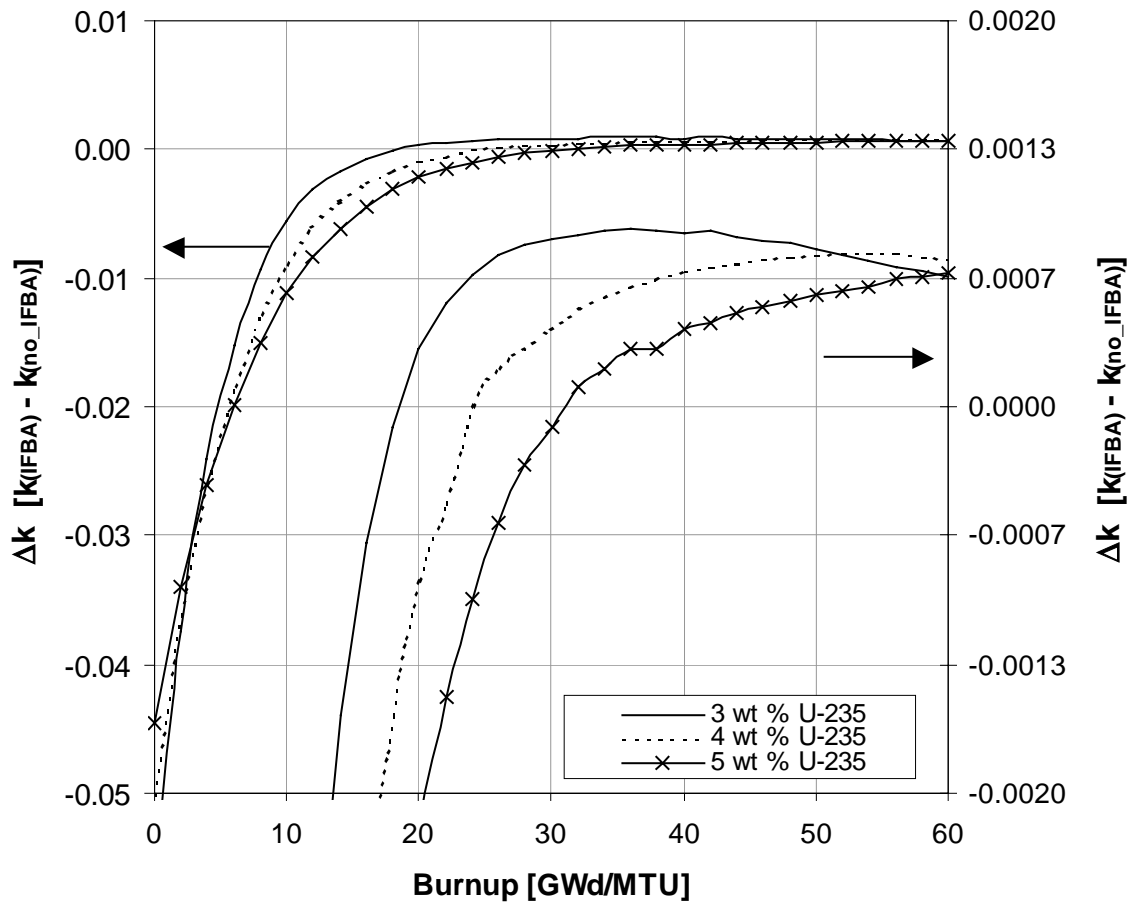


Figure 40 Comparison of Δk values versus burnup with the 32 IFBA loading pattern showing varying ^{235}U enrichments. The results are also plotted on the enlarged scale on the right-hand-side y-axis for clarity.

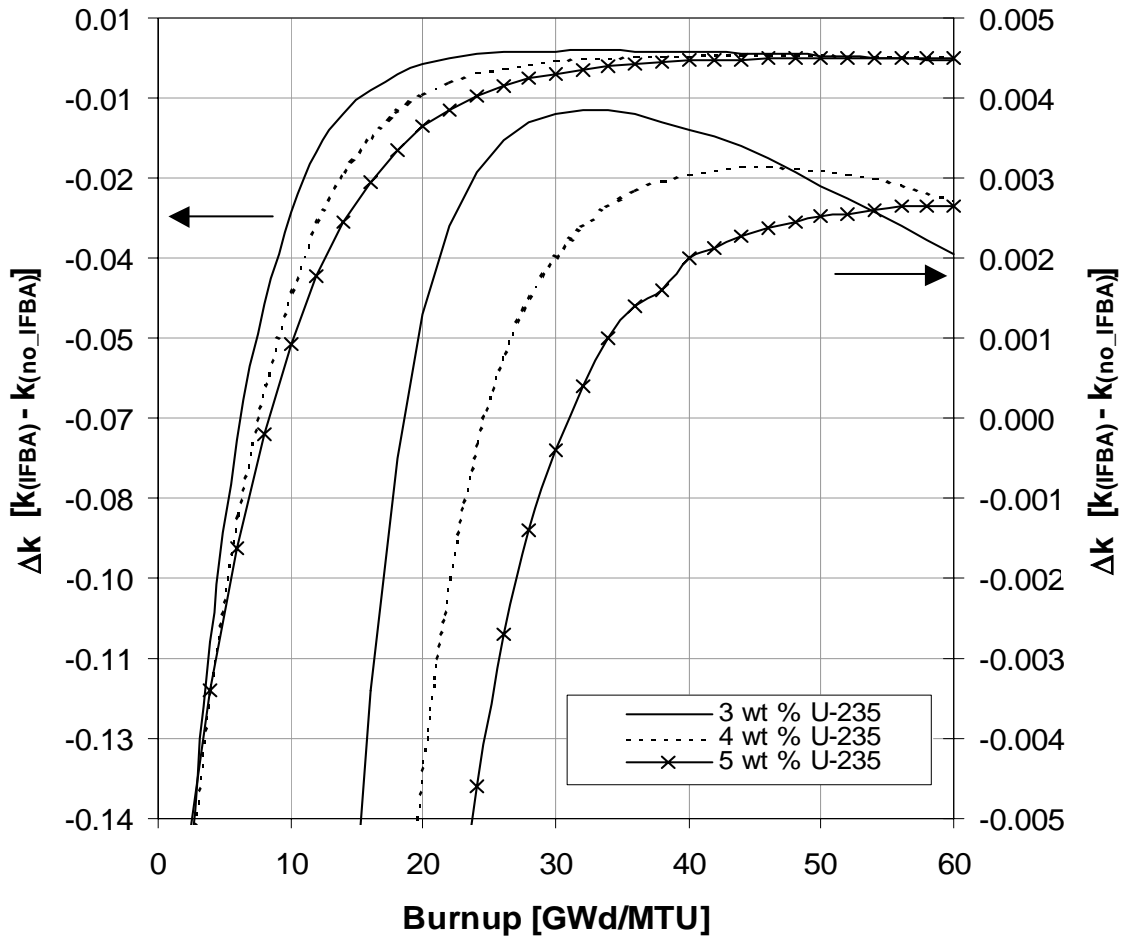


Figure 41 Comparison of Δk values versus burnup with the 156 IFBA loading pattern showing varying ^{235}U enrichments. The results are also plotted on the enlarged scale on the right-hand-side y-axis for clarity.

Table 8 Summary of maximum positive Δk values observed for IFBA cases

IFBA loading pattern	Enrichment (wt % ^{235}U)		
	3.0	4.0	5.0
32	0.0009	0.0008	0.0007
64	0.0018	0.0015	0.0013
80	0.0020	0.0016	0.0014
104	0.0026	0.0021	0.0018
128	0.0031	0.0026	0.0022
156	0.0038	0.0031	0.0027

3.3.5.2 Residual Reactivity Effect of Integral Burnable Absorbers

Sections 3.3.1 and 3.3.2 demonstrate that the Δk values become positive for fuel assembly designs containing IFBA rods but remain negative for gadolinia-bearing fuel assembly designs. To understand this different behavior, a study looked at the residual effects of the gadolinium in the $\text{UO}_2\text{-Gd}_2\text{O}_3$ rods, as well as the boron poison in the IFBA rods. The analyses for the residual effects of gadolinium were performed for the Siemens 17×17 fuel design referred to as M1 (see Table 5 for fuel assembly data).

In order to observe the residual effects of gadolinium, the reactivity worth ($\Delta k/k$) was calculated by artificially setting various compositions to zero in the criticality calculation model. Two additional calculations were performed for comparison to the unaltered condition. The first calculation featured the M1 fuel design with the non-fission product (FP) gadolinium artificially set to zero. The second calculation, performed for the M1 fuel design, artificially set the non-FP minor gadolinium isotopes (^{152}Gd , ^{154}Gd , ^{156}Gd , ^{158}Gd , and ^{160}Gd) to zero. The results of these calculations and the results from the unaltered condition were used to calculate the reactivity worth of the two sets of gadolinium isotopes, which are displayed in Figure 42 as a function of burnup. It can be seen that there is a negative residual effect associated with the presence of the gadolinium isotopes.

Analyses were also performed for the Westinghouse IFBA design containing 64 IFBA rods, 1.57 $^{10}\text{B}/\text{in.}$ boron loading, and 4.0 wt % initial fuel enrichment to study the residual effects of ^{10}B and ^{11}B . The reactivity worth was calculated by setting ^{10}B and ^{11}B to zero during the calculation. The results, plotted versus burnup in Figure 43, demonstrate that there are no significant residual reactivity effects with IFBA rods.

These analyses show that there is a negative residual effect for gadolinia-bearing fuel but no such effect for fuel designs with IFBA rods. The main difference between the $\text{UO}_2\text{-Gd}_2\text{O}_3$ rods and the IFBA rods is that gadolinium is an integral part of the fuel matrix in the $\text{UO}_2\text{-Gd}_2\text{O}_3$ rod while the boron is placed as a thin coating on the outer surface of the fuel pellets in the IFBA rod. The gadolinium isotopes displace uranium in the $\text{UO}_2\text{-Gd}_2\text{O}_3$ rod, resulting in reduced reactivity (due to the reduction in heavy metal mass). The IFBA coating does not displace uranium, and thus, there is no negative residual effect.

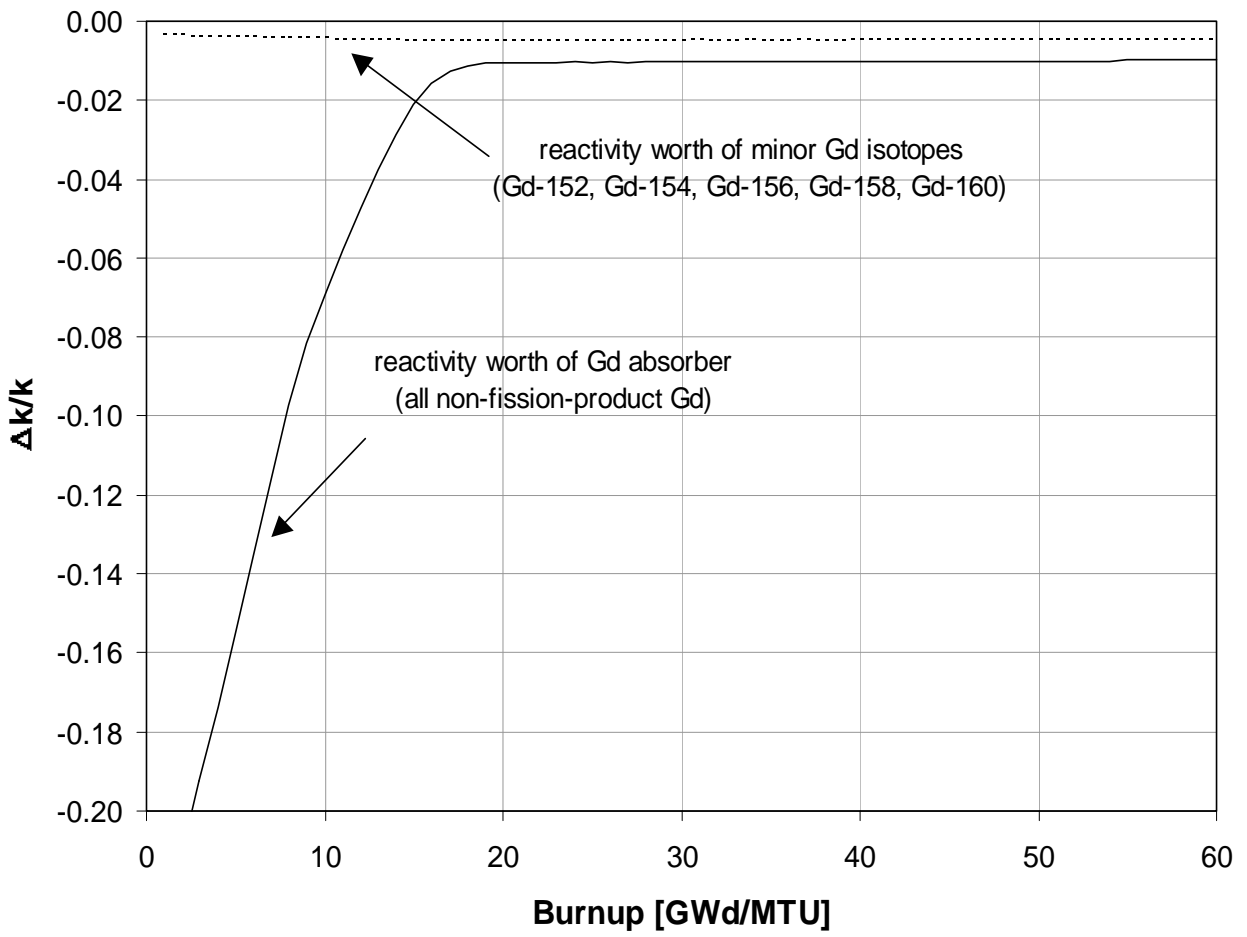


Figure 42 Reactivity worth of gadolinium isotopes versus burnup for M1 assembly

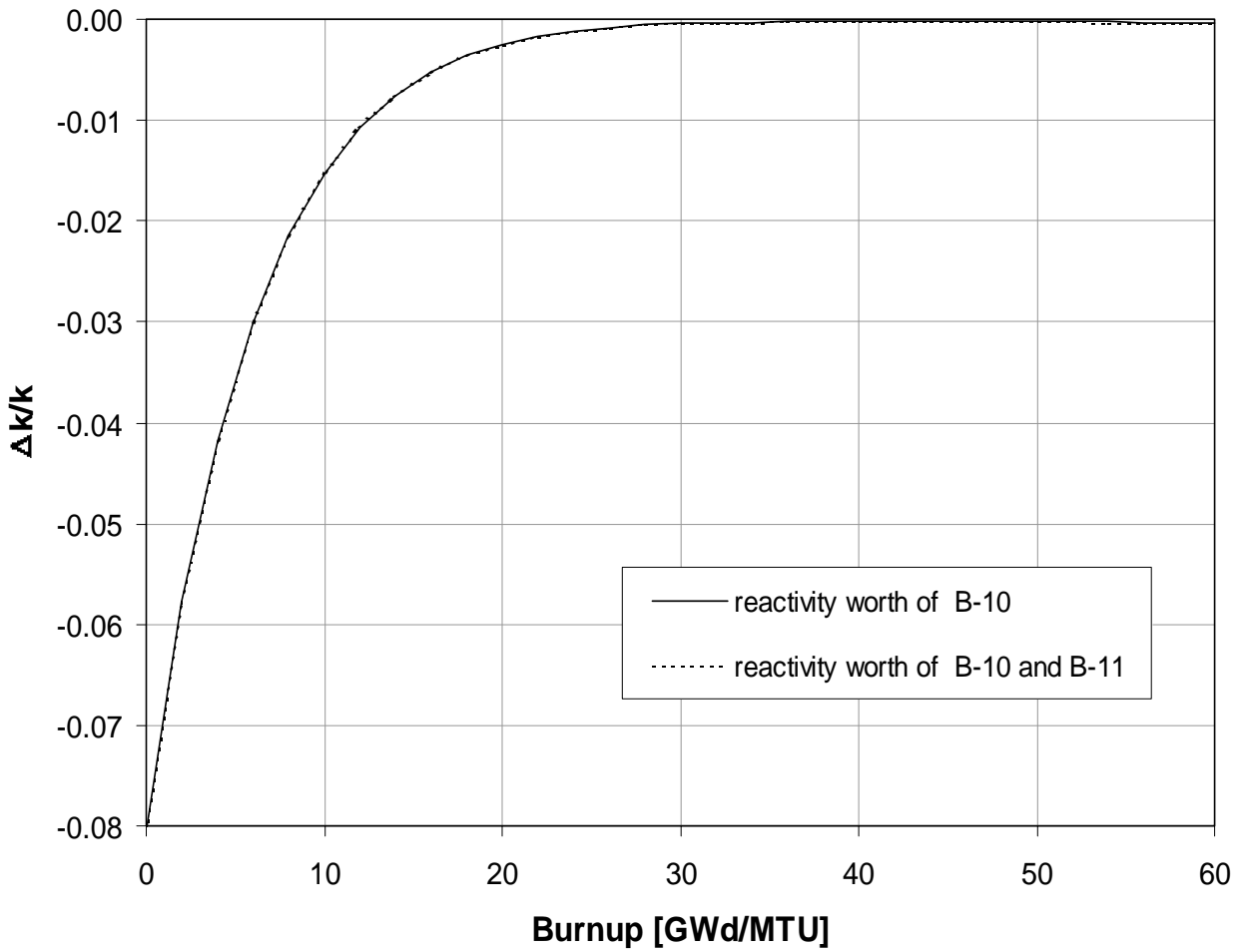


Figure 43 Reactivity worth of boron versus burnup for a Westinghouse 17×17 fuel assembly containing 64 IFBA rods

3.3.5.3 Cooling Time

To study the effects of cooling time, a few calculations were performed at cooling times other than zero. The fuel assembly employed for the study was the design containing 104 IFBA rods with a poison loading of 1.57 mg ¹⁰B/in. and 4.0 wt % ²³⁵U enrichment. Infinite assembly array calculations were performed for cooling times of 5, 20, and 40 years. The results (Δk as a function of burnup) are displayed in Figure 44. It can be seen that cooling time has little impact on the Δk values, and thus, the results at zero cooling time are expected to be applicable within the time frame relevant to cask storage and transportation.

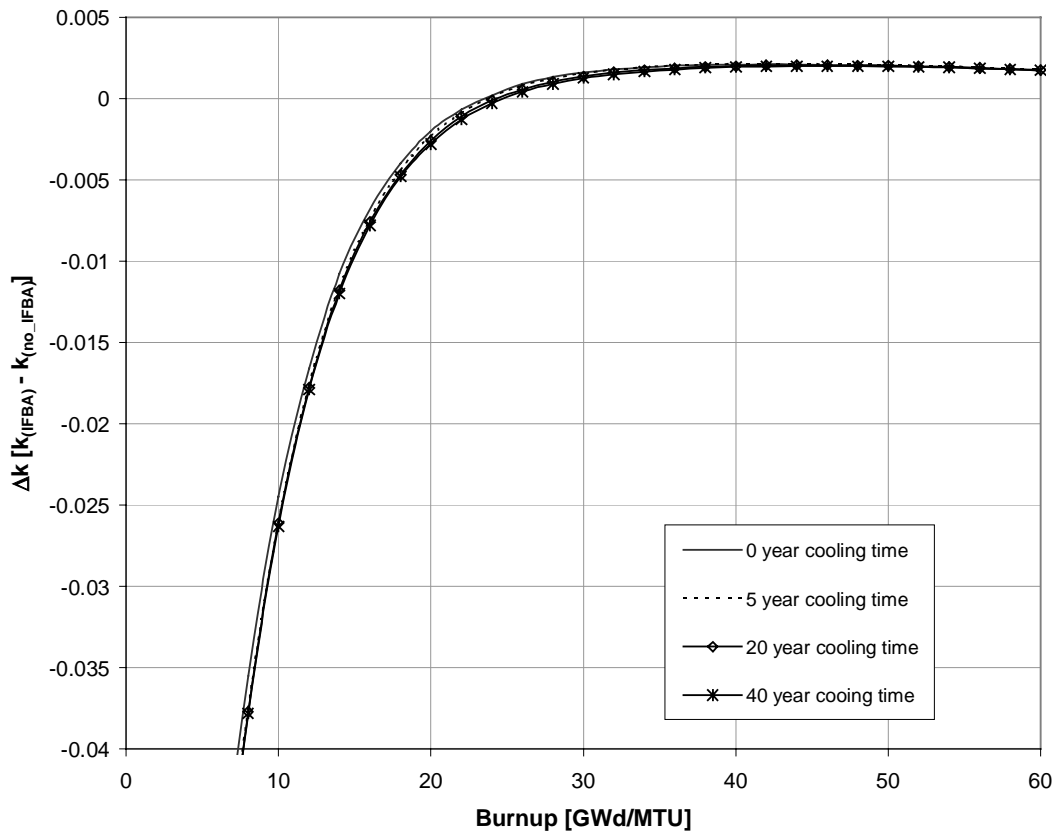


Figure 44 Comparison of Δk values as a function of burnup and cooling time between assemblies with and without IFBA rods (104 IFBA rods) for and initial enrichment of 4.0 wt % ²³⁵U

3.3.5.4 Reactivity Behavior in a Poisoned Storage Cell

The presence of fixed absorbers (e.g., boral panels), which are commonly used in SNF storage cells, affect the neutron spectrum; and thus, their presence can be an important consideration in burnup credit analyses. This is particularly true when estimating the reactivity worth of thermal neutron absorbers (e.g., fission products) because the absorbers compete for neutrons with the poison (e.g., boron) in the fixed absorber panels. For example, it has been shown that the reactivity worth of fission products is reduced by the presence of fixed absorber panels,¹¹ as compared to estimates of the reactivity worth of fission products in a configuration without fixed absorbers panels (e.g., an infinite pin lattice). To evaluate the impact of fixed absorbers, a number of the HELIOS calculations were repeated using an infinite array of poisoned storage cells from the GBC-32 cask, which is a generic 32-PWR assembly cask developed to be representative of actual burnup credit casks designed by industry. The boron loading in the boral panels in the GBC-32 cask is 0.225 g $^{10}\text{B}/\text{cm}^2$; detailed specifications for the GBC-32 cask are available in Ref. 12.

Calculations were performed for the Westinghouse 17×17 design with various IFBA loading and initial fuel enrichments, and the Δk values were compared to the Δk values from the IFBA calculations, which were based on an infinite array of assemblies. The results (Δk as a function of burnup) are shown in Figure 45, where it can be seen that the reactivity effects are nearly the same in both environments. The cask environment produces slightly higher Δk , especially early in burnup, because the residual IBA material competes with the poison in the absorber panels for thermal neutrons, thereby reducing the relative reactivity worth of the fixed absorber panels. The maximum positive Δk values for the various IFBA cases modeled in a cask environment are summarized in Table 9.

The Siemens M1 and M3 designs were also modeled in the GBC-32 cell. The results (Δk as a function of burnup) are shown in Figure 46, where it can be seen that the Δk values are less negative in the storage cell geometry. However, the Δk values do remain negative throughout burnup.

While only the results for the IFBA and $\text{UO}_2\text{-Gd}_2\text{O}_3$ IBA designs are presented here, studies for all the IBA designs were performed in the poisoned storage cell. The results from these calculations confirm the validity of the infinite assembly array calculations. However, it is noted that the positive Δk effect of IFBAs is slightly larger in the poisoned storage cell.

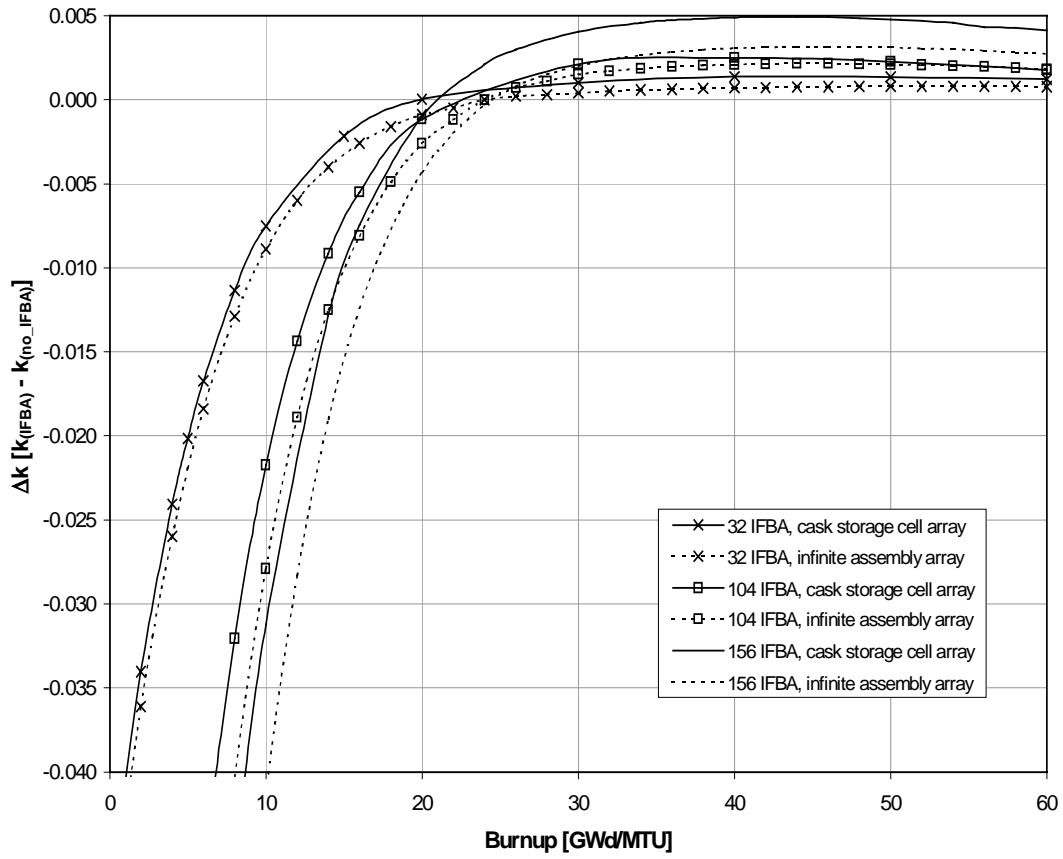


Figure 45 Comparison of Δk values as a function of burnup for IFBA assemblies in differing geometric configurations

Table 9 Summary of maximum positive Δk values observed for IFBA cases in a cask environment

IFBA loading pattern	Enrichment (wt % ^{235}U)		
	3.0	4.0	5.0
32	0.0014	0.0013	0.0012
80	0.0024	0.0020	0.0018
104	0.0029	0.0025	0.0021
156	0.0054	0.0049	0.0044

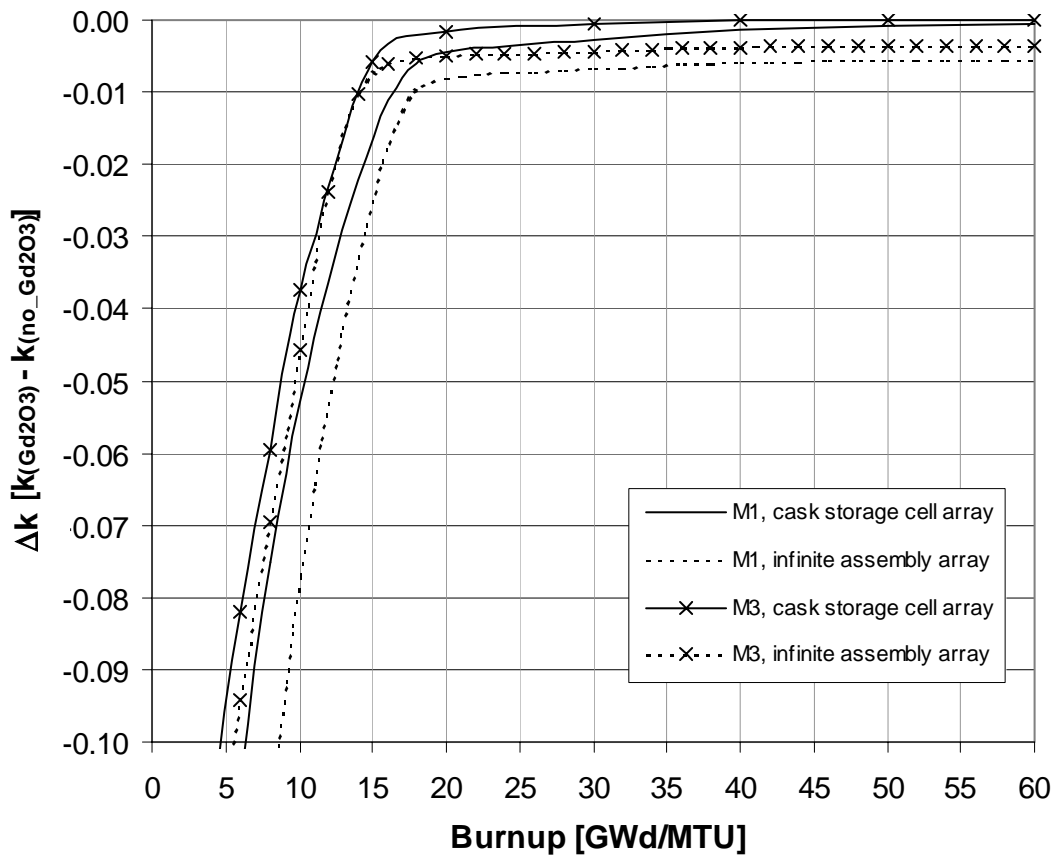


Figure 46 Comparison of Δk values as a function of burnup for assemblies with $\text{UO}_2\text{-Gd}_2\text{O}_3$ rods in differing geometric configurations

3.3.5.5 Axial Burnup

To evaluate the effect of IBAs with an axial burnup distribution present, a few 3-D criticality calculations were performed using the KENO V.a module of the SCALE system,¹³ employing spent fuel isotopics calculated by HELIOS. The KENO V.a criticality calculations used the 238-group cross-section library, which is based primarily on ENDF/B-V data. For this analysis, the GBC-32 cask and Westinghouse 17 × 17 assembly with 4.0 wt % ²³⁵U initial enrichment were used. Calculations were performed for (1) a fuel assembly with 104 IFBA rods (poison loading of 1.57 mg ¹⁰B/in.) and (2) a fuel assembly with no IFBA rods. The active fuel length of the assemblies was divided into 18 equal-length axial regions to facilitate the axial variation in SNF and IFBA coating compositions due to the axial burnup distribution. The axial profile suggested in Ref. 14 for PWR fuel with assembly-average discharge burnup greater than 30 GWd/MTU was used for this study.

While individual fuel pin (fuel and IFBA coating) compositions are tracked and utilized in the HELIOS depletion and criticality calculations, lattice-average compositions (for both fuel and IFBA coating) were used in the KENO V.a calculations. With this approximation, the KENO V.a calculations include lattice-average fuel and IFBA coating compositions for each of the 18 axial fuel regions modeled [(1 UO₂ fuel pin composition) + (1 IFBA coating composition) × (18 axial regions) = 36 fuel-related compositions], as opposed to separate fuel and IFBA compositions for each axial region of each fuel pin [neglecting symmetry, (264 UO₂ fuel pin compositions) + (104 IFBA coating compositions) × (18 axial regions) = 6624 fuel-related compositions]. Therefore, the following KENO V.a calculations and comparisons contain an approximation and associated uncertainty that is not present in the previous HELIOS comparisons.

The KENO criticality calculations were performed with subsets of the available nuclides compositions from HELIOS. The use of a subset of actinides in burnup credit calculations is referred to as “actinide-only” burnup credit. The nuclides used here for actinide-only calculations are consistent with those specified in a Department of Energy (DOE) Topical Report on burnup credit,¹⁴ with the exception that ²³⁶U and ²³⁷Np are also included. The use of a subset of actinides and fission products is referred to herein as “actinide + fission product” burnup credit. The fission product nuclides used here for actinide + fission product calculations are consistent with those identified in Table 2 of Ref. 15 as being the most important for criticality calculations.

Table 10 displays the results from calculations assuming the IFBA coating extends the entire length of the fuel (i.e., 144 inches), and shows that the cases with IFBA rods present yield a slightly lower effective neutron multiplication factor, k_{eff} , than the cases without IFBA rods. This is due to the residual IBA material in the underburned end regions, which dominate the neutron multiplication in the SNF. Hence, the difference between cases with and without IFBAs decreases with burnup; for high burnups (e.g., 60 GWd/MTU) the difference is very small.

A review of the relevant literature, however, indicates that the IFBA coating seldom (if ever) extends over the entire active fuel length. Rather, the IFBA coating may vary in axial location and length depending on particular core design requirements. Reference 16 indicates that the typical IFBA coating (or stack) length is in the range of 116 to 134 inches, while Ref. 17 cites a minimum IFBA coating length of 108 inches. Therefore additional calculations were performed for reduced IFBA coating lengths of 120 and 108 inches, assuming the IFBA coating is centered with respect to the active fuel length. The results for the cases corresponding to 120 and 108-inch IFBA coating lengths are given in Tables 11 and 12, respectively. The results in Tables 11 and 12 show that for these shorter IFBA coating lengths, a case with IFBA rods can yield higher k_{eff} values than a corresponding case without IFBA rods. Further, the results in Tables 10–12 demonstrate that as the IFBA length decreases, the difference (Δk) between cases with and without IFBA

rods present becomes positive earlier in burnup. This is because the lower-burnup end regions no longer contain any residual IBA material due to the shorter IFBA coating lengths.

These results are important because they show that the small positive effect for fuel with IFBA rods that was shown with 2-D calculations (infinite radial assembly arrays and infinite radial arrays of assemblies in poisoned storage cells) does not exist in a 3-D cask model that includes the axial burnup distribution and full-length axial poison loading. However, the results also show that the effect of the IFBA rods is dependent on the axial length of the poison loading; for typical IFBA coating lengths (i.e., 116 to 134 inches) there is a small positive effect associated with the IFBA rods. Finally, the results support the expectation that assemblies with the other types of IBAs over the full axial length of the fuel are less reactive, as compared to assemblies without IBAs, than what was shown with the 2-D calculations.

Table 10 Comparison of k_{eff} results in the GBC-32 cask for fuel with full-length (144 inch) IFBA rods when the axial burnup distribution is included

Burnup (GWd/MTU)	$k_{eff} \pm 1-\sigma$		Δk ($k_{IFBA} - k_{no_IFBA}$)
	Reference case (no IFBAs present)	IFBA case (104 IFBAs present)	
Actinide-only			
15	1.0621 \pm 0.0006	1.0518 \pm 0.0006	-0.0103 \pm 0.0008
30	0.9933 \pm 0.0006	0.9844 \pm 0.0005	-0.0089 \pm 0.0008
45	0.9419 \pm 0.0005	0.9350 \pm 0.0005	-0.0069 \pm 0.0007
60	0.8959 \pm 0.0006	0.8934 \pm 0.0006	-0.0025 \pm 0.0008
Actinides and fission products			
15	1.0235 \pm 0.0006	1.0137 \pm 0.0005	-0.0098 \pm 0.0008
30	0.9406 \pm 0.0005	0.9336 \pm 0.0006	-0.0070 \pm 0.0008
45	0.8782 \pm 0.0006	0.8729 \pm 0.0006	-0.0053 \pm 0.0009
60	0.8223 \pm 0.0007	0.8209 \pm 0.0007	-0.0014 \pm 0.0010

Table 11 Comparison of k_{eff} results in the GBC-32 cask for fuel with IFBA rods when the axial burnup distribution is included and the IFBA coating corresponds to the central 120 inches of the axial fuel length

Burnup (GWd/MTU)	$k_{eff} \pm 1-\sigma$		Δk ($k_{IFBA} - k_{no_IFBA}$)
	Reference case (no IFBAs present)	IFBA case (104 IFBAs present)	
Actinide-only			
15	1.0621 \pm 0.0006	1.0530 \pm 0.0006	-0.0091 \pm 0.0008
30	0.9933 \pm 0.0006	0.9872 \pm 0.0006	-0.0061 \pm 0.0008
45	0.9419 \pm 0.0005	0.9496 \pm 0.0006	0.0077 \pm 0.0008
60	0.8959 \pm 0.0006	0.9045 \pm 0.0006	0.0086 \pm 0.0008
Actinides and fission products			
15	1.0235 \pm 0.0006	1.0155 \pm 0.0005	-0.0080 \pm 0.0008
30	0.9406 \pm 0.0005	0.9357 \pm 0.0006	-0.0049 \pm 0.0008
45	0.8782 \pm 0.0006	0.8843 \pm 0.0006	0.0061 \pm 0.0008
60	0.8223 \pm 0.0007	0.8295 \pm 0.0006	0.0072 \pm 0.0008

Table 12 Comparison of k_{eff} results in the GBC-32 cask for fuel with IFBA rods when the axial burnup distribution is included and the IFBA coating corresponds to the central 108 inches of the axial fuel length

Burnup (GWd/MTU)	$k_{eff} \pm 1-\sigma$		Δk ($k_{IFBA} - k_{no_IFBA}$)
	Reference case (no IFBAs present)	IFBA case (104 IFBAs present)	
Actinide-only			
15	1.0621 \pm 0.0006	1.0566 \pm 0.0006	-0.0055 \pm 0.0008
30	0.9933 \pm 0.0006	0.9996 \pm 0.0006	0.0063 \pm 0.0008
45	0.9419 \pm 0.0005	0.9501 \pm 0.0006	0.0082 \pm 0.0008
60	0.8959 \pm 0.0006	0.9048 \pm 0.0006	0.0089 \pm 0.0008
Actinides and fission products			
15	1.0235 \pm 0.0006	1.0213 \pm 0.0007	-0.0022 \pm 0.0008
30	0.9406 \pm 0.0005	0.9476 \pm 0.0006	0.0070 \pm 0.0008
45	0.8782 \pm 0.0006	0.8857 \pm 0.0005	0.0075 \pm 0.0008
60	0.8223 \pm 0.0007	0.8304 \pm 0.0006	0.0081 \pm 0.0008

4 SUMMARY AND IMPLICATIONS

Numerous IBA types have been used in commercial nuclear fuel assembly designs to suppress initial reactivity. Variations in the IBA poison material, composition, placement within rods, and rod configurations exist among current PWR IBA fuel assembly designs. These IBA characteristics are varied in combination with the initial fuel assembly enrichment and core location to achieve core operating and fuel management goals. To assess the potential impact of these IBAs on the reactivity of SNF, analyses have been presented in this report for all IBA types widely used in U.S. PWRs. These IBA types include IFBA rods, $\text{UO}_2\text{-Gd}_2\text{O}_3$ rods, $\text{UO}_2\text{-Er}_2\text{O}_3$ rods, and $\text{Al}_2\text{O}_3\text{-B}_4\text{C}$ rods. Based on the available data, analyses were performed for a realistic range of fuel initial enrichment and poison loading combinations based on actual assemblies.

Assemblies with IBAs are designed such that the poison material is effectively depleted during the first third of the assembly life. As a result, depending on the IBA type and loading, the assembly reactivity may actually increase with burnup to a maximum or peak at which the IBA is essentially depleted. At this point (or beyond), the reactivity of an assembly with IBAs may equal or exceed the reactivity of a nonpoisoned equivalent enrichment assembly. To determine if any of the assemblies with IBAs exceed the reactivity of nonpoisoned equivalent enrichment assemblies, this evaluation compared k_{inf} values, throughout burnup, between fuel assemblies with and without IBAs. The premise was that if assemblies with IBAs yield lower k_{inf} values (throughout burnup) than assemblies without IBAs, burnup credit criticality safety analyses may conservatively neglect the presence of IBAs. Thus, for each unique IBA assembly design considered, a calculation was performed for (1) the actual assembly specification (including the presence of the IBA) and (2) an artificial condition in which the IBA was neglected (nonpoisoned equivalent enrichment case). The difference between the calculated k_{inf} values (Δk) from these two cases was used to assess the reactivity effect of each of the IBA types.

First, 2-D analyses were performed for Westinghouse assembly designs with IFBA rods, including varying numbers of IFBA rods, varying boron loadings, and various initial fuel enrichments. The results (as a function of burnup) indicate that the k_{inf} values for fuel assemblies containing IFBA rods may exceed the k_{inf} values for fuel assemblies without IFBA rods. In fact, all IFBA assembly designs considered were shown to have a small, positive reactivity effect, as compared to assemblies without IFBA rods. For a fixed initial fuel enrichment, the positive reactivity effect was shown to increase with increasing poison loading (i.e., both increasing ^{10}B loading and increasing number of IFBA rods). Additionally, for a fixed poison loading, the positive reactivity effect was shown to increase with decreasing initial fuel enrichment. For all of the IFBA cases considered, the maximum positive Δk value was found to be $\sim 0.5\%$. However, this maximum value corresponds to a very heavily poisoned, atypical assembly design and, based on the available data, is not representative of typical IFBA assemblies. The positive reactivity effect for typical IFBA assembly designs (designs that are used in significant numbers) appears to be less than $\sim 0.3\%$.

Second, analyses were performed for assembly designs with $\text{UO}_2\text{-Gd}_2\text{O}_3$ rods, including variations in gadolinia loadings (wt % Gd_2O_3 and number of gadolinia-bearing rods) and initial fuel enrichment. The calculations showed that, throughout burnup, the k_{inf} values for fuel assemblies containing $\text{UO}_2\text{-Gd}_2\text{O}_3$ rods remain less than the k_{inf} values for fuel assemblies without $\text{UO}_2\text{-Gd}_2\text{O}_3$ rods. Therefore, it is concluded that gadolinia-bearing rods yield a negative reactivity effect. The negative reactivity effect was found to increase with increasing gadolinia loading (wt % Gd_2O_3 and number of gadolinia-bearing rods) and increasing initial fuel enrichment. For all of the actual fuel assembly designs considered, the k_{inf} values for fuel assemblies with gadolinia-bearing rods were always less (by as much as 0.5%) than the k_{inf} values for fuel assemblies without gadolinia-bearing rods.

Third, analyses were performed for assembly designs with $\text{UO}_2\text{-Er}_2\text{O}_3$, including variations in the number of $\text{UO}_2\text{-Er}_2\text{O}_3$ rods. For the assembly designs considered, the k_{inf} values for the non-erbia-bearing fuel assemblies consistently remained higher than the k_{inf} values for the erbia-bearing fuel assemblies. The amount by which the k_{inf} values for the erbia-bearing fuel were less than the k_{inf} values for the non-erbia-bearing fuel increased with increasing numbers of $\text{UO}_2\text{-Er}_2\text{O}_3$ rods. Therefore, it is concluded that erbia-bearing rods yield a negative reactivity effect.

Finally, analyses were performed for assembly designs with $\text{Al}_2\text{O}_3\text{-B}_4\text{C}$ rods, including variations in the number $\text{Al}_2\text{O}_3\text{-B}_4\text{C}$ rods. For the assembly designs considered, the k_{inf} values for the fuel assemblies with $\text{Al}_2\text{O}_3\text{-B}_4\text{C}$ rods consistently remained lower than the k_{inf} values for the fuel assemblies without $\text{Al}_2\text{O}_3\text{-B}_4\text{C}$ rods. The amount by which the k_{inf} values for the fuel assemblies with $\text{Al}_2\text{O}_3\text{-B}_4\text{C}$ rods were less than the k_{inf} values for the fuel assemblies without $\text{Al}_2\text{O}_3\text{-B}_4\text{C}$ rods increased with increasing numbers of $\text{Al}_2\text{O}_3\text{-B}_4\text{C}$ rods. Therefore, it is concluded that $\text{Al}_2\text{O}_3\text{-B}_4\text{C}$ rods yield a negative reactivity effect.

In summary, the analyses presented in Sections 3.3.1–3.3.4 demonstrate that the neutron multiplication factor for an assembly without IBAs is always greater (as a function of burnup) than the neutron multiplication factor for an assembly using any of the following IBA types: $\text{UO}_2\text{-Gd}_2\text{O}_3$, $\text{UO}_2\text{-Er}_2\text{O}_3$, or $\text{Al}_2\text{O}_3\text{-B}_4\text{C}$ rods. Conversely, the neutron multiplication factor for an assembly with IFBA rods present was found to exceed (maximum of 0.4% Δk) the neutron multiplication factor for an assembly without IFBA rods. Therefore, neglecting the IBAs in a burnup-credit criticality safety analysis will yield conservative results for assembly designs with $\text{UO}_2\text{-Gd}_2\text{O}_3$, $\text{UO}_2\text{-Er}_2\text{O}_3$, or $\text{Al}_2\text{O}_3\text{-B}_4\text{C}$ IBA rods and nonconservative results for assembly designs with IFBA rods. In all cases, for burnups characteristic of discharge, the reactivity effect of IBAs is relatively small (less than $\sim 1.0\%$ Δk) and generally well behaved.

These results are consistent with previous work, which provided illustrative examples of the reactivity effects of several of the IBA types based on a 2-D analysis of a single case for each type.³ However, 3-D cask calculations performed for this study (Section 3.3.5.5) demonstrated that when the axial burnup distribution is included, assemblies with IFBA rods are actually less reactive than corresponding assemblies without IFBA rods because of the residual absorber in the low-burnup end regions. The amount by which the IFBA assemblies are less reactive decreases with burnup, as the residual absorber in the end regions is depleted. This finding supports the expectation that assemblies with the other types of IBAs over the full axial length are also less reactive than what was shown with the 2-D calculations. However, the results also show that the effects of the IFBA rods is dependent on the axial length of the poison loading and that for typical IFBA coating lengths (i.e., 116 to 134 inches) there is a small positive effect associated with the IGBA rods.

These results are important to burnup credit because they demonstrate that assembly designs with IFBA $\text{UO}_2\text{-Gd}_2\text{O}_3$, $\text{UO}_2\text{-Er}_2\text{O}_3$, or $\text{Al}_2\text{O}_3\text{-B}_4\text{C}$ IBA rods are less reactive throughout burnup than their corresponding designs without the IBA rods (i.e., nonpoisoned equivalent enrichment). Consequently, with the notable exception of assemblies with IFBA rods, neglecting the presence of IBAs in a burnup credit criticality safety evaluation will yield slightly conservative results. For assembly designs with IFBA rods, the positive reactivity effect is small and dependent on the axial length of the IFBA coating.

5 RECOMMENDATIONS

The analyses presented in this report provide a technical basis for revising NRC's Interim Staff Guidance (Ref. 2) to allow burnup credit for assembly designs with IBAs. Although the analyses do not address the issue of validation of depletion methods for assembly designs with IBAs, they do demonstrate that the effect of the IBAs is relatively small (at or near target discharge burnups) and generally well behaved. Furthermore, the recommended approaches for addressing fuel assemblies with IBAs, as described below, do not involve explicit analyses with IBAs present and thus do not necessitate validation of the depletion methods for assembly designs with IBAs. Therefore, it is concluded that the effect of the various IBA types may be adequately calculated and that the current restriction on assemblies with IBAs should be eliminated.

The analyses described in this report conclusively demonstrate that, with the exception of the Westinghouse IFBA rods, the neutron multiplication factor for an assembly without IBAs is always greater (throughout burnup) than the neutron multiplication factor for an assembly with IBAs, including $\text{UO}_2\text{-Gd}_2\text{O}_3$, $\text{UO}_2\text{-Er}_2\text{O}_3$, and $\text{Al}_2\text{O}_3\text{-B}_4\text{C}$ rods. Therefore, for those IBAs other than IFBAs, burnup credit criticality safety analyses may simply and conservatively neglect the presence of the IBAs by assuming nonpoisoned equivalent enrichment fuel. Considering the variations in IBA assembly designs, neglecting the presence of the IBAs is an important simplifying assumption that does not add significant unnecessary conservatism.

For assembly designs with IFBA rods, 2-D (radially infinite) calculations have demonstrated that the neutron multiplication factor is slightly greater (maximum of 0.4% Δk) than the neutron multiplication factor for assembly designs without IFBA rods. Three-dimensional cask calculations showed that when the axial burnup distribution is included, assemblies with full-axial length IFBA coatings are less reactive than corresponding assemblies without IFBA rods, because of the residual absorber in the low-burnup end regions. However, the results also indicated that the effect of the IFBA rods is dependent on the axial length of the poison loading and that for typical IFBA coating lengths (i.e., 116 to 134 inches), there is a small positive effect associated with the IFBA rods. Consequently, the positive reactivity effect due to the presence of IFBA rods should be considered in any burnup-credit criticality safety analysis seeking to qualify IFBA assemblies as acceptable contents. Due to the significant variations in IFBA assembly designs, simple strategies for addressing the positive reactivity effect are desirable. Two possible strategies for consideration include: (1) the inclusion of a small reactivity bias to bound the effect of the IFBA rods, or (2) demonstration that the effect of the IFBA rods is bounded by the effect of other modeling assumptions (e.g., BPR exposure). The use of a reactivity bias will require justification for the value of the bias. Alternatively, it may be simpler and less burdensome to demonstrate that the effect of the IFBA rods is bounded by the BPR modeling approach. Comparison of the reactivity effect of IFBA rods (shown in this report) to the reactivity effect of BPRs (as quantified in Ref. 1), clearly demonstrates that the reactivity effect of the IFBA rods is significantly less than the reactivity effect due to BPRs. Furthermore, considering the fact that BPRs are seldom used within assemblies that have IFBA rods, and when used, are employed in a limited way (e.g., a small number of BPRs may be used in conjunction with an assembly that has a relatively light IFBA loading), reliance on the BPR modeling to account for the effect of IFBA rods is justified. However, this approach would only be applicable to analyses that consider BPR exposure.

6 REFERENCES

1. J. C. Wagner and C. V. Parks, "Impact of Burnable Poison Rods on PWR Burnup Credit Criticality Safety Analyses," *Trans. Am. Nucl. Soc.* **83**, 130–134 (2000).
2. "Spent Fuel Project Office Interim Staff Guidance – 8, Rev. 1 – Limited Burnup Credit," U.S. Nuclear Regulatory Commission, July 30, 1999.
3. P. M. O’Leary and M. L. Pitts, "Effects of Integral Burnable Absorbers on PWR Spent Nuclear Fuel," *Trans. Am. Nucl. Soc.* **83**, November 2000.
4. J. J. Casal, R. J. J. Stamm’ler, E. A. Villarino, and A. A. Ferri, "HELIOS: Geometric Capabilities of a New Fuel-Assembly Program," Vol. 2, p. 10.2.1 113 in *Proc. International Topical Meeting on Advances in Mathematics, Computations, and Reactor Physics*, April 28–May 2, 1991, Pittsburgh, PA.
5. R. J. Cacciapouti and S. Van Volkinburg, *Axial Burnup Profile Database for Pressurized Water Reactors*, YAEC-1937, Yankee Atomic Electric Company, Auburn, MA, May 1997.
6. M. A. Tremblay and J. P. Gorski, *Seabrook Station Cycle 5 Nuclear Design Report*, YAEC-1927, Yankee Atomic Electric Company, Auburn, MA, November 1995.
7. M. Schlieck, H.-D. Borger, and A. Neufert, "Optimized Gadolinia Concepts for Advanced in-Core Fuel Management in PWRs," *Nucl. Eng. Des.* **205**, 191 (2001).
8. *System Description for Reactor Core for Ulchin 5&6 Nuclear Power Plants*, N0696-RE-SD280, KOPEC, 1997.
9. Calvert Cliffs Nuclear Power Plant UFSAR, Rev. 26 Constellation Nuclear.
10. R. J. Ellis, *System Definition Document: Reactor Data Necessary for Modeling Plutonium Disposition in Catawaba Nuclear Station Units 1 and 2*, ORNL/TM-1999/255, UT-Battelle, LLC, Oak Ridge National Laboratory, November 2000.
11. D. E. Carlson, C. J. Withee and C. V. Parks, "Spent Fuel Burnup Credit in Casks: An NRC Perspective," pp. 419–436 in *Proc. of the Twenty-Seventh Water Reactor Safety Information Meeting*, NUREG/CP-0169, U.S. Nuclear Regulatory Commission, October 25–27, 1999, Bethesda, MD, March 2000.
12. J. C. Wagner, *Computational Benchmark for Estimation of Reactivity Margin from Fission Products and Minor Actinides in PWR Burnup Credit*, NUREG/CR-6747 (ORNL/TM-2000/306), U.S. Nuclear Regulatory Commission, Oak Ridge National Laboratory, September 2001.
13. *SCALE: A Modular Code System for Performing Standardized Computer Analysis for Licensing Evaluation*, NUREG/CR-0200, Rev. 6 (ORNL/NUREG/CSD-2/R6), Vols. I, II, and III, May 2000. Available from Radiation Safety Information Computational Center at Oak Ridge National Laboratory as CCC-545.

14. *Topical Report on Actinide-Only Burnup Credit for PWR Spent Nuclear Fuel Packages*, DOE/RW-0472, Rev. 2, U.S. Department of Energy, Office of Civilian Radioactive Waste Management, Washington, D.C., September 1998.
15. C. V. Parks, M. D. DeHart, and J. C. Wagner, *Review and Prioritization of Technical Issues Related to Burnup Credit for LWR Fuel*, NUREG/CR-6665 (ORNL/TM-1999/303), U.S. Nuclear Regulatory Commission, Oak Ridge National Laboratory, February 2000.
16. S. E. Cunningham, M. G. Balfour, R. S. Miller, and H. W. Keller, “ZrB₂ Integral Fuel Burnable Absorber Rod Performance,” pp. 343–347 in *Proc. of the International Topical Meeting on LWR Fuel Performance*, April 17–20, 1988, Williamsburg, VA.
17. W. A. Boyd, R. F. Schmidt, R. D. Erwin, R. R. Wojnarowski, and J. D. Martin, “IFBA Credit in the Shearon Harris Fuel Racks with Vantage 5 Fuel,” pp. 304–311 in *Proc. of the International Topical Meeting on Safety Margins in Criticality Safety*, November 26–30, 1989, San Francisco, CA.

INTERNAL DISTRIBUTION

1. S. M. Bowman, 6011, MS-6370
2. B. L. Broadhead, 6011, MS-6370
3. W. C. Carter, 6011, MS-6370
4. M. D. DeHart, 6011, MS-6370
5. M. E. Dunn, 6011, MS-6370
6. K. R. Elam, 6011, MS-6370
7. R. J. Ellis, 6025, MS-6363
8. M. B. Emmett, 6011, MS-6370
9. I. C. Gauld, 6011, MS-6370
10. J. C. Gehin, 6025, MS-6363
11. S. Goluoglu, 6011, MS-6370
12. D. F. Hollenbach, 6011, MS-6370
13. C. M. Hopper, 6011, MS-6370
14. D. T. Ingersol, 6025, MS-6363
15. B. L. Kirk, 6025, MS-6362
16. M. A. Kuliasha, 6025, MS-6435
17. A. Loebel, 6025, MS-6435
18. S. B. Ludwig, NTRC, MS-6472
19. G. E. Michaels, 4500N, MS-6210
20. C. I. Moser, 4500N, MS-6199
21. B. D. Murphy, 6011, MS-6370
22. C. V. Parks, 6011, MS-6370
23. L. M. Petrie, 6011, MS-6370
24. R. T. Primm III, 6025, MS-6363
25. B. T. Rearden, 6011, MS-6370
26. J.-P. Renier, 6025, MS-6363
27. C. E. Sanders, 6011, MS-6370
28. J. G. Simpson, 4500N, MS-6210
29. J. C. Wagner, 6011, MS-6370
30. R. M. Westfall, 6011, MS-6370
31. Laboratory Records-RC
4500N, MS-6285
32. Central Research Library
4500N, MS-6191
- 33–50. Return extra ORNL copies to:
W. C. Carter, 6011, MS-6370

EXTERNAL DISTRIBUTION

51. M. L. Anderson, Bechtel SAIC Company, LLC, 1261 Town Center Drive, Las Vegas, Nevada 89134
52. S. Anton, Holtec International, 555 Lincoln Drive West, Marlton, NJ 08053
53. A. C. Attard, U.S. Nuclear Regulatory Commission, NRR/DSSA/SRXB, MS O10-B1, Washington, DC 20555
54. M. G. Bailey, U.S. Nuclear Regulatory Commission, NMSS, MS T8-A23, Washington, DC 20555-0001
55. A. S. Barto, U.S. Nuclear Regulatory Commission, NMSS/SFPO/TRA, MS O13-D13, Washington, DC 20555-0001
56. C. J. Benson, Bettis Atomic Power Laboratory, P.O. Box 79, West Mifflin, PA 15122
57. G. H. Biding, NUMEC, 17016 Cashell Road, Rockville, MD 20853
58. J. Boshoven, Transnuclear West, Inc., 39300 Civic Center Drive, Suite 280, Fremont, CA 94538
59. M. C. Brady Raap, Battelle, Pacific Northwest National Laboratory, P.O. Box 999 / MS K8-34, Richland, WA 99352

60. R. J. Cacciapouti, Duke Engineering and Services, 400 Donald Lynch Boulevard, Marlborough, MA 01752
61. D. E. Carlson, U.S. Nuclear Regulatory Commission, RES/DSARE/REAHFB, MS T10F-13A, Washington, DC 20555-0001
62. J. M. Conde López, Consejo de Seguridad Nuclear, Jefe de Area de Ingeniería Nuclear, Subdirección General de Tecnología Nuclear, Justo Dorado, 11, 28040 Madrid, Spain
63. D. R. Connors, Bettis Atomic Power Laboratory, P.O. Box 79, West Mifflin, PA 15122
64. P. Cousinou, Institut de Protection et de Sûreté Nucleaire, Département de Recherches en Sécurité, CECI B.P. 6 - 92265 Fontenzy-Aux-Roses, Cedex, France
65. T. W. Doering, Bechtel SAIC Company, LLC, 1261 Town Center Drive, Las Vegas, Nevada 89134
66. E. P. Easton, U.S. Nuclear Regulatory Commission, NMSS/SFPO/TRD, MS T9-F3, Washington, DC 20555-0001
67. F. Eltawila, U.S. Nuclear Regulatory Commission, NRR/DE, MS O9-E2, Washington, DC 20555-0001
68. K. T. Erwin, U.S. Nuclear Regulatory Commission, NMSS/SFPO/TRB, MS O13-D13, Washington, DC 20555-0001
69. L. R. Foulke, Bechtel Bettis, Inc., Bettis Atomic Power Laboratory, P.O. Box 79, West Mifflin, PA 15122
70. A. S. Giantelli, U.S. Nuclear Regulatory Commission, NMSS/SFPO/TRA, MS O13-D13, Washington, DC 20555-0001
71. R. N. B. Gmal, Gesellschaft für Anlagen-und Reaktorsicherheit (GRS) mbH, Leiter der Gruppe Kritikalität, Forschungsgelände, 85748 Garching b. München
72. P. Grimm, Paul Scherrer Institute, CH-5232 Villigen PSI, Switzerland
73. N. Gulliford, Winfrith Technology Centre, 306/A32, AEA Technology PLC, Winfrith, Dorchester, Dorset DT2 8DH, United Kingdom
74. J. Guttman, U.S. Nuclear Regulatory Commission, NMSS/SFPO/TRD, MS O13-D13, Washington, DC 20555-0001
75. A. Haghghat, Nuclear and Radiological Engineering Department, 202 Nuclear Sciences Building, University of Florida, P.O. Box 118300, Gainesville, FL 32611-8300
76. S. Hanauer, U.S. Department of Energy, RW-22, Washington, DC 20545
77. G. Harms, Sandia National Laboratory, PO Box 5800, Mail Stop 1143, Albuquerque, New Mexico 87185-1143
78. L. A. Hassler, Framatome ANP, 3315 Old Forest Road, P.O. Box 10935, Lynchburg, VA 24506-0935
79. D. Henderson, Framatome ANP, 3315 Old Forest Road, P.O. Box 10935, Lynchburg, VA 24506-0935
80. M. W. Hodges, U.S. Nuclear Regulatory Commission, NMSS/SFPO/TRD, MS O13-D13, Washington, DC 20555-0001
81. Hae Ryong Hwang, Radiation Safety Analysis Group, KOPEC, 150, Duckjin Dong, Taejon, South Korea 305-600
82. H. Kühl, Wissenschaftlich-Technische Ingenieurberatung GMBH, Karl-Heinz-Beckurts-Strasse 8, 52428 Jülich
83. W. H. Lake, Office of Civilian Radioactive Waste Management, U.S. Department of Energy, RW-46, Washington, DC 20585
84. D. B. Lancaster, Nuclear Consultants.com, 320 South Corl Street, State College, PA 16801

85. C. Lavarenne, Institut de Protection et de Sûreté Nucléaire, Department of Prevention and Studies of Accidents, Criticality Studies Division, CEA - 60-68, avenue de Général Leclerc, B.P. 6 - 92265, Fontenay - Aux - Roses, Cedex, France
- 86-90. R. Y. Lee, U.S. Nuclear Regulatory Commission, RES/DSARE/SMSAB, MS T10-K8, Washington, DC 20555-0001
91. W. J. Lee, NAC International, 655 Engineerig Drive, Norcross, GA 30092
92. M. Mason, Transnuclear, Two Skyline Drive, Hawthorne, NY 10532-2120
93. A. J. Machiels, Electric Power Research Institute, Advanced Nuclear Technology, Energy Conervation Division, 3412 Hillview Ave., Palo Alto, CA 94304-1395
94. L. Markova, Ustav jaderneho vyzkumu Rez, Theoretical Reactor Physics, Nuclear Research Institute, Czech Republic, 25068 REZ
95. Daniel Marloye, Belgonucléaire, Av. Ariane 4, B-1200, Brussels, Belgium
96. J. R. Massari, Constellation Nuclear Services, 2200 Defense Highway, Suite 405, Crofton, MD 21114-2404
97. C. W. Mays, Framatome ANP, 3315 Old Forest Road, P.O. Box 10935, Lynchburg, VA 24506-0935
98. J. N. McKamy, U.S. Department of Energy, Office of Engineering Assistance and Site Interface, EH-34, 19901 Germantown Rd., Germantown, MD 20874
99. N. B. McLeod, JAI Corporation, 4103 Chain Bridge Road, Suite 200, Fairfax, VA 22030
100. D. Mennerdahl, E. Mennerdahl Systems, Starvägen 12, S-183 57 Täby, Sweden
101. R. L. Murray, 8701 Murray Hill Drive, Raleigh, NC 27615
102. J. A. Myers, U. S. Nuclear Regulatory Commission, NMSS/SFPO/TRD, MS O13-D13, Washington, DC 20555-0001
103. K. A. Neimer, Duke Engineering & Services, 400 S. Tyron St., WC26B, P.O. Box 1004, Charlotte, NC 28201-1004
104. P. Noel, Bechtel SAIC Company, LLC, 1261 Town Center Drive, Las Vegas, Nevada 89134
105. I. Nojiri, Japan Nuclear Cycle Development Institute, Environment and Safety Division, Tokai Works, Muramatsu Tokai-mura, Naka-gun Ibaraki-ken 319-1194, Japan
106. J. C. Neuber, SIEMENS AG, KWU NS-B, Berliner Str. 295-303, D-63067 OFFENBACH AM MAIN, Germany
107. A. Nouri, OECD/NEA Data Bank, Le Seine-Saint Germain, 12 Boulevard des Iles, F-92130 Issy-les-Moulineaux, France
- 108-109. Office of Scientific and Technical Information, U.S. Department of Energy, P.O. Box 62, Oak Ridge, TN 37831
110. Office of the Assistant Manager for Energy Research and Development, Department of Energy Oak Ridge Operations (DOE-ORO), P.O. Box 2008, Oak Ridge, TN 37831
111. H. Okuno, Japan Atomic Energy Research Institute, Department of Fuel Cycle, Safety Research, 2-4 Shirakata-Shirane, 319-1195 Tokai-mura, Naka-Gun, Ibaraki-ken, Japan
112. P. M. O'Leary, Framatome ANP, 3315 Old Forest Road, P.O. Box 10935, Lynchburg, VA 24506-0935
113. J. R. Massari, Constellation Nuclear Services, 2200 Defense Highway, Suite 405, Crofton, MD 21114-2404
114. N. L. Osgood, U.S. Nuclear Regulatory Commission, Office of Nuclear Materials Safety and Safeguards, MS O13-D13, Washington, DC 20555-0001
115. T. Parish, Department of Nuclear Engineering, Texas A & M University, College Station, TX 77843-3313

116. V. A. Perin, U.S. Nuclear Regulatory Commission, NMSS/FCSS/SPB, MS T8-A33, Washington, DC 20555-0001
117. B. Petrovic, Westinghouse Electric Company, Science and Technology Department, 1344 Beulah Road, Pittsburgh, PA 15235
118. J. S. Philbin, Sandia National Laboratory, PO Box 5800, Mail Stop 1143, Albuquerque, New Mexico 87185-1143
119. M. L. Pitts, Framatome ANP, 3315 Old Forest Road, PO Box 10935, Lynchburg, VA 24506-0935
120. M. Rahimi, U.S. Nuclear Regulatory Commission, NMSS/DWM/HLWB, MS T7-F3, Washington, DC 20555-0001
121. E. L. Redmond II, Holtec International, 555 Lincoln Drive West, Marlton, NJ 08053
122. Frederik Reitsma, Reactor Theory, Building 1900, Pelindaba, NECSA, PO Box 582, 0001 PRETORIA, South Africa
123. C. Rombough, CTR Technical Services, Inc., 5619 Misty Crest Dr., Arlington, TX 76017-4147
124. J. E. Rosenthal, U.S. Nuclear Regulatory Commission, RES/DSARE/SMSAB, MS T10-K8, Washington, DC 20555-0001
125. D. Salmon, Bechtel SAIC Company, LLC, 1261 Town Center Drive, Las Vegas, Nevada 89134
126. A. Santamarina, Commissariat A L'Energie Atomique, Nuclear Reactor Division, Reactor Studies Department, Reactor and Cycle Physics Service, CEA/CADARACHE/DRN/DER/SPRC Bat. 230, 13108 Saint-Paul-Lez-Durance, Cedex, France
127. E. Sartori, OECD/NEA Data Bank, Le Seine-Saint Germain, 12 Boulevard des Iles, F-92130 Issy-les-Moulineaux, France
128. J. J. Sapyta, Framatome ANP, 3315 Old Forest Road, P.O. Box 10935, Lynchburg, Virginia 24506-0935
129. D. Schrire, Hot Cell Laboratory, Studsvik Nuclear, Nyköping 61182, Sweden
130. H. H. Schweer, Bundesamt fuer Strahlenschutz, Willi Brandt Str. 5, D-38226 SALZGITTER, Germany
131. M. Smith, Virginia Power Co., P.O. Box 2666, Richmond, VA 23261
132. N. R. Smith, AEA Technology, A32 Winfrith, Dorchester, Dorset DT2 8DH, United Kingdom
133. Rudi Stamm'ler, Studsvik Scandpower AS, Gasevikveien 2, P O Box 15, NO-2027 Kjeller Norway
134. J. T. Stewart, Department of Environment, Transport, and Re, RMTD, 4/18, GMH, 76 Marsham Street, London SW1P 4DR, United Kingdom
135. T. Suto, Power Reactor and Nuclear Fuel Development Corporation, Technical Service Division, Tokai Reprocessing Plant, Tokai Works, Tokai-Mura, Naka-gun, Ibaraki-ken, Japan
136. H. Taniuchi, Kobe Steel, Ltd., 2-3-1 Shinhamma, Arai-Cho, Takasago, 676 Japan
137. D. A. Thomas, Bechtel SAIC Company, LLC, 1261 Town Center Drive, Las Vegas, Nevada 89134
138. P. R. Thorne, British Nuclear Fuels plc (BNFL), Nuclear and Radiological Safety, R101 Rutherford House, Risley Warrington WA3 6AS, United Kingdom
139. J. R. Thornton, Duke Engineering & Services, 230 S. Tyron St., P.O. Box 1004, Charlotte, NC 28201-1004
140. S. E. Turner, Holtec International, 230 Normandy Circle East, Palm Harbor, FL 34683
141. A. P. Ulses, U.S. Nuclear Regulatory Commission, NRR/DSSA/SRXB, MS O10-B3, Washington, DC 20555-0001

142. M. E. Wangler, U.S. Department of Energy, EH-33.2, Washington, DC 20585-0002
143. M. D. Waters, U.S. Nuclear Regulatory Commission, NMSS/SFPO/SLID, MS O13-D13, Washington, DC 20555-0001
144. A. Wells, 2846 Peachtree Walk, Duluth, GA 30136
145. S. A. Whaley, U.S. Nuclear Regulatory Commission, NMSS/SFPO/TRD, MS O13-D13, Washington, DC 20555-0001
146. B. H. White, U.S. Nuclear Regulatory Commission, NMSS/SFPO/TRD, MS O13-D13, Washington, DC 20555-0001
147. R. Wilson, Rocky Flats Field Office, USDOE, 10808 Highway 93, Golden, CO 80403-8200
148. C. J. Withee, U.S. Nuclear Regulatory Commission, NMSS/SFPO/TRD, MS O13-D13, Washington, DC 20555-0001

NRC FORM 335 (2-89) NRCM 1102 3201, 3202	U.S. NUCLEAR REGULATORY COMMISSION BIBLIOGRAPHIC DATA SHEET <i>(See instructions on the reverse)</i>	1. REPORT NUMBER (Assigned by NRC, Add Vol., Supp., Rev., and Addendum Numbers, if any.) NUREG/CR-6760 ORNL/TM-2000/321				
2. TITLE AND SUBTITLE Study of the Effect of Integral Burnable Absorbers for PWR Burnup Credit	3. DATE REPORT PUBLISHED	<table border="1"> <tr> <td style="text-align: center;">MONTH</td> <td style="text-align: center;">YEAR</td> </tr> <tr> <td style="text-align: center;">March</td> <td style="text-align: center;">2002</td> </tr> </table>	MONTH	YEAR	March	2002
	MONTH	YEAR				
	March	2002				
4. FIN OR GRANT NUMBER W6479						
5. AUTHOR(S) C. E. Sanders and J. C. Wagner	6. TYPE OF REPORT Technical					
	7. PERIOD COVERED <i>(Inclusive Dates)</i>					
8. PERFORMING ORGANIZATION — NAME AND ADDRESS <i>(If NRC, provide Division, Office or Region, U.S. Nuclear Regulatory Commission, and mailing address; if contractor, provide name and mailing address.)</i> Oak Ridge National Laboratory Managed by UT-Battelle, LLC Oak Ridge, TN 37831-6370						
9. SPONSORING ORGANIZATION — NAME AND ADDRESS <i>(If NRC, type "Same as above"; if contractor, provide NRC Division, Office or Region, U.S. Regulatory Commission, and mailing address.)</i> Division of Systems Analysis and Regulatory Effectiveness Office of Nuclear Regulatory Research U.S. Nuclear Regulatory Commission Washington, DC 20555-0001						
10. SUPPLEMENTARY NOTES R. Y. Lee, NRC Project Manager						
11. ABSTRACT <i>(200 words or less)</i> <p>The Interim Staff Guidance on burnup credit issued by the U.S. Nuclear Regulatory Commission's Spent Fuel Project Office recommends restricting the use of burnup credit to assemblies that have not used burnable absorbers. This restriction eliminates a large portion of the currently discharged spent fuel assemblies from cask loading, and thus severely limits the practical usefulness of burnup credit. This report examines the effect of integral burnable absorbers (IBAs) on reactivity to provide technical justification for relaxing the current restriction for dry storage and transportation, and subsequently, for developing the necessary guidelines for relaxing the current restriction. The effect of IBAs on reactivity for various IBA designs is shown and discussed. Further, the reactivity effect of IBAs for typical initial fuel enrichment and absorber loadings is quantified as a function of burnup. The report concludes with a discussion of the issues for consideration and preliminary recommendations to expand the use of burnup credit to include spent fuel assemblies with IBAs.</p>						
12. KEY WORDS/DESCRIPTORS <i>(List words or phrases that will assist researchers in locating the report.)</i> criticality safety, burnup credit, transportation, dry storage, integral burnable absorbers	13. AVAILABILITY STATEMENT unlimited					
	14. SECURITY CLASSIFICATION <i>(This Page)</i> unclassified					
	<i>(This Report)</i> unclassified					
	15. NUMBER OF PAGES					
16. PRICE						